Structural studies on
β$_2$-glycoprotein I and
von Willebrand factor A3 domain

Barend Bouma

Structural studies on
β₂-glycoprotein I and
von Willebrand factor A3 domain

Structuuranalyse van β₂-glycoproteïne I en
het A3 domein van von Willebrand factor

(Met een samenvatting in het Nederlands)

Proefschrift

ter verkrijging van de graad van doctor aan de Universiteit Utrecht op gezag van de Rector Magnificus, Prof. Dr. H.O. Voorma, ingevolge het besluit van het College voor Promoties in het openbaar te verdedigen op dinsdag 19 september 2000 des ochtends te 10.30 uur

door

Barend Bouma

geboren op 21 november 1972, te Deventer

--- Contents ---

*"**b**-wetenschap, ja, wat is dat nu eigenlijk?"*[a]

Nou, zoiets dus……….

[a] Permanent gespreksthema binnen de gelijknamige discussiegroep (Utrecht, 1995-2000)

--- Chapter I ---

Introduction

Protein crystallography

The widespread and important role of X-ray crystallography in current structural research has its origin in the discovery by Röntgen in the year 1895 of mysterious rays that passed through the human body, which he termed 'X-rays'. The first X-ray crystallographic experiment was performed in 1912 by von Laue, Friedrich and Knipping. They measured the X-ray diffraction pattern of a crystal of copper sulfate. The use of X-ray crystallography in the biological sciences is marked by an impressive milestone in 1953. In that year Watson and Crick[1] published the structure of DNA based on diffraction data. The breakthrough in protein crystallography came within one decade with the crystal-structure determinations of hemoglobin and myoglobin as the important hallmark[2,3]. Nowadays, protein crystallography has become a major technique for rational structure-based drug design, for the emerging field of structural genomics and for understanding biological processes, with the structure elucidation of the complete 50S subunit of the ribosome as a very recent and impressive result[4].

The increasing contribution of protein crystallography to structural studies of bio-macromolecules is based on dramatic developments in data collection and structure elucidation. Important developments have been third-generation synchrotron radiation[5,6], multiple anomalous dispersion (MAD)[a] technique[7,8] and improvements both in phasing and refinement methods[9,10], that use the still increasing computer power. Furthermore, advances in molecular biology enable the production of more and more complex proteins in sufficient amounts. New crystallization techniques and increasing insights into protein crystallization[11] result in faster screening and reproducible crystallization of nearly every protein of interest. Current challenges in structural biology include structure elucidation of large functional complexes consisting of multiple proteins and structure determination of eukaryotic integral membrane proteins. For these studies protein crystallography remains the primary technique, which can be combined with nuclear magnetic resonance (NMR) spectroscopy to study e.g. the dynamic behavior of molecules, and may be complemented by electron microscopy in the study of large structures (e.g. viruses and ribosomes). Progress in the field of macromolecular structure determination is reflected by the nearly exponential increase in known three-dimensional structures, *i.e.* ~300 in 1991, ~4,500 in 1997, ~12,000 in 2000 (Ref. 12).

X-ray crystallography in a nutshell
X-ray crystallography is a very powerful experimental technique that provides the three-dimensional structure of (macro)molecules. Crystallography gives information ranging from high-resolution structural details to global folds and quarternary structures of protein complexes. The first requirement for a successful X-ray diffraction experiment is a high-quality crystal. Such a crystal is a highly ordered array of unit cells containing one or more molecules repeated in three-dimensions in identical orientations and conformations.

---

[a] Abbreviations used: aβ2ab, anti-β2gpI auto-antibody; aCL, anti-cardiolipin auto-antibody; aPL, anti-phospholipid auto-antibody; APS, anti-phospholipid syndrome; AvWD; acquired von Willebrand disease; β2gpI, β2-glycoprotein I; CK, cysteine knot; CL, cardiolipin; CNS, *Crystallography & NMR System*; ESRF, European Synchrotron Radiation Facility; gpIb, platelet-receptor glycoprotein Ib; HFH, human factor H; MAD, multiple anomalous dispersion; MIDAS, metal-ion dependent adhesion-site; NMR, nuclear magnetic resonance; PS, phosphatidylserine; SCR, short concensus repeat; SDS PAGE, sodiumdodecylsulphate polyacrylamide gel-electrophoresis; SLE, systemic lupus erythematosus; TTP, thrombotic thrombocytopenic purpura; VCP, vaccinia virus complement control protein; vWD, von Willebrand disease; vWf, von Willebrand factor.

Comparing macromolecular X-ray crystallography with NMR spectroscopy reveals two major differences[13]. Firstly, the X-ray diffraction technique provides less information on the dynamic behavior of the molecule than is obtained from an NMR spectroscopy experiment. Secondly, with NMR spectroscopy only structures of relatively small molecules with an molecular weight of up to ~30 kDa can be solved, whereas X-ray crystallography is used for structure solution of molecules as large as viruses and ribosomes.

With X-ray crystallography the average electron density of all periodically assembled macromolecules in the crystal is reconstructed from diffraction data. A diffraction experiment is based on the property of X-rays to be scattered upon hitting the electron clouds of atoms whose distances are comparable to the wavelength of the X-rays (*i.e.* in the Angstrom range). This scattering occurs only constructively in specific directions due to the periodic nature of the crystal structure. Reconstruction of the molecular electron density needs calculation of the electron density distribution in the unit cell using equation:

$$r(x,y,z) = \frac{1}{V} \sum_h \sum_k \sum_l |F(hkl)| e^{ij\,(hkl)} e^{-2pi(hx+ky+lz)}$$

The observations obtained from the X-ray diffraction experiment are intensities I, that diffract in directions specified by indices (hkl). From the measured intensities the amplitudes |F(hkl)| can be derived. Phase angles φ(hkl) of the diffracted rays, that are essential for calculation of electron density with the *equation*, can, however not retrieved directly from the experiment, which is known as the 'phase problem' in crystallography. Several methods have been developed to circumvent this phase problem. These methods are all based on an indirect and initial estimation of the phases: single or multiple wavelength anomalous diffraction (SAD/MAD), single or multiple isomorphous replacement (SIR/MIR), sometimes with the additional use of anomalous diffraction (SIRAS/MIRAS), and molecular replacement. With a first estimation of the phases an electron-density map is calculated which is used for construction of a first atomic model of the macromolecule. This initial model is built automatically (ARP/wARP; 14, 15) or interactively with the use of computer graphics[16], dependent on data quality and resolution. Subsequent cycles of refinement and rebuilding of the initial model, using measured X-ray diffraction data and available geometrical information from data bases, are performed until convergence. Finally, the refined model is validated using available biochemical data and databases with geometrical data derived from high-resolution models (WHATIF, PROCHECK; 17,18).

Advantages of (third-generation) synchrotron-radiation sources

Nowadays, almost every published crystal structure of a protein has been elucidated with the use of synchrotron radiation. Advantages of, especially, third-generation synchrotron radiation over X-rays produced by conventional sources, such as rotating anodes, are numerous[5].

Third-generation synchrotron-radiation sources provide X-ray beams which have orders of magnitude higher flux and brilliance over conventional X-ray sources. This allows for higher resolution data sets to be collected. For example, crystals of fully-glycosylated human plasma β_2-glycoprotein I diffracted only to 3.8 Å resolution at our in-house X-ray source, whereas 2.6-3.0 Å resolution data-sets were collected routinely at the European Synchrotron Radiation Facility (ESRF) in Grenoble, France (beam lines ID14-EH1, -EH3 and -EH4, See *Chapter II*, *Chapter IV* and the *Appendix* to *Chapter IV*). The very high

intensity of the beams also allows for structure determination using weakly diffracting crystals of very large molecules. For example, the crystal structure of the 50S ribosomal subunit has been elucidated to 2.7 Å resolution[10]. Very intense synchrotron beams also allow for data collection in time periods smaller than a second, opening the way to time-resolved structural studies of, for example, enzymatic reactions[5,6]. In addition, the high brilliance of current synchrotron beams makes data collection possible from crystals tens of cubic microns in size[19]. The lower mosaicity of small crystals improves the quality of the data collected.

Synchrotrons provide very intense and tunable beams. These are requirements for using the MAD technique[7,8]. The major advantage of this technique is that phase determinations are not hampered by non-isomorphism between crystals.

One disadvantage of intense X-ray sources is radiation damage, which causes a global and non-specific decay of the crystal. This decay can be largely prevented by measuring data at cryogenic temperature[20,21]. Recent studies on irradiation of protein crystals with very intense beams of the third-generation synchrotron source at the ESRF (Grenoble, France), showed that even cryo-cooling cannot prevent highly specific structural radiation damage[22-24]. Specific damage to the protein molecule is observed as breaking of disulfide bonds, decarboxylation of acidic amino-acid residues and release of hydroxyl groups and thio groups from tyrosine and methionine residues, respectively. These insights initiated the search for compounds that can act as preservatives against radiation damage.

The use of the highly intense synchrotron beams has been facilitated by advantages of new detection systems[25] and new data-processing software (DENZO; 26). In addition, developments in data-collection technology have been complemented with important developments in computer programs that aid phase determination (SOLVE: 10; SnB: 27, 28; SHELXL: G.M. Sheldrick), model building (ARP/wARP: 14, 15) and model refinement (Maximum Likelihood: 29; CNS: 9). Structure determinations described in this thesis made fruitfully use of SOLVE and CNS. The program SOLVE fully automates the process of crystal-structure solution using the MAD and MIR(AS) methods through integration of all separate steps in an optimization procedure using Z-score criteria. The procedures used in SOLVE have remarkably reduced the time needed for often difficult and time-consuming elucidation of crystal structures. The quality of a calculated phase set is assessed directly from electron-density output. With SOLVE we obtained an interpretable map with the MIRAS method using data of poorly diffracting crystals of human plasma β_2-glycoprotein I (See *Chapter II*). An important advantage of the *Crystallography & NMR System* (CNS; 9) for crystallographic refinement is its usage of the maximum likelihood procedure[29]. This procedure maximizes the probability distribution of the observed amplitudes given the calculated amplitudes from a model that may be partial or partially incorrect. In this way, the effect of model bias is reduced in the refinement process.

In summary, advances of protein crystallography in structural biology are made possible by improvements throughout all stages of the structure-determination process, *i.e.* by dramatic developments in data-collection technology, in structure-determination methodology, in computer technology and in microbiology.

β₂-Glycoprotein I

Primary structure of β₂-glycoprotein I

β₂-Glycoprotein I (β2gpI) is a mammalian glycoprotein present in blood plasma in a concentration ranging from 10 to 200 µg ml^{-1} (0.25-5.0 µM)[30-32]. β2gpI is a monomer in solution, whereas dimers[33,34] and tetramers[35] are observed during sodiumdodecyl-sulphate polyacrylamide gel-electrophoresis (SDS PAGE). *b2gpI* mRNA is expressed in endothelial cells[36], central nervous-system cells[37], hepatocytes[38] and in the placenta[39]. β2gpI is synthesized as a single-chain polypeptide consisting of 326 amino-acid residues and with a calculated molecular mass of 36.3 kDa. Sequencing of human *b2gpI* DNA[38, 40] and amino-acid sequencing of human β2gpI[41] and bovine β2gpI[42] revealed 22 cysteines all involved in intramolecular disulfide bonds, and a relatively high content of prolines (*i.e.* 31). In addition, four potential Asn-X-Ser/Thr N-glycosylation motifs were identified in human β2gpI (Fig. 1). Lozier *et al.* (41) and Walsh *et al.* (43) showed that N-glycans were indeed attached to these four sites. In addition, Gambino *et al.* (44, 45) indicated that β2gpI contains O-glycans. The glycans account for approximately 20% w/w of the total molecular mass of β2gpI (42-50 kDa), as observed with SDS PAGE[32,35,41]. Apart from variations in plasma levels of β2gpI, carbohydrate heterogeneity among subfractions of β2gpI isolated from plasma of a single donor[46,47], as well as genetic heterogeneity in human populations[48-50] have been observed. Carbohydrates differed in their content of sialic acid residues. Observed genetic heterogeneity in human β2gpI was a Val247Leu polymorphism[38,51], a Cys306Gly mutation[52] and a Trp316Ser mutation[52,53].

Domain organization of β2gpI

The mature β2gpI sequence of 326 amino-acid residues consists of five contiguous repeating units of the same type. These units are termed Sushi domains, complement control protein domains or short concensus repeat (SCR) domains and are present in many proteins that function in the complement system, as well as in many other mammalian adhesive proteins[54]. SCR domains consist of about 60 residues and have two fully conserved disulfide bonds. In many proteins consecutive repeating stretches of SCR domains are found, e.g. in complement receptor 2, factor H and complement receptor 1, which contain up to 15, 20 and 30 SCR domains. Two structures of single SCR domains, domains 5 and 16 of human factor H (HFH)[55,56], and two structures of two SCR domains in tandem, domains 15-16 of HFH and domains 3-4 of vaccinia virus complement control protein (VCP)[57,58] have been determined with NMR spectroscopy. Furthermore, crystal structures of a tandem of two SCR domains of human CD46 (Ref. 59) and of a construct of a single SCR domain and a serine-protease domain of human complement C1s (Ref. 60) have been reported. The structures of these eight SCR domains revealed a common globular fold with a hydrophobic core, consisting of a four-stranded central β-sheet flanked by two short two-stranded β-sheets (Fig. 1A). Furthermore, sequence alignment based on sequential and structural homology revealed a set of 16 conserved mainly hydrophobic residues and a sequence homology among SCR domains ranging from 20 to 40%. (Fig. 1B). Alignment of the amino-acid sequence of β2gpI to sequences of the eight SCR domains with known structure indicates that the first four SCR domains of β2gpI have a regular fold (Fig. 1B). The amino-acid sequence of the C-terminal fifth domain of β2gpI is aberrant. It contains a six-residue insertion and a 19-residue C-terminal extension, which is C-terminally cross-linked by an additional disulfide bond. In

Chapter II we present the three-dimensional model of human plasma β2gpI, obtained with X-ray crystallography.

Adhesive properties of β2gpI: binding to anionic phospholipids

β2gpI is also referred to as 'apolipoprotein H', due to its property to adhere to lipoproteins[61,62]. It has been established, however, that β2gpI not only binds to lipoproteins but more in general to any negatively charged surface present in the blood circulation, *i.e.* it also binds to apoptotic bodies[63,64], chylomicrons[65], blood platelets[66,67], and liposomes[68,69]. β2gpI adheres specifically to anionic phospholipids, *i.e.* cardiolipin (CL) and phosphatidylserine (PS), exposed on the negatively charged membrane surfaces[69-72]. The phospholipid-binding site of β2gpI has been mapped to its fifth aberrant SCR domain[73-75]. Cationic residues Lys282, Lys284, Lys286, Lys287, Lys308 and Lys324 have been implicated in charge interactions between β2gpI and negatively charged head groups of anionic phosphoplipids[34,73,76] (Fig. 1B). In addition, Wang *et al.* (77, 78) have shown that hydrophobic interactions were also important in lipid adhesion, which has been confirmed by mutagenesis studies that revealed a critical role for the hydrophobic sequence Leu313-Ala-Phe-Trp316 (Ref. 52, 53, 79). The integrity of the fifth SCR domain is another important factor in lipid adhesion. Enzymatic cleavage at one of two scissile bonds Leu314-Phe315 and Lys317-Thr318 inhibits binding to anionic lipids[32,80-82]. Furthermore, genetically determined mutation Cys306Gly present in part of the population disrupts a conserved disulfide bond and affects the ability of β2gpI to adhere to anionic lipids[52]. We determined the crystal structure of two isoforms of β2gpI (*Chapter II* and *Chapter IV*). Combined with available biochemical data we proposed a model for membrane adhesion of β2gpI and for inhibition of membrane adhesion.

Adhesive properties of β2gpI: protein-protein interactions

β2gpI binds to several self-proteins in blood plasma and in kidney cells. It forms complexes with protein C, protein S and C4B binding protein[83-85], that function in the protein C-dependent anticoagulant-pathway[86-89]. Klaerke *et al.* (90) and Rojkjaer *et al.* (91) reported very high-affinity complexes between renal-filtered β2gpI and calmodulin, an intracellular protein that plays a major role in the regulation of many enzymes and in a wide variety of cellular events[92]. Renal filtered β2gpI also binds to the endocytic receptor megalin, which actively transfers β2gpI from kidney cells back into the circulation[93]. β2gpI has been identified as a physiological ligand for plasma lipoprotein(a) and binds specifically to the kringle IV domain of the glycoprotein apolipoprotein(a) in this low-density lipoprotein-apolipoprotein(a) complex[94]. Furthermore, β2gpI binds to the endothelial cell-surface protein annexin II[95]. β2gpI also forms complexes with various non-self proteins, e.g. it binds to surface protein Sbi of the bacterium *Staphylococcus aureus*[96], to surface antigens of human immuno-deficiency virus[97] and to surface antigens of hepatitis B virus[98,99]. Although binding properties of β2gpI to self- and non-self proteins have been extensively studied, for none of the above listed protein-protein interactions the binding site of β2gpI has been determined. We studied formation of complexes between β2gpI and several proteins present in blood plasma and kidney cells for further determination of the adhesive properties of β2gpI (*Chapter III*).

Title:
(1_1.eps)
Creator:
Adobe Illustrator(R) 8.0
Preview:
This EPS picture was not saved
with a preview included in it.
Comment:
This EPS picture will print to a
PostScript printer, but not to
other types of printers.

Function of β₂-glycoprotein I

Despite intensive research on human β2gpI, initiated by Schultze *et al.* (100), the physiological function of this plasma protein is still not clear. Moreover, a β2gpI deficiency does not result in noticeable complications[30,31], prompting to the question whether β2gpI has a physiological function at all. In contrast, an important role for β2gpI is suggested by the observation that high plasma levels of β2gpI influence metabolism of triglyceride-rich lipoproteins[70,101] and cholesterol[102]. High plasma levels of β2gpI also correlate with several diseases[103,104], whereas decreased levels of β2gpI are associated with coagulation disorders[105,106]. β2gpI synthesis in placenta and involvement of β2gpI in auto-immune disease-related fetal loss indicate a putative, yet undetermined role in pregnancy[39,107-109]. Connected with these observations, a variety of processes in haemostasis, metabolism and apoptotic-cell clearance are identified in which a regulatory role for β2gpI is indicated.

Nowadays, the main research on β2gpI function addresses topics related to the observation that autologous β2gpI appears highly immunogenic. Auto-antibodies elicited against self-β2gpI are detected in plasma of subsets of patients with auto-immune disease anti-phospholipid syndrome (APS)[110-112] or with other disorders, e.g. non-auto-immune liver disease[113] and auto-immune disease systemic lupus erythematosus[103,114-116], as well as in plasma of healthy subjects[117]. In addition, the presence of anti-β2gpI auto-antibodies (aβ2ab) in plasma is indicated as an important risk factor for myocardial infarction and atherosclerosis[118,119].

Procoagulant activity of β2gpI by inhibition of protein C-dependent anticoagulant reactions upon passive occupation of anionic lipid surfaces by β2gpI has been observed *in vitro*[120,121]. In contrast, β2gpI prevents coagulation by promoting anionic phospholipid vesicles – macrophage interaction and likely by subsequently stimulating uptake of these procoagulant lipid vesicles[122]. β2gpI has also been indicated as a direct inhibitor of a series of anionic-membrane mediated coagulation processes[66,67,123-130], as well as a positive cofactor in protein C/protein S-dependent anticoagulant processes[83,83,105,106]. The influence of β2gpI on coagulation processes is strongly dependent on the presence of anionic phospholipids, suggesting that the regulatory role of β2gpI is associated with its adhesion to negatively charged lipid layers. Both pro- and anticoagulant activity of β2gpI have only been demonstrated in *in vitro* assays, whereas *in vivo* these activities have not yet been proven.

Whether β2gpI has a critical role in clearance of apoptotic cells from the circulation is a matter of debate. Price *et al.* (31) showed that β2gpI binds specifically to the anionic phospholipid surface of PS-expressing apoptotic bodies. Work of Balasubramanian *et al.* (63, 64) indicated that binding and subsequent internalization of apoptotic cells by macrophages was enhanced after opsonization of these apoptotic cells with β2gpI. Although an absolute requirement for β2gpI in clearance of apoptotic cells was not deduced, these results suggested that β2gpI may at least serve a stimulatory role. In contrast, Dombroski *et al.* (132) showed that β2gpI reduces uptake of membranes containing PS, that are representatives for apoptotic cells, by endothelial cells. Manfredi *et al.* (133) indicated with their experiments that β2gpI did not influence apoptotic cell clearance at all. Moreover, there is for many years concensus in the field of research on apoptosis that PS is the specific ligand at the surface of apoptotic cells which triggers recognition by macrophages[134,135]. Recently, Fadok *et al.* (136) identified the specific PS receptor of the macrophages. These results prompted further doubt whether β2gpI has a role in apoptotic cell clearance.

In summary, in all proposed physiological functions the common activity of β2gpI consists of a non-specific occupation or neutralization of anionic phospholipid layers[105]. In addition, the important and well-characterized gain-of-function for β2gpI in the auto-immune disease APS is also fully dependent on the availability of exposed anionic phospholipids[111]. With the research described in this thesis we aimed at gaining more insight into potential functions of β2gpI by studying protein-protein complexes involving β2gpI (*Chapter III*) and by determining the aspects that influence the lipid-adhesive properties of β2gpI (*Chapter IV*).

β2gpI and auto-immunity

β2gpI has a well-defined gain-of-function associated with the presence of aβ2ab in plasma of patients with the auto-immune disease APS[111,137-140]. Abnormalities associated with aβ2ab-β2gpI complexes in APS are arterial and venous thrombosis, thrombo-embolic complications (e.g. cardial infarction), thrombocytopenia, neurological disorders and (recurrent) fetal loss[112]. Intensive research focused on identification of the auto-antibodies and on the role of auto-immunity to β2gpI in APS. It has become evident that aβ2ab are not only markers of APS but in fact (partly) cause the observed abnormalities[110]. The aspects responsible for the high immunogenicity of β2gpI are not fully understood. The existence of genetically determined features of β2gpI[51,103,104,141] and several physiological abnormalities[142-146] potentially cause APS by breaking the tolerance for autologous β2gpI.

Initially, auto-antibodies in APS were identified as anti-phospholipid auto-antibodies (aPL) elicited against anionic lipid surfaces. Galli *et al.* (147), McNeill *et al.* (148), and Koike and Matsuura (149) demonstrated that aPL were in fact aβ2ab raised against β2gpI bound to a lipid layer. aβ2ab are an intra- and inter-individually heterogeneous group of auto-antibodies. Epitopes for aβ2ab are localized in all five SCR domains of β2gpI[150-153], including the C-terminal fifth domain, which contains the adhesion site for anionic phospholipids[154,155]. This diversity may correlate with the observed variety of clinical manifestations in patients with APS[117,156]. Controversy exists on the parameters that define affinity of aβ2ab for β2gpI, when β2gpI is membrane bound. High affinity of aβ2ab for immobilized β2gpI is possibly explained by exposure of cryptic epitopes upon adhesion of β2gpI to anionic membranes, as evidenced by enzyme-linked immunosorbent assays[75,157-161]. This hypothesis is supported by circular dichroism spectroscopy[162]. Alternatively or additionally, occurrence of (aβ2ab)$_2$-β2gpI complexes at membrane surfaces and not free in solution may depend on the increase in avidity provided by two aβ2ab-β2gpI interactions in combination with two β2gpI-lipid interactions per complex[110]. Fab fragments of aβ2ab do not induce adhesion of β2gpI to anionic lipids upon binding to β2gpI, providing evidence for this second potential mechanism[163,164].

The central role for β2gpI in the auto-immune response leading to severe coagulation disorders makes this protein a target for potential treatment of anti-phospholipid syndrome[153,165].

von Willebrand factor

Multimeric configuration of vWf

von Willebrand factor (vWf) is a glycoprotein present as multimers in endothelial cells, megakaryocytes and platelets, and in plasma in an approximate concentration of 10 μg ml^{-1} with large variations among individuals (See for reviews: 166-168, and references therein). The *vWf* gene is expressed in vascular endothelial cells and in bone-marrow megakaryocytes. The resulting precursor polypeptide, referred to as pre-pro-vWf, consists of 2,813 amino-acid residues, including a signal peptide of 22 amino-acid residues and a large propeptide of 741 residues[169,170] (Fig. 2A). During biosynthesis of pre-pro-vWf the signal peptide and the propeptide are released, resulting in fully processed mature vWf. This mature vWf subunit consists of 2,050 amino-acid residues and has a molecular weight of 230-280 kDa. Ten to twenty percent of the molecular mass is accounted by ten O-linked carbohydrates and twelve N-linked carbohydrates, two of which are additionally sulfated. The N-linked carbohydrates of vWf are part of the ABO-blood group determinants. The mature protein is highly cysteine rich with most of the 169 cysteines involved in intramolecular disulfide bonds[171]. Intermolecular disulfide bonds near the carboxy terminus of pro-vWf are formed in the Endoplasmic Reticulum, forming vWf dimers (Fig. 2B). In the Golgi subsequent formation of intermolecular disulfide bonds near the amino terminus links mature vWf-dimers to higher-order multimers. These polymers consist of up to as many as 100 vWf monomers and have molecular weights ranging from 1,000 kDa to over 20,000 kDa. In the circulation vWf multimers have, either a compact 'ball-of-yarn' conformation, or an extended string-like shape of the disulfide-bond-linked vWf monomers[172-174]. The latter conformation is formed under influence of high shear stress at high blood pressure[174].

Storage and secretion of vWf

Directly after synthesis in vascular endothelial cells major part of the vWf pool is secreted constitutively[175]. The remainder part of vWf is stored in Weibel-Palade bodies inside the endothelial cells. In megakaryocytes and platelets derived from them vWf is stored in granules. After stimulation of cells during haemostatic imbalance stored vWf is released via a regulated pathway. Secreted vWf, either by the constitutive pathway, or by the regulated pathway, is released into the blood circulation and into the subendothelial matrix of the vessel wall. vWf secreted upon activation consists of relatively large multimers, which are more effective in the haemostatic system.

Domain organization of vWf and function of individual domains

A mature vWf subunit consists of domains D'-D3-A1-A2-A3-D4-B1-B2-B3-C1-C2-CK, whereas pre-pro-vWf is N-terminally extended with the 22-residue signal sequence and with the propeptide consisting of domains D1-D2 (Fig. 2). Evidence is evolving which suggests that individual domains of vWf are independent structural motifs with discrete functional activities[176-180]. Domains D1-D2 in the pro-vWf subunit have a function in the process of multimerization by cross-linking vWf dimers via disulfide bonds. Domains D'-D3 contain the binding site for coagulation cofactor VIII[181] and a binding site for heparin. Mutations in D' result in von Willebrand-disease (vWD) type 2N, resulting in a vWf molecule which can not bind factor VIII (For reviews see: 182-184, and references therein). Cysteine residues in D3 link N-termini of vWf dimers[171]. The A1 domain has a binding site for platelet-receptor glycoprotein Ib (gpIb), heparin, that inhibits binding of A1 to platelet gpIb, collagen type

VI[185,186], sulfatides, snake venom botrocetin and antibiotic ristocetin, that induce binding of vWf to platelets without prior immobilization of vWf[187,188]. Furthermore, A1 putatively contains a cryptic binding site for the vWf-A3 domain, that may only then become available after adhesion of vWf to collagen[189]. In addition, domain A1 is, like A2, prone to many vWD mutations. No binding sites reside in the A2 domain, but it contains a cleavage site for a metalloproteinase. This proteinase cleaves vWf under conditions of high shear stress, *i.e.* when vWf has its extended conformation, resulting in decreased haemostatic activity of the shortened vWf multimers. In this way, the proteinase prevents spontaneous platelet aggregation by large multimers of vWf. The binding sites for collagen types I and III[180,190] and for snake venom bitiscetin, that induces binding of platelets to the A1 domain[189], reside in domain A3. No functions and adhesion sites are designated to domains D4, B1, B2, B3 and C2. The C1 domain binds to the integrin platelet-surface receptor $\alpha_{IIb}\beta_3$ once platelets are activated. The RGD amino-acid sequence of C1 is essential for its cell-adhesive properties[191] and has been found in other proteins that interact with integrin receptors[168]. The cysteine-knot (CK) domain near the carboxy terminus is involved in dimerization of vWf molecules[177] and has no additional adhesive function. Finally, vWf binds fibrin, but the binding site has not been assigned to a specific domain[192].

Title:
(1_2.eps)
Creator:
Adobe Illustrator(R) 8.0
Preview:
This EPS picture was not saved
with a preview included in it.
Comment:
This EPS picture will print to a
PostScript printer, but not to
other types of printers.

Fig. 2. Domain organization of von Willebrand factor. (**A**) The domain structure of pre-pro-vWf is shown, with a 22 amino-acid residue signal peptide, that is cleaved off in pro-vWf, and a 741 amino-acid residue propeptide, that is subsequently cleaved off in the 2,050 amino-acid residue mature vWf molecule. Location of domains is indicated by labeled boxes. Cysteines that link two pro-vWf monomers forming dimers are located in the CK domain; disulfide bonds between dimers forming higher-order multimers with varying size are formed between cysteines located in the D3 domain of mature vWf. The location of cysteines that are involved in intermolecular disulfide bonds are indicated with S-atoms. The scissors indicates the location of the metalloproteinase cleavage-site in domain A2. (**B**) Schematic representation of a pro-vWf dimer (left) and a mature vWf multimer (right). Positions of the D3 and CK domains are indicated. In healthy individuals vWf multimers consist of as many as up to 100 monomers, whereas unusual or ultra large vWf multimers, found in plasma of patients suffering from thrombotic thrombocytopenic purpura, consist of even higher numbers of monomers.

Crystal structures of the vWf-A1 and A3 domain (Ref. 193-196; R. Romijn, unpublished results) show a so-called Rossman fold, dinucleotide fold, or α/β fold consisting of a central hydrophobic β-sheet flanked by α-helices on each side (Fig. 3). This classical fold is also observed for the crystal structures of the I domains of integrins $\alpha_M\beta_2$, $\alpha_L\beta_2$ and $\alpha_2\beta_1$, of which the latter, like vWf-A3, binds to collagen[197-199]. In contrast to the I domains, both the A1 and A3 domain lack the typical metal-ion dependent adhesion-site (MIDAS) motif and a metal ion bound to this motif. For all known integrin I domains this motif, located in the 'top face' of the molecule, and a bound divalent cation are involved in ligand binding. The crystal structure of the I domain of integrin $\alpha_2\beta_1$ in complex with a triple-helical collagen peptide has confirmed the importance of the MIDAS motif in collagen binding[200]. Comparison of the structure of the I domain of integrin $\alpha_2\beta_1$ with the structure of vWf-A3 revealed no shared features and, in addition, mutation of amino-acid residues in the top face of A3 homologous to residues of $\alpha_2\beta_1$ that are involved in collagen binding, had no influence on collagen binding by A3[193,201]. These observations prompt doubt whether the collagen-binding site of A3 is located in its top face (Fig. 3A). With a structural study by means of X-ray crystallography, of the vWf-A3 domain in complex with a function-inhibiting Fab fragment, we aimed at providing more insight into the binding site of A3 for collagen (*Chapter V*).

Studies with A1 using site-directed mutagenesis[188] and the crystal structure of the vWf-A1 domain in complex with a Fab fragment of an antibody that blocks adhesion of A1 to gpIb[195], have pointed to the binding sites for gpIb, ristocetin and botrocetin (Fig. 2B). Binding sites for these three ligands are located outside the top face of A1 and do not involve the vestigial MIDAS motif. The observations that gpIb, ristocetin and botrocetin do not bind to the top face of A1 and that collagen likely does not bind to the top face of A3, leaves this adhesion site in A1 and A3 available for putative alternative, yet unknown roles in functional interactions.

The haemostatic balance

Plasma protein vWf has an important function in the very first response in case of vascular damage. Thereby, activity of vWf is part of our haemostatic system, which is critical in preservation of the integrity of the blood circulation and prevention of blood loss at sites of vascular damage, termed physiological homeostasis. The haemostatic system is a complex system consisting of five major components; blood vessel walls, blood platelets, pro- and anticoagulation system, rheology and fibrinolytic factors, that act in concert in integrated pathways during haemostasis. At a site of a ruptured blood vessel three mechanisms respond instantaneously to arrest the blood loss; *i.* vessel wall contraction, *ii.* formation of a plug by platelet adhesion and aggregation, activities in which vWf plays an essential role, and *iii.* blood coagulation, formation of a fibrin mesh. Anticoagulant proteins prevent occlusion of veins and arteries by thrombi and prevent extension of the procoagulant response outside the direct vicinity of the damaged vessel wall. Clot-dissolving fibrinolytic factors restore normal blood flow by gradual lysis of a haemostatic plug, *i.e.* by fibrinolysis. Haemostasis is a complex tightly balanced system of stimulating and inhibitory pathways that respond fast and strict locally to arrest haemorrhage at sites of vascular damage and that initiate subsequent longer-term restoring events. Imbalance in the haemostatic system may result in excessive and life-threatening bleeding even from a trivial trauma, or may result in arrest of circulation to vital organs by uncontrolled formation of thrombo-embolic occlusions in the blood-vessel system.

Fig. 3. Ribbon diagrams of the vWf-A1 domain and the vWf-A3 domain. Positions of residues that are involved in the vestigial MIDAS motif in the top face of the A1 and A3 domain are indicated with gray spheres. The intramolecular disulfide bond within A1 and A3, located near the carboxy and amino termini at the bottom face of both domains, is represented in ball-and-stick. Figures are generated with MOLSCRIPT[202] and RASTER3D[203]. (**A**) Schematic drawing of the human vWf-A3 domain (vWf residues 920 to 1111) (pdb code 1ATZ, 194). The collagen-binding site in the top face of the structurally related I domain of integrin $\alpha_2\beta_1$[200] is indicated with a circle in the model of A3. Amino-acid mutations in the top face of A3 that had no influence on collagen binding by an A3 construct[193], or by full-length vWf[201] are indicated by black spheres. Residues Asp934, Ser936 and Ser938, that form the vestigial MIDAS motif, were also mutated and are represented as gray spheres. (**B**) Schematic drawing of the human vWf-A1 domain (vWf residues 508 to 709, R. Romijn, unpublished data). The putative binding sites for gpIb and for botrocetin, that induce spontaneous binding of A1 to gpIb, determined by using point-mutated constructs of A1, are located on the front side of the domain, and are indicated with boxes[188,195,196]. The position of vWD Type 2B mutations, that also induce spontaneous platelet binding by A1, are located at the bottom and back side of A1, opposite to the putative location of the gpIb and botrocetin binding sites.

Function of vWf in haemostasis

One of the two known haemostatic functions of vWf is to adhere to platelets and to plasma-exposed subendothelial components of a damaged arterial vessel wall, thereby initiating haemostasis under conditions of high shear stress[166-168]. At a site of vascular injury the A3 domain of vWf binds to collagen types I and III. Once vWf is bound to the subendothelial connective tissue the A1 domain binds with high affinity and reversibly to the platelet receptor gpIb. In this way tethered platelets are slowed down, which allows for their irreversible adherence to components of the vessel wall via the platelet receptor $\alpha_{IIb}\beta_3$. At high shear stress, *i.e.* in small arterioles, arterial capillaries and next to atherosclerotic plaques, binding of platelets to vWf is essential for the activity of vWf in haemostasis and disease. When tethered to vWf, activated platelets aggregate and bind simultaneously to fibrin that incorporates into a network, resulting in formation of a blood clot that closes the ruptured vessel wall. In parallel, thrombin is formed by the coagulation cascade, which

results in additional activation of platelets and conversion of soluble fibrinogen to fibrin. This results in formation of a permanent and fibrous clot that arrests blood loss.

vWf also functions in the haemostatic system as the carrier molecule of glycoprotein factor VIII[204,205]. When non-covalently bound to vWf factor VIII is protected for enzymatic degradation by protein C. Factor VIII is a cofactor with procoagulant activity, that is triggered upon cleavage by thrombin. The physiological reason of stabilization of factor VIII by vWf is not known, but an important role for vWf in translocating factor VIII to sites of vascular injury is suggestive.

Activation of vWf during haemostatic imbalance

vWf in the circulation does not bind spontaneously to platelet-receptor gpIb. Platelet tethering to vWf occurs, *i.* upon binding of vWf to components of a damaged vessel wall, *ii.* in case of naturally occurring so-called vWD 'type 2B' mutations in the 'bottom face' of domain A1, or *iii.* upon binding of, either snake venom botrocetin, or antibiotic ristocetin to A1. Another important aspect in activation of platelet adhesion by vWf is the presence of shear stress[167]. At low blood pressure vWf has a globular ball-of-yarn conformation, that does neither adhere to exposed constituents of the vessel wall at sites of vascular damage, nor to platelets. In small arterioles and arterial capillaries, *i.e.* at high shear stress, multimeric vWf adopts an extended chain conformation that allows for collagen binding and subsequent gpIb binding. Furthermore, platelet adhesion depends on the multimeric size of vWf; monomers are not functional active at all, activity increases with multimeric size and ultra-large multimers are able to bind platelets spontaneously, an event that occurs in patients suffering from thrombotic thrombocytopenic purpura (TTP). All data together may point to activation of vWf by, either an allosterically controlled pathway, or an entropically controlled pathway, or by an integrated pathway which contains contributions of both models[167].

The allosteric model has been proposed for the vWf-A1 domain[195,196], based on the crystal structure of A1 and based on the observed conformational changes upon ligand binding in the structurally related I domain of integrin $\alpha_M\beta_2$[198,206,207]. Activation mechanisms of A1 indeed point to the possible existence of a low-affinity conformation that switches to a high-affinity state upon, *i.* stimulation by modulators for which A1 has binding sites outside its gpIb-binding site (e.g. botrocetin, ristocetin), *ii.* introduction of gain-of-function mutations, also located outside the gpIb-binding site (e.g. vWD Type 2B), or, *iii.* immobilization of vWf at a damaged vessel wall. A mechanism in which A3, adhered to collagen, activates A1 by induction of conformational changes via direct A3-A1 interactions, is often suggested[189,193] but has not been proven. Indirect evidence that supports a mechanism in which activity of A1 is modulated by A3, is provided by auto-antibodies that inhibit binding of vWf to collagen as well as binding of vWf to gpIb upon binding of the antibodies to epitopes in A1 or A3[208,209]. Additional support for the hypothesis comes from snake venom bitiscetin, that binds to A3, thereby inhibiting platelet binding to the A1 domain[189].

Alternatively or additionally, the entropic model is supported by the observations that, *i.* larger vWf multimers are more active in haemostasis, *ii.* vWf exposes hidden domains under high shear-rate conditions, and *iii.* unusually large vWf multimers bind to platelets spontaneously, without the prior need of activation or immobilization of vWf. Affinity of individual A1 domains for gpIb may be too low for effective binding, as is observed for collagen binding by the isolated A3 domain[201]. Adhesion of stretched vWf multimers to sites of vascular damage via multivalent A3-collagen interactions will effectively increase the local concentration of A1 contact sites, available for interactions with gpIb. Intrinsic low

14

affinity of A1 for gpIb is now circumvented by increased avidity of multiple A1-gpIb interactions.

von Willebrand factor and blood-coagulation disorders

Qualitative and quantitative alterations of vWf have dramatic impact on its activity during maintenance of homeostasis, resulting in a variety of haemostatic diseases. These diseases are defined, either by bleeding tendencies (vWD, acquired vWD), or by thrombotic complications (auto-immune response to vWf, e.g. in lupus anticoagulant, SLE, APS), or by both (TTP).

The rare disease thrombotic thrombocytopenic purpura is defined by sustained qualitative alterations of vWf accompanied by a periodic quantitative deficiency of vWf. Patients with TTP show spontaneous intravascular aggregation of platelets in their microcirculation resulting in severe thrombocytopenia, neurological disorders, haemolysis, fever and renal dysfunction (For reviews see: 210-212). In most cases TTP is correlated with the presence of auto-antibodies elicited against the metalloproteinase that specifically cleaves the A2 domain of vWf. Impairment of proteolytic breakdown of vWf results in the presence of ultra large vWf multimers in the circulation, that aggregate platelets spontaneously. Absence of the metalloproteinase is permanent in plasma of patients with familial chronic relapsing TTP[210]. A single acute episode of TTP seems correlated with the presence of function-inhibiting auto-antibodies elicited against the enzyme. Acute TTP is often associated with auto-immune diseases SLE and APS[213], although direct correlation remains doubtful[214]. In between episodes of TTP, the concentration of ultra large vWf multimers in plasma is apparently below a threshold level, producing only non-severe amounts of platelet aggregates. Increased endothelial cell activation or cell damage, possibly triggered by viral or bacterial infection, auto-immune disorders, bone marrow transplantation, cancer, therapeutics and pregnancy, releases additional stored ultra large vWf multimers form endothelial cells, which then results in the observed aggregation of platelets and in the pathogenic mechanisms of TTP.

Von Willebrand disease is a clinically heterogeneous and common inherited bleeding disorder which originates from qualitative or quantitative defects of vWf, caused by mutations in the *vWf* gene[182-184]. vWD has been classified in several subtypes based on the observed molecular defects: vWD Type 1 (mild quantitative vWf deficiency), Type 2 (altered vWf function), Type 3 (severe quantitative vWf deficiency). vWD Type I is characterized by a reduced amount of vWf multimers whereas the multimer distribution of vWf is normal. vWD Type 3 is a rare disease but most life threatening among vWD variants. Patients with vWD Type 3 suffer from severe bleeding correlated with the virtual absence of vWf in the circulation. The qualitative Type 2 vWD variants have been further divided into subgroups 2A, 2B, 2M, and 2N, based on heterogeneous pathophysiology. Bleeding tendencies result from amino-acid point mutations or gene insertions or deletions in the D domains or in the A domains (Fig. 2A). vWD Type 2A and B is characterized by the absence of large multimers. For Type 2A the absence of large multimers is due to mutations in the A2 domain that result in increased susceptibility of vWf for the metalloproteinase, which cleaves the A2 domain. For Type 2B the absence of large multimers is due to spontaneous binding of the largest vWf multimers to platelets. In Type 2M activity of vWf is decreased, whereas concentration and distribution of vWf over the normal range of multimer sizes is normal. Patients with vWD Type 2N have a normal vWf multimer distribution, but binding of vWf to factor VIII is reduced or abolished.

Acquired von Willebrand disease (AvWD, auto-immune vWD) is a rare disease that occurs in combination with an array of disorders, e.g. infectious diseases, tumours, metabolic or hormonal disorders[215-217]. A predominant amount of cases is associated with auto-immune disorders, including SLE and APS[215,218,219]. Clinical manifestations of AvWD are similar to those observed in patients with inherited vWD. In most cases of AvWD abolished vWf function, due to the lack of large vWf multimers, is observed accompanied by function-inhibiting or vWf-clearance accelerating anti-vWf antibodies, or by a general auto-immune response. Auto-antibodies specific for the A1 and A3 domains of vWf, which abolish platelet-gpIb binding or collagen binding, or both, may be present[208,209,220]. Alternatively, auto-antibodies in patients with APS, lupus anticoagulant or SLE, that are not elicited against vWf, induce bleeding tendencies and thrombotic complications by stimulation of vWf release from endothelial cells[221-223].

Scope and outline of thesis

In this thesis crystallographic structure analyses are described of human plasma β_2-glycoprotein I and the recombinant A3 domain of human plasma von Willebrand factor. Common aspects of β2gpI and vWf are, *i.* the necessity to adhere to a suitable surface as part of their activation, *ii.* their interaction with multiple proteins that function in the haemostatic system, and *iii.* their implication in several coagulation disorders. Five-domain β2gpI binds specifically with its fifth short concensus repeat domain to anionic phospholipid layers. This shielding of negatively charged surfaces in the circulation is likely the important aspect of β2gpI in anti- and procoagulant processes. Multi-domain vWf contains a major binding site for fibrilar collagen located in its A3 domain. When an arterial vessel wall is ruptured binding of the A3 domain to exposed collagen is one of the first steps in haemostasis, that facilitates recruitment of platelets from the circulation for formation of a blood clot. Structural insights into the adhesive mechanisms of β2gpI to lipids and of vWf-A3 to collagen are of valuable help in understanding the role of β2gpI and vWf in the haemostatic balance and in diseases, that affect the integrity of the circulation.

In *Chapter II* elucidation of the crystal structure of fully-glycosylated β2gpI, purified from human plasma, is reported. Based on the β2gpI structure and available biochemical data a model for membrane adhesion is proposed. In *Chapter III* investigation by means of gel-filtration chromatography of the interaction of β2gpI with several proteins that function in blood coagulation or in renal excretion is described. *Chapter IV* describes the biophysical analysis and the crystal structure of an isoform of β2gpI that is present in plasma of patients who suffered from severe oxidative stress. The structure and thin-layer chromatography revealed that the β2gpI isoform contains a neutral phospholipid molecule, with possible implications for the function of β2gpI. In the *Appendix* to *Chapter IV* effects of radiation damage on the local and global structure of β2gpI are analyzed. This analysis was required for a proper comparison of the structures of β2gpI isoforms. In *Chapter V* we address the localization of the collagen-binding site of the vWf-A3 domain. For this purpose the crystal structure was solved of the recombinant seleno-methionine A3-domain of human vWf in complex with a Fab fragment of antibody RU5, that blocks adhesion of vWf to collagen.

--- Chapter II ---

Crystal structure of β₂-glycoprotein I: model for adhesion to phospholipids

Barend Bouma, Philip G. de Groot[1], Jean M.H. van den Elsen, Raimond B.G. Ravelli[2], Arie Schouten, Marleen J.A. Simmelink[1], Ronald H.W.M. Derksen[3], Jan Kroon and Piet Gros

Department of Crystal and Structural Chemistry, Bijvoet Center for Biomolecular Research, Utrecht University, Padualaan 8, 3584 CH, [1]Haemostasis and Thrombosis Laboratory and [3]Rheumatology and Clinical Immunology, PO Box 85500, 3508 GA Utrecht, The Netherlands and [2]EMBL Grenoble outstation, 6 Rue Jules Horowitz, B.P. 156, 38042 Grenoble Cedex 9, France.

Summary

Human β_2-glycoprotein I is a heavily glycosylated five-domain plasma membrane-adhesion protein, that has been implicated in coagulation and clearance of apoptotic bodies from the circulation. It is also the key antigen in the auto-immune disease anti-phospholipid syndrome. The crystal structure of β_2-glycoprotein I isolated from human plasma reveals an elongated fish-hook like arrangement of the globular short-consensus repeat domains. Half of the C-terminal fifth domain deviates strongly from the standard fold, as observed in domains one to four. This aberrant half forms a specific phospholipid-binding site. A large patch of 14 positively charged residues provides electrostatic interations with anionic phospholipid headgroups and an exposed membrane-insertion loop yields specificity for lipid layers. The observed spatial arrangement of the five domains suggests a functional partitioning of protein adhesion and membrane adhesion over the N- and C-terminal domains, respectively, separated by glycosylated bridging domains. Coordinates are in the Protein Data Bank (accession code 1QUB).

Introduction

Human β_2-glycoprotein I (β2gpI)[a], also known as apolipoprotein H, is a membrane-adhesion glycoprotein present in blood plasma in a concentration of ~150 to 300 μg ml^{-1} (Ref. 163). It consists of 326 amino-acid residues[40,41] with approximately 20% w/w carbohydrates attached. β2gpI is the key antigen in the auto-immune disease anti-phospholipid syndrome (APS), defined by thrombo-embolic complications and the presence of anti-phospholipid auto-antibodies (aPL's) in the blood. β2gpI has been indicated as a natural anticoagulant[106] and has a role in clearance of apoptotic bodies from the circulation[64,131,133]. β2gpI belongs to a super-family of proteins characterized by repeating stretches of ~60 amino-acid residues, each with a set of 16 conserved residues and two fully conserved disulfide bonds. More than 50 mammalian, mainly complement, proteins belong to this family including CR2, factor H and CR1, which contain up to 15, 20 and 30 of these consecutive repeating stretches, respectively[54]. These repeating units have been termed short consensus repeat (SCR), complement control protein or Sushi domains and are in many cases involved in protein-protein interactions, with typically two to four consecutive domains forming an interaction site[59,224-227]. NMR structures of two single SCR domains, domains 5 and 16 of human factor H (HFH)[55,56], and two SCR domains in tandem, domains 15-16 of HFH and domains 3-4 of Vaccinia virus complement control protein (VCP)[57,58], have been determined. Recently, the crystal structure of the N-terminal two SCR domains of CD46 has been published[59]. β2gpI consists of five of these SCR domains. The first four domains are regular SCR domains with respect to their amino-acid sequences. The fifth C-terminal domain contains a six-residue insertion and a 19-residue C-terminal extension, which is C-terminally cross-linked by an additional disulfide bond. This aberrant domain is responsible for adhesion to anionic phospholipids[34,73,76]. Adhesion to membranes is very likely an essential aspect of β2gpI, that is common to the observed effects of β2gpI in APS, coagulation and apoptosis.

The auto-immune disorder APS is characterized by the presence of a group of heterogeneous auto-antibodies in blood plasma and the occurrence of thrombo-embolic complications in both the arterial and venous vasculature of patients[112]. The symptoms appear predominantly in women at age 25-35. A particular problem in understanding the pathophysiology of aPL's has been the apparent contradiction between the *in vivo* observed thrombosis and the *in vitro* observed prolonged coagulation time[106]. An important observation has been that the real antigen for aPL's is the plasma-protein β2gpI[147] and not phospholipids[228]. The affinity of β2gpI for anionic phospholipids increases strongly in the presence of aPL's, which is explained by the formation of divalent (β2gpI)$_2$-aPL complexes[163]. Binding of these complexes to phospholipids interferes with binding of other phospholipid-binding proteins in plasma, such as coagulation proteins, resulting in the *in vitro* prolongation of coagulation[150]. *In vivo*, the (β2gpI)$_2$-aPL complexes possibly inhibit the anticoagulant activity of protein C at phospholipid surfaces, explaining the thrombo-embolic risk[229].

---

[a] Abbreviations used: Å, Angstrom, 10^{-10} m; aPL, anti-phospholipid auto-antibodies; APS, anti-phospholipid syndrome; β2gpI, β_2-glycoprotein I; GlcNAc, *N*-acetylglucosamine; HFH, human factor H; IEF, iso-electric focusing; MALDI TOF, matrix-assisted laser/desorption time-of-flight; Man, mannose; MIRAS, multiple isomorphous replacement method using anomalous scattering; r.m.s.d., root-mean-square deviation; SCR, short concensus repeat; SDS PAGE, sodium dodecyl polyacrylamide gel-electrophoresis; VCP, vaccinia virus complement control protein.

We have determined the crystal structure to 2.7 Å resolution of the glycosylated five-domain human β2gpI purified from blood plasma. The structure aids in characterization of the epitopes for the heterogeneous pool of aPL's and yields insights into the spatial arrangement and functional partitioning over the multiple consecutive SCR domains and the mechanism of binding to anionic phospholipids.

Structure determination

Crystals of β2gpI grew in the orthorhombic space group $C222_1$. Significant non-isomorphism was observed between crystals, as indicated by an R_{iso} of 20.9% between data sets Native I and II (Table I). Structure determination of β2gpI with the multiple-isomorphous replacement method using anomalous scattering (MIRAS) revealed one β2gpI molecule in the asymmetric unit with a remarkably high solvent content of 86% and a large V_m of 8.5 Å^3 Da^{-1} (Table II, Fig. 1). The initial map using Native I and derivatives I was of low quality due to poor phasing statistics (Table II) and was improved dramatically by solvent flattening using a solvent fraction of 70%. A first model was built at 3.75 Å resolution using the NMR structure of the 15th SCR domain of HFH[57]. Rigid-body refinement of this initial model against data set Native II yielded a decrease in R-factor from 52.6% to 48.0% and in free R-factor from 52.0% to 47.8%. Phase information to 2.7 Å resolution obtained at a later stage (derivative sets II) was used to validate and correct the model (Fig. 2). Refinement used the maximum-likelihood method and a bulk-solvent correction (see Materials & Methods). Electron density corresponding to residues Ser311-Lys317 is not visible in the final $2|F_o|-|F_c|$ map and, therefore, these residues have not been included in the final model. Seven carbohydrate residues are identified in the electron-density maps at the four N-glycosylation sites. The final structure is refined to 2.7 Å resolution with an R-factor of 24.9% and a free R-factor of 26.9%, and displays good stereochemistry (Table II). Coordinates and structure factors have been deposited with the Protein Data Bank (accession code 1QUB).

Table I
Crystal characteristics showing non-isomorphism

Crystal	Res. (Å)	m (°)[*]	a, b, c (Å)			$\Delta V/V$[§]	T[†]
Native I	29-3.75	1.0	161.53	163.73	114.99	0.0	120
Native II	40-2.7	1.0	161.17	166.49	114.51	+ 1.0	100
K_2OsO_4 (I)	39-3.0	0.6	160.95	161.33	114.65	- 2.1	100
Na_3IrCl_6 (I)	38-3.1	0.5	160.55	163.11	113.98	- 1.9	100
K_2PtCl_6 (I)	39-3.2	0.8	161.38	161.86	113.98	- 2.1	100
K_2OsO_4 (II)	40-2.7	0.4	160.86	166.26	115.35	+ 1.0	100
K_2PtCl_6 (II)	40-2.9	0.5	162.43	165.42	114.76	+ 1.0	100

[*] Mosaicity
[§] Native I is taken as a reference, cell-volume differences are given as a percentage and are mainly caused by changes in the *b*-axis
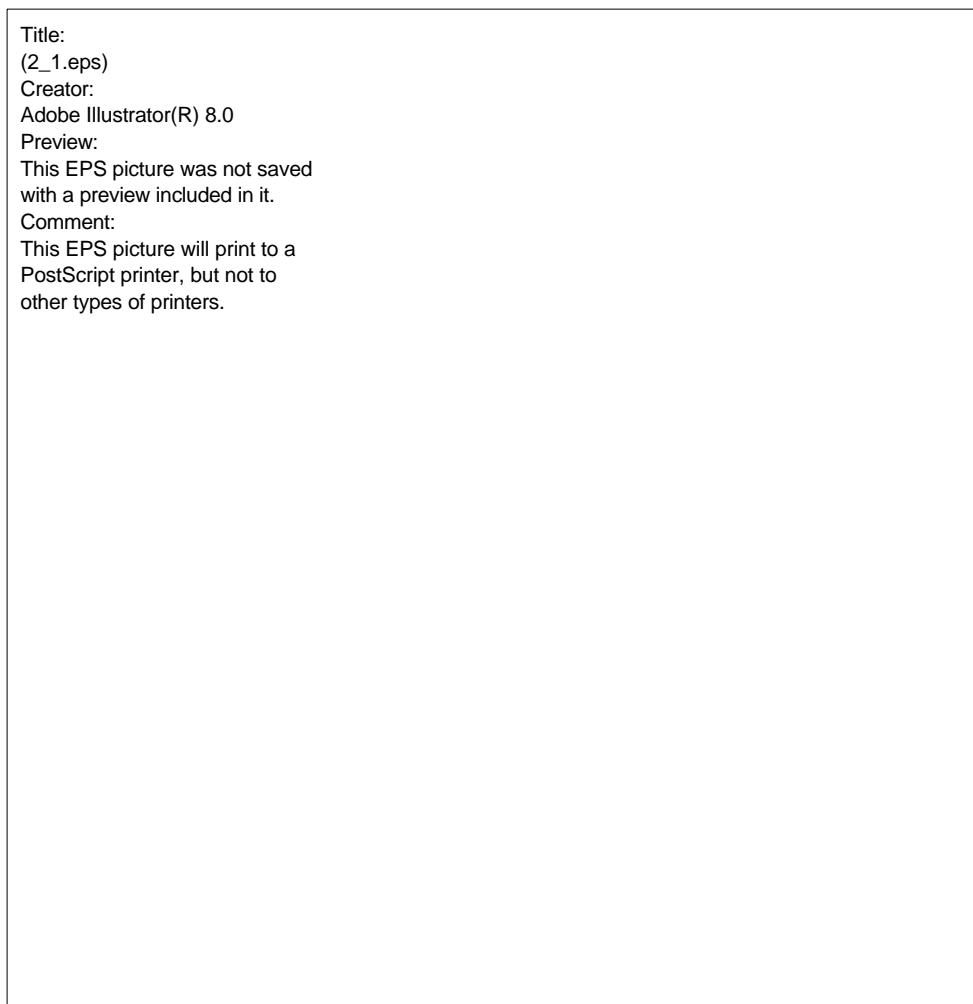[†] Temperature in K during data collection

Title:
(2_1.eps)
Creator:
Adobe Illustrator(R) 8.0
Preview:
This EPS picture was not saved
with a preview included in it.
Comment:
This EPS picture will print to a
PostScript printer, but not to
other types of printers.

Fig. 1. Structural representations of human blood-plasma β2gpI revealing the extended chain of the five SCR domains. (**A**) Ribbon drawing of β2gpI with consecutive domains labeled I to V. N-linked glycans as well as the position of the putative O-linked glycan, Thr130, are indicated by ball-and-stick model. β-Strands are shown in green and helices in red. (**B**) Topology diagram of β2gpI. The central β-sheets of all five domains are labeled B2(-B2'')-B3-B4(-B5), the N- and C-terminal β-sheets are labeled B1'-B2' and B4'-B5', the α-helix and the 3/10 helix are denoted A1 and A2 and numbers of residues delimiting secondary structure elements are given. Disulfide bonds are indicated with dashed lines. Positions of N-glycosylation are given by hexagons; a diamond indicates the putative O-glycan. Horizontal dashed lines mark domain boundaries. (**C**) Ribbon representation of domain III of β2gpI with labeled secondary structure elements. The two fully conserved disulfide bonds are shown in yellow. (**D**) Ribbon representation of domain V of β2gpI with labeled secondary structure elements. The three disulfide bonds are indicated in yellow. The aberrant face, that contains the membrane-binding site, is located on the right side.

```
Title:
(2_2.eps)
Creator:
Adobe Illustrator(R) 8.0
Preview:
This EPS picture was not saved
with a preview included in it.
Comment:
This EPS picture will print to a
PostScript printer, but not to
```

Fig. 2. Electron density map near Trp53 calculated with phases from the refined model. The $2|F_o|$-$|F_c|$ electron-density map at 2.7 Å resolution is contoured at 1 σ.

Structure description

The structure of β2gpI shows an extended chain of five SCR domains with an overall fish-hook like appearance with dimensions of 130 Å (vertical direction in Fig. 1A), 85 Å (horizontal) and 130 Å from the N- to the C-terminal extremity. The distance from the N- to the C-terminal end along the curve of the molecule is ~190 Å. The fish-hook shape is mostly flat, but slightly bent around domain III. The elongated structure contradicts a hypothetical model of Koike *et al.* (230), who describe the molecule as being folded into a compact particle.

Domains I to IV of β2gpI have common SCR folds (Fig. 1B). They consist of a central anti-parallel β-sheet, comprising strands B2-B3-B4, with two extended loops typically flanked by short two-stranded anti-parallel β-sheets, B1'-B2' and B4'-B5', at the N- and C-terminal side (Fig. 1C). Disulfide bridges located at opposite ends of a domain cross-link the short flanking β-sheets with the central β-sheet (B1' to B4 and B3 to B5'). Domain II has slightly deviating structural elements; its central sheet is extended by one more anti-parallel strand denoted B5 and residues at the position of strand B1'-B2' do not adopt a β-sheet conformation. These four domains of β2gpI have a sequence homology ranging from 24 to 45%[231] and superimpose within 1.2 to 1.9 Å root-mean-square (r.m.s.) coordinate difference (see Methods section). A similar range of homology, 21 to 41%, and a similar range of r.m.s. coordinate difference, 1.4 to 2.3 Å, is observed when comparing β2gpI I-IV with SCR domains available in the Protein Data Bank, HFH-15, 16 (Ref. 57) and VCP-3, 4 (Ref. 58). This indicates that the SCR fold is very well conserved. The largest differences with respect to amino-acid length and structure are observed in the B2-B2' loops, referred to as 'hyper-variable' by Barlow *et al.* (57).

The fifth C-terminal domain deviates significantly from the common SCR fold (Fig. 1D). Similar to the SCR fold it has the central anti-parallel β-sheet encompassing β-strands B2, B3 and B4 and the two disulfide bonds common to all SCR domains. In domain V strands B3 and B4 of the central sheet are extended and are part of a larger and strongly twisted anti-parallel β-sheet. Domain V has an insertion of six residues in the region of the hyper-variable loop. This region now forms an additional β-strand (B2"), that participates in the central β-sheet, followed by a short α-helix (A1). The C-terminal extension contains a short 3/10 helix (A2) and is C-terminally cross-linked by a third disulfide bond. Residues

22

311-317 of this extension are not visible in the electron-density map. This exposed loop is possibly mobile or disordered due to potential cleavage at Ala314-Phe315 or Lys317-Thr318 (Ref. 76, 80). In conclusion, domain V may be considered to consist of a core that is reminiscent of the consensus SCR fold with unique structural elements A1, A2 and B2" and the exposed loop 311-317 forming a completely new face of this domain in respect to other known SCR domains.

Table II
Structure-determination statistics

Diffraction-data statistics[1]

Crystal	Res. (Å)	Redundancy	No. unique refl.	$<I>/<\sigma(I)>$	Completeness (%)	R_{merge}^2 (%)
Native I	29-3.75	4.0	15447	5.2 (4.1)	97.8 (97.7)	14.7 (31.1)
Native II	40-2.7	3.8	42494	5.8 (2.0)	99.8 (99.6)	8.9 (36.3)
K_2OsO_4 (I)	39-3.0	3.3	30431	8.8 (2.6)	96.6 (88.4)	7.4 (28.9)
Na_3IrCl_6 (I)	38-3.1	3.7	23790	9.0 (4.4)	83.8 (77.3)	6.9 (20.0)
K_2PtCl_6 (I)	39-3.2	3.2	23516	8.2 (2.6)	93.6 (67.0)	7.8 (25.1)
K_2OsO_4 (II)	40-2.7	8.9	42498	9.7 (3.3)	100 (99.8)	7.4 (40.3)
K_2PtCl_6 (II)	40-2.9	10.4	34609	12.0 (5.4)	99.5 (97.4)	8.9 (33.1)

Phasing statistics

Derivative	R_{iso}^3	R_{ano}^4	No. sites	Phasing power[5] Cent.	Acent.	R_{cullis}^6	FOM[7]
K_2OsO_4 (I)	0.230	0.050	3	0.65	0.73	0.67	0.43
Na_3IrCl_6 (I)	0.130	0.031	2	0.26	0.35	0.81	0.43
K_2PtCl_6 (I)	0.181	0.047	1	0.40	0.40	0.79	0.43
K_2OsO_4 (II)	0.207	0.063	4	0.68	0.76	0.70	0.34
K_2PtCl_6 (II)	0.213	0.056	1	0.47	0.53	0.76	0.34

Refinement statistics

Resolution	40-2.7 Å
R-factor/R_{free}[8]	0.249 / 0.269
R.m.s.d. bond distances	0.019 Å
R.m.s.d. angles	1.92°
Average B-factor	49 Å²
No. non-hydrogen atoms	2,608
No. protein residues	319
No. sugar residues	7
No. solvent molecules	32

1 Numbers in parentheses indicate statistics for highest resolution shells.
2 $R_{merge} = \Sigma_h \Sigma_i |I_{hi} - <I_h>|/\Sigma_h \Sigma_i |I_{hi}|$
3 $R_{iso} = \Sigma |F_{ph}^2 - F_p^2| / |\Sigma(F_{ph}^2 + F_p^2)$
4 $R_{ano} = \Sigma |F_{(+)}^2 - F_{(-)}^2| / |\Sigma(F_{(+)}^2 + F_{(-)}^2)$
5 Phasing power is the r.m.s. value of the heavy-atom structure-factor amplitude divided by the r.m.s. residual lack-of-closure
6 R_{cullis} is the mean residual lack-of-closure error divided by the isomorphous difference
7 FOM , figure of merit
8 A 5% test set of reflections was used for calculation of the free R-factor

Oligosaccharide antennae

As indicated by Kristensen *et al.* (40), human β2gpI contains four N-glycosylation sites. The electron density shows seven carbohydrate residues at these four sites, *viz.* GlcNAc-(β1-N)-Asn143, GlcNAc-(β1-N)-Asn164, Man-(β1-4)-GlcNAc-(β1-4)-GlcNAc-(β1-N)-Asn174 and GlcNAc-(β1-4)-GlcNAc-(β1-N)-Asn234. Weak density at Thr130 indicates the position of an O-linked sugar[45], which is in agreement with the sequence context of glycosylated threonines[232]. Four glycans (at positions 130, 143, 164 and 174) are located on domain III and one (at 234) on domain IV. Three glycans are positioned in the inner-curve of the fish-hook, filling the niche formed by the molecule (Fig. 1A). The remaining two glycans are located on domain III at the outer-curve of the fish-hook. The five glycans point into large solvent channels present in the crystal. Crystal packing is dominated by interactions involving domains I, II and V. Very few crystal contacts involve domains III and IV (Fig. 3). Moreover, domains III and IV, which carry the glycans, appear to bridge between the contacts made by the N- and C-terminal domains I, II and V. The observed shielding of the domains III and IV may reflect an indirect functional role of the glycans.

Title:
(2_3.eps)
Creator:
Adobe Illustrator(R) 8.0
Preview:
This EPS picture was not saved
with a preview included in it.
Comment:
This EPS picture will print to a
PostScript printer, but not to
other types of printers.

Fig. 3. Crystal packing of β2gpI. Shown are C_α-traces of one molecule with its four neighboring molecules. Crystal contacts involve predominantly domains I, II and V. Contacts with glycosylated domains III and IV are restricted to the N-terminal bottom and C-terminal top of the domains III and IV, respectively. In the crystal the glycosylated domains bridge the crystal contacts made by the N- and C-terminal domains.

Inter-domain flexibility

The domains in β2gpI are connected by short linker regions of three (domains IV-V) and four residues (all others), *i.e.* counting the number of residues between the C-terminal cystine of the first domain and the N-terminal cystine of the second domain. Between domains II-III and III-IV these linking residues form β-strands that connect sheets B4'-B5' of the N-terminal domain with B1'-B2' of the C-terminal domain (Fig. 1A, B). The interactions observed at the interfaces are hydrophobic contacts and one hydrogen bond between domains I-II, II-III and III-IV and two hydrogen bonds between domains IV-V. Only a small amount (10 to 15%) of surface is buried at the inter-domain interfaces: 422, 242, 445 and 492 Å^2 for domains I-II up to IV-V, respectively.

The four inter-domain orientations observed in β2gpI display tilt angles φ varying from 128 to 160° and twist angles ψ varying from 41 to 137° (Table III, Fig. 4). Slightly different angles (up to 6° differences) are observed for the low-resolution data Native I, for which the *b*-axis is 2.8 Å shorter. The observed tilt angles φ in all known SCR domain-domain structures are obtuse and range from 120 to 162° (Table III). The range observed for the twist angle ψ is much larger, 22 to 180°, which indicates a large variability in precise domain-domain interactions. Electron microscopy for CR2 (Ref. 233) and HFH[234], that contain 15 and 20 SCR repeats, also shows elongated and winding structures. In these proteins up to eight residues link the separate domains yielding further flexibility. These electron microscopy, NMR and X-ray data suggest that multiple SCR repeats likely form elongated and rather flexible chains.

Title:
(2_4.eps)
Creator:
Adobe Illustrator(R) 8.0
Preview:
This EPS picture was not saved
with a preview included in it.
Comment:
This EPS picture will print to a
PostScript printer, but not to
other types of printers.

Fig. 4. Domain-domain orientations in β2gpI. (**A**) Stereo view of domain-domain orientations of the four sets of consecutive SCR domain pairs. The N-terminal domains of tandems II-III, III-IV and IV-V are superposed on domain I of tandem I-II. C-termini are indicated with the domain labels II to V. (**B**) The variation in domain orientations is expressed in a tilt angle φ and a twist angle ψ determined by the principal inertia axes *a* and *b* (See the Methods section and Table III).

Membrane binding

The fifth domain of β2gpI has been implicated in membrane binding[73]. In β2gpI we observe a large positively charged area of ~2,000 Å^2 on domain V (Fig. 5). This patch is formed by side chains of 12 lysines, one arginine and one histidine located at the outer-curve of the fish hook. It includes four lysines from the loop Cys281-Cys288 and lysines 308 and 324, that are important for phospholipid binding[34,73,76]. Other residues of this patch are Lys246, Lys250, Lys251, Arg260, Lys262, Lys266, Lys268 and His310. The flexible loop Ser311-Lys317, containing Trp316 that is essential for phospholipid binding[52], is located within this charged region (indicated in Fig. 5B).

The structural and biochemical data indicate a relatively simple membrane-binding mechanism. The positive charges on domain V interact with the anionic phospholipid headgroups and the flexible loop Ser311-Ser-Leu-Ala-Phe-Trp-Lys317 putatively inserts into the lipid layer and positions Trp316 at the interface region between acyl chains and phosphate headgroups of the lipids, thereby anchoring the protein molecule to the membrane (Fig. 5C). Furthermore, the combination of Trp, Phe or Tyr, followed by a Lys is of particular importance for the interaction with the interfacial region between the lipid phosphate group and the acyl chains of lipids[235-238]. Comparison of β2gpI sequences of bovine, canine, mouse, rat and human shows that the putative membrane-insertion loop Ser 311-Lys 317 is identical among these species and that substitutions with respect to a positively charged patch on domain V are conserved. Interestingly, all residues responsible for the unique function in membrane binding of domain V are located on the aberrant non-SCR like half of this domain.

Reduced affinity for anionic phospholipids, as observed for the two naturally occurring mutants Cys306Gly and Trp316Ser[52,53] and for two cleaved isoforms of β2gpI, with scissile bonds between residues 314-315 and 317-318 (Ref. 76, 80), can readily be explained by the proposed membrane-binding model. Both mutations and the two scissile bonds disrupt the integrity of the putative membrane-insertion loop 311-317. We think that *in vitro* observed binding properties to heparin of β2gpI with the single mutation Trp316Ser[53] and of two isoforms which are proteolytically cleaved between Lys317 and Thr318, and native β2gpI[32] show an aspecific behaviour of the protein, which is not affected by alterations or disruptions of the membrane-insertion loop and which is brought about solely by charge interactions. The loop Ser311-Ser-Leu-Ala-Phe-Trp-Lys317, then, gives β2gpI its specificity for phospholipid interfaces by introducing specific hydrophobic interactions between amino-acid residues and acyl chains of phospholipids, in addition to the large number of charge interactions.

Table III
Inter-domain orientations

	Tilt angle φ (°)	Twist angle ψ (°)
β2gpI[†] I-II	160, 162	137, 136
β2gpI II-III	160, 159	83, 78
β2gpI III-IV	128, 125	41, 46
β2gpI IV-V	131, 137	80, 76
HFH 15-16[‡]	130	130
CD46 1-2[§]	120	180
VCP 3-4[*]	121	22

† Two values are given: the first value is obtained from β2gpI in crystal form II (*cf.* Native II), the second value refers to β2gpI in form I (Native I).
‡ Reported standard deviations are 13° in φ and 17° in ψ[58]
§ Between the six copies of the molecule in the asymmetric unit a difference of 15° in φ is reported[59]
* Reported standard deviations are 4° in φ and 6° in ψ[58]

Binding of anti-phospholipid auto-antibodies

The group of auto-antibodies, aPL's, detected in blood plasma of patients with APS is both inter- and intra-individually heterogeneous. Indeed, the extended shape of β2gpI offers many

potential sites for antibody binding, particularly at the non-glycosylated domains I, II and V. So far aPL binding to domains I, III, IV and V and to the inter-domain region between I and II, has been reported[76,151-154]. Wang *et al.* (154) have identified two potential epitope sequences, Gly274-Phe280 and Ala314-Pro325. Based on the structure both sequences are unlikely to be epitopes of aPL's. Gly274-Phe80 forms the central β-strand B3 of domain V, which is largely inaccessible to the solvent (17% solvent accessibility). It is, thus, unlikely to be, either an epitope, or a cryptic epitope, without fully disrupting the fifth domain. The second peptide, Ala314-Pro325 contains part of the putative membrane-insertion loop Ser311-Lys317. Binding of aPL to these residues will directly interfere with, if not fully abolish, membrane binding of β2gpI. This analysis shows that the crystal structure of β2gpI is an important tool for the evaluation of potential epitopes. It will guide mutational studies of β2gpI and aid in characterization of antibodies related to APS.

Conclusions

The crystal structure of the intact and glycosylated adhesion protein β2gpI from human blood plasma reveals that the five consecutive SCR domains of β2gpI form an elongated chain yielding an overall fish-hook shape of the molecule. Multiple consecutively arranged domains are common in adhesion molecules. However, very few structures of these repetitive domains have been resolved (see e.g. Ref. 239-241), let alone of complete adhesion molecules. The structure of complete β2gpI shows that the first four domains display regular SCR folds, that are common to many mammalian complement proteins. The fifth domain has an aberrant fold. Constructed onto a SCR-like core, a six-residue insertion and 19-residue C-terminal extension together with some rearrangement of existing elements create a completely new face on this domain. Strikingly, the structural and biochemical data strongly suggest that this new face of domain V is fully responsible for membrane binding of β2gpI. The proposed mechanism of membrane binding consists of two major aspects: *i.* a large positive patch of 14 charges binds to the anionic surface, and *ii.* a flexible and partly hydrophobic loop inserts into the lipid layer and positions a Trp and a Lys at the interfacial region, thereby providing specificity for negatively charged phospholipid layers. Membrane adhesion of β2gpI very likely underlies the diverse effects of this protein in blood coagulation, apoptosis and the APS immune disorder, in which auto-antibodies enhance membrane affinity by divalent cross-linking of β2gpI. The observed crystal structure even bears relevance for how β2gpI domains are positioned, when the molecule is membrane bound. It implies that association of the binding site, located at the top and outer curve of the fish hook of β2gpI, with a membrane layer results into pointing domain IV to I far into the solution. Similar to what is observed in the crystal, the glycosylated domains III and IV are partly shielded from protein-protein interactions by the glycans and may, therefore, possibly be regarded as linker or 'bridging' domains. The N-terminal domains are exposed most to the solution and most likely provide binding sites in e.g. apoptosis. Thus, the crystal structure of the complete and glycosylated adhesion molecule β2gpI suggests a functional partitioning over its three-dimensional structure, that is probably a general phenomenon for many elongated multi-domain adhesion molecules, as is already observed for e.g. factor H[225] and C4BP[227].

Title:
(2_5.eps)
Creator:
Adobe Illustrator(R) 8.0
Preview:
This EPS picture was not saved
with a preview included in it.
Comment:
This EPS picture will print to a
PostScript printer, but not to
other types of printers.

Fig. 5. Binding of β2gpI to an anionic phospholipid surface. (**A**) Two views, related by 180° rotation, of the electrostatic surface potential of β2gpI. Domains are labeled I to V. The electrostatic potential is scaled from red for negative charge to blue for positive charge. (**B**) Positively charged patch on the aberrant half of domain V. The 14 residues contributing to this patch and the position of the disordered loop Ser311-Lys317 are indicated. (**C**) Cartoon of the proposed model for binding of β2gpI to anionic phospholipids. The positively charged patch on the surface of domain V is indicated with '+', acidic phospholipids are depicted with '-' and the putative membrane-insertion loop Ser311-Ser-Leu-Ala-Phe-Trp-Lys317 is shown to insert into the phospholipid layer. Positions of N-glycans are indicated with hexagons and the putative site for O-linked glycosylation is indicated with a diamond.

Materials and Methods

Protein purification

β2gpI was isolated from freshly-frozen citrated human plasma of three healthy donors (Dutch Blood Bank) as described before[242]. Purified β2gpI appeared as a single band of 42 kDa on an SDS-PAGE gel under non-reducing conditions and as at least seven bands between pH 5.3 and 6.8 on a silver-stained Pharmacia PhastGel IEF 3-9. MALDI-TOF mass-spectrometry analysis revealed a protein mass of 45 ± 2 kDa (calculated mass 36.3 kDa), indicative for heterogeneity of the carbohydrate content and the presence of approximately 40 to 60 carbohydrate residues.

Crystallization, heavy-atom derivatives and data collection

Crystallization trials using the hanging-drop vapor diffusion method at 4°C were performed with β2gpI concentrated to 6.5 mg ml^{-1} in 150 mM NaCl, 50 mM Tris-HCl pH 7.3. Crystallization conditions were essentially as described[243]. Reservoir solutions contained, either 1.5 M $(NH_4)_2SO_4$, 2% v/v glycerol, 20 mM $CdCl_2$ and 0.1 M HEPES pH 7.5 (Native II), or 1.5 M $(NH_4)_2HPO_4$ and 0.1 M Na-acetate pH 5.6 (Native I). Large (0.4x0.4x0.3 mm^3) crystals with irregular shape grew within 10 days in set-ups of 1 μl protein solution and 1 μl reservoir solution. Crystals obtained with both conditions were in the orthorhombic space group C222$_1$ and were used for further experiments (Table I). Heavy-atom derivatives were prepared by soaking crystals for four days in solutions containing, either 3 mM K_2OsO_4, or Na_3IrCl_6, or K_2PtCl_6. Crystals were flash-frozen in a liquid nitrogen stream after

equilibration in solutions with 43% v/v (Native I) or 30-35% v/v glycerol. X-ray data were collected using a Mar345 imaging plate (Hamburg, EMBL outstation at the DESY synchrotron, beamline BW7B for data sets K_2OsO_4 (I), Na_3IrCl_6 (I) and K_2PtCl_6 (I)), a MacScience DIP2020 imaging plate mounted on a Nonius FR-571 rotating anode (for Native I) and an ADSC 2x2 CCD camera (Grenoble, EMBL outstation at the ESRF synchrotron, beamline ID14-EH4, for Native II, K_2OsO_4 (II) and K_2PtCl_6 (II)). Data collection was aided by use of STRATEGY[244] and data were processed and scaled using, either DENZO and SCALEPACK[26], or the CCP4 Program Suite[245]. Unit-cell dimensions are given in Table I. Differences in cell volumes of up to 3.1% were mainly caused by differences in the length of the *b*-axis.

Structure determination

Three heavy-atom derivatives were used for phasing by the MIRAS method (Table II). Heavy-atom positions were located and refined and a set of phases was calculated with SOLVE[10] using data sets Native I, K_2OsO_4 (I), Na_3IrCl_6 (I) and K_2PtCl_6 (I). We could determine the presence of one β2gpI molecule in the asymmetric unit in the first electron density map phased at 3.75 Å resolution. Phases were improved by solvent flattening with a solvent fraction of 70% using the program suite CNS[9]. The NMR structure of SCR domain 15 of HFH[57] was used for global positioning of the five SCR domains of β2gpI. A first model was constructed consisting of all 326 residues with 102 residues replaced by Ala. At a later stage phase information to 2.7 Å resolution was obtained from K_2OsO_4 (II) and K_2PtCl_6 (II) using Native II (Table II). The model was validated and adjusted to the new map. The initial model was for the most part correct with respect to domains I to IV and contained chain-trace errors in domain V. Refinement was started with this adjusted model consisting of residues 1-131, 139-203, 210-282, 287-298 and 300-326.

Structure refinement

The model was refined against the Native II data set at 2.7 Å resolution. Cycles of rebuilding using O[16] and positional- and B-factor refinement using model phases, using CNS, were performed until convergence. Cross validation was used throughout the refinement. Refinement used the Maximum Likelihood algorithm[29] and bulk solvent correction was applied as calculated by CNS. No electron density was visible for the loop Ser311-Lys317 in the final $2|F_o|-|F_c|$ electron-density map, although some density indicated its position in the maps calculated with MIRAS phases at 2.7 and 3.75 Å resolution. This ill-defined solvent-exposed region could not be modeled satisfactorily. In the vicinity of the four N-glycosylation sites, electron density was seen accounting for a total of seven carbohydrate residues, *viz.* GlcNAc-(β1-N)-Asn143, GlcNAc-(β1-N)-Asn164, Man-(β1-4)-GlcNAc-(β1-4)-GlcNAc-(β1-N)-Asn174 and GlcNAc-(β1-4)-GlcNAc-(β1-N)-Asn234, which are included in the model. No electron density accounting for fucose units, linked to GlcNac-Asn, was seen. The mobility of the oligosaccharide antennae is reflected by high B-factors of the carbohydrate units, ranging from 50 to 99 Å^2. Between Thr130 and Gly1 of a symmetry related molecule electron density was seen, which can possibly be ascribed to an O-linked oligosaccharide antenna attached to Thr130 (Ref. 45, 232). Additional electron density, that may be accounted for by cadmium ions, is observed near His172, His216 and near Glu309. Near Tyr207's hydroxyl group additional weak density is present which might be indicative for partial sulfatation. Side-chain positions of residues Arg2, Arg39, Lys59, Lys110, Arg135, Gln158, Lys177, Lys208, Lys251, Lys284, Glu285, Lys286, Lys287, Lys308 and Glu309 are

29

poorly defined. The average B-factors for the main-chain atoms (C_α, C, O, N) of the domains (labeled I to V) are 41.6 $Å^2$ (I), 38.1 $Å^2$ (II), 52.7 $Å^2$ (III), 53.8 $Å^2$ (IV) and 57.9 $Å^2$ (V) with an average B-factor for all domains of 46.9 $Å^2$. For all non-hydrogen protein atoms (*i.e.* excluding glycans) the B-factors are 42.1 $Å^2$ (I), 39.3 $Å^2$ (II), 53.8 $Å^2$ (III), 54.8 $Å^2$ (IV) and 59.2 $Å^2$ (V), with an average B-factor for all domains of 48.0 $Å^2$. The final model comprises β2gpI residues Gly1-His310, residues Thr318-Cys326, one mannose and six *N*-acetylglucosamine carbohydrate residues, which accounts for ~80% of the total mass of a β2gpI molecule, and 32 ordered water molecules.

Crystal structure analysis
Superpositions of SCR domains are calculated in O using first cystine residues only, followed by superpositioning of C_α positions of spatially related residues (distance cut-off 3.8 Å). Root-mean-square coordinate differences of 1.2 to 2.3 Å are observed for superimposing 39 to 59 residues of β2gpI domains I to IV, HFH domains 15, 16 and VCP domains 3, 4. Domain-domain orientations of β2gpI were calculated using 27 C_α-atoms from each domain, which superimposed with r.m.s. coordinate differences of 1.17 to 1.50 Å , as calculated with O. All domains were translated to one origin and for each domain inertia tensors were calculated and diagonalized. One domain was rotated with respect to its preceding domain in such a way that their eigenvectors with the smallest eigenvalues, *i.e.* the main axis of the domains (labeled *a* and *a'* in Fig. 4B), were aligned (tilt angle φ). Next, a second rotation (twist angle ψ) was performed to align the eigenvectors (labeled *b* and *b'* in Fig. 4B) with the second-smallest eigenvalues. Definition of the tilt angle φ and of the twist angle ψ is according to Bork *et al.* (54). Molecular surfaces and electrostatic potentials were calculated with GRASP[246]. The model quality was checked with WHATIF[17] and PROCHECK[18]. The Ramachandran plot for the final model comprising 319 amino-acid residues, shows that 87.4% of these residues fall in the most favored region with no residues in disallowed regions. Domain-domain contacts were calculated with LIGPLOT[247]. Fig. 1A, C, D and 4A were generated using MOLSCRIPT[202] and RASTER3D[203].

Acknowledgements

--- Chapter III ---

Interaction of human β₂-glycoprotein I with proteins related to coagulation and renal excretion

Summary

Human β_2-glycoprotein I (β2gpI) is a plasma protein that has been implicated in blood coagulation, clearance of apoptotic bodies from the circulation, and in the auto-immune disease anti-phospholipid syndrome. β2gpI binds to megalin, an endocytic receptor that transfers renal-filtered β2gpI back into the circulation, to activated protein C, protein S and C4B binding protein, that function in anticoagulant processes, to the cellular protein calmodulin and to auto-antibodies in patients with the anti-phospholipid syndrome *in vitro,* when β2gpI or its protein ligand is immobilized on a suitable surface. In the present study we focussed on β2gpI-protein complex formation in solution using gel-filtration chromatography. β2gpI formed a stable complex in solution with the lupus anticoagulant-positive IgG 22F6. This indicates that adhesion to membranes is not in all cases a prerequisite for formation of β2gpI-auto-antibody complexes. β2gpI did not form complexes in solution with activated protein C and protein S. High-affinity binding of a small fraction of β2gpI to C4B binding protein could not be excluded based on our experiments. Even in the presence of β2gpI protein S-C4B binding protein complex was very stable. Therefore, no further evidence was revealed that supports an anticoagulant function of β2gpI by maintaining the level of free protein S. Our binding experiments did not establish previously reported high-affinity complex formation between β2gpI and calmodulin. Stable complexes putatively only form *in vivo* when β2gpI is bound to a lipid surface. Binding of extreme negatively charged calmodulin to the positively charged membrane-adhesion site of β2gpI may, then, block β2gpI-lipid interaction. This may be a prerequisite for the translocation of renal excreted β2gpI back into the circulation by the transporter megalin.

Keywords: activated protein C, anti-beta2 glycoprotein I antibody, beta2 glycoprotein I, C4B binding protein, calmodulin, coagulation, gel-filtration chromatography, lupus anticoagulant, protein-protein complex, protein S, renal excretion

Introduction

Human β_2-glycoprotein I (β2gpI)[a] is a heavily-glycosylated plasma protein that is present in a concentration of ~150 to 300 μg ml^{-1} (~3.3-6.6 μM), of which about 4% is bound to lipoproteins[62]. β2gpI is an important antigen in the auto-immune disease anti-phospholipid syndrome (APS), defined by recurrent fetal loss, occurrence of thrombo-embolic complications in both the arterial and venous vasculature and the presence of anti-phospholipid auto-antibodies (aPL's, lupus anticoagulants, LA's) in the blood, of which a subset is directed against β2gpI[147,148]. β2gpI has been indicated as an anticoagulant[84,85,106,121], as well as a procoagulant[248,249]. β2gpI may have a role in clearance of apoptotic bodies from the circulation[64,131,133]. Recently, we elucidated the crystal structure of human β2gpI purified from blood plasma[250], which has been confirmed by Schwarzenbacher *et al.* (251) at a later stage. Based on the crystal structure and available biochemical data, we proposed a membrane-adhesion model for β2gpI in which the fifth C-terminal short concensus repeat (SCR) domain binds specifically to anionic phospholipids. Spatial arrangement of the five SCR domains of β2gpI suggested that adhesion of the fifth domain to phospholipids points the four N-terminal domains away from the lipid surface. These four fully exposed N-terminal SCR domains may then be available for protein-protein interactions.

The membrane-adhesion mechanism and lipid specificity of β2gpI have been extensively investigated[34,52,73,76-79]. In contrast, little is known about protein ligands that may form functional complexes with β2gpI in apoptosis or coagulation, and about the mechanism that triggers formation of auto-antibodies that are elicited against β2gpI[112,116,252].

The affinity of β2gpI for anionic phospholipids increases strongly in the presence of aPL's and LA's. These aPL's and LA's have varying affinity for β2gpI and epitopes are identified in all five SCR domains of β2gpI[76,151-154]. The increased affinity is explained by formation of divalent (β2gpI)$_2$-auto-antibody complexes[163,253]. Adhesion of these complexes to phospholipid layers inhibits the protein C-dependent anticoagulant cascade[248,249,254]. This may explain the observed thrombo-embolic complications in patients with APS[229].

In vitro binding studies with immobilized proteins suggested that β2gpI interacts with protein S[83-85], a positive cofactor in the protein C-dependent anticoagulant pathway[86-89]. Complement-regulator C4B binding protein (C4Bbp) inhibits the stimulatory anticoagulant activity of protein S by formation of C4Bbp-protein S complexes. Formation of β2gpI-protein S complexes has shown to prevent formation of C4Bbp-protein S complexes, and, thereby, may keep at least part of the protein S pool available for its anticoagulant function. In addition to binding of β2gpI to protein S, Sim and Devine (85) reported binding of β2gpI to activated protein C (APC) and to C4Bbp. Observed modulation of β2gpI-APC and β2gpI-C4Bbp complex formation by protein S suggested a complicated allosterically controlled role for β2gpI in the APC-dependent anticoagulant pathway. Binding of β2gpI to protein S has been confirmed with an enzyme-linked immuno-sorbent assay (ELISA) set-up, whereas binding of β2gpI to APC or to C4Bbp was not established (M. Simmelink, unpublished results).

---

[a] Abbreviations used: APC, activated protein C; aPL, anti-phospholipid auto-antibody; APS, anti-phospholipid syndrome; β2gpI, β_2-glycoprotein I; CaM, calmodulin; C4Bbp, C4B binding protein; ELISA, enzyme-linked immuno-sorbent assay; IgG, immunoglobulin G; LA, lupus anticoagulant; MW, molecular weight; PDB, Protein Data Bank; SCR, short concensus repeat; TBS, Tris-buffered saline, 50 mM Tris-HCl pH 7.5, 150 mM NaCl; V_e, elution volume.

Klaerke *et al.* (90) and Rojkjaer *et al.* (91) reported very high-affinity complexes between renal-filtered β2gpI and calmodulin (CaM). In contrast, low-affinity β2gpI-CaM complex was observed in an ELISA set-up (M. Simmelink, unpublished results). CaM is a ubiquitous intracellular protein that is found in all tissues and that plays a major role in the Ca^{2+}-dependent regulation of a multitude of enzymes and in a wide variety of cellular events[92]. Renal filtered β2gpI also binds to the endocytic receptor megalin, which actively transfers β2gpI from kidney cells back into the circulation[93]. Megalin is a large multi-domain trans-membrane receptor of approx. 600 kDa. It is a member of the low-density lipoprotein receptor family and was first identified as the antigen in the renal auto-immune disease Heymann nephritis[255]. Megalin is a receptor for plasminogen and its activated form plasmin[256,257], of which the latter partly inactivates lipid-binding ability of β2gpI by cleaving it at Lys317-Thr318 *in vitro*[32]. Furthermore, megalin adheres to and facilitates cellular uptake of lipoprotein(a) and low-density lipoproteins[255,258], which are also known ligands for β2gpI[61,65,94].

In the present study, we focussed on interaction of β2gpI with proteins that function in coagulation, APS and putatively renal filtering, *i.e.* protein S, activated protein C, C4B binding protein, LA-active IgG 22F6 and calmodulin. Previously, several binding studies were performed in which, either β2gpI, or its putative protein ligand was immobilized on a solid surface. Addressing physiological relevance of observed β2gpI-protein interactions needs consideration of experimental shortcomings that may result in artificial binding properties. Firstly, it has previously been shown that absorption and immobilization of proteins at a solid surface, as in an ELISA set-up, can induce denaturation and conformational changes[260,261]. Absorption-induced exposure of artificial epitopes may, therefore, result in non-physiological properties of the protein. Secondly, when one of the proteins in a complex is immobilized on a solid surface, its effective concentration is enormously enhanced. As a result, very low-affinity complexes can form that have no functional relevance *in vivo*. Thirdly, Tsutsumi *et al.* (141) demonstrated that binding properties of β2gpI from separate purifications can vary among different ELISA set-ups. Furthermore, for formation of β2gpI-protein S complexes Merrill *et al.* (84) used β2gpI that was purified from perchloric acid-treated plasma. This method introduces alterations in the physical properties of the protein[262] and may, therefore, give rise to new non-physiological activities of β2gpI, due to conformational changes or chemical modifications. To gain further insight into previously reported β2gpI-protein complex formations, we chose an experimental set-up for direct detection of protein-protein interactions in solution, *i.e.* gel-filtration chromatography. Based on our results and previous reports we discuss a role for β2gpI-CaM complexes in renal re-absorption by megalin, and for β2gpI-C4Bbp complexes with respect to anticoagulant activity of β2gpI.

Methods

Protein solutions

β2gpI was purified from pooled plasma of three healthy human donors (designated 'Pool A') (Dutch Blood Bank, Utrecht, the Netherlands) according to Horbach et al. (232). Characterization of native β2gpI revealed that it was contaminated with a small amount of an isoform of β2gpI, referred to as 'β2gpI *1' (Ref. 32; *Chapter IV*). β2gpI *1 is cleaved at position Lys317-Thr318 and lost its ability to adhere to anionic membranes. β2gpI *1 was

purified from a separate pool of blood plasma from three healthy human donors, which is referred to as 'Pool B', and was a kind gift of D. Horbach (Haemostasis and Thrombosis Laboratory, University Medical Center Utrecht). Purified β2gpI was stored in Tris-buffered saline (TBS). Lyophilized CaM was purchased from Pharmacia Biotech (Uppsala, Sweden). CaM was either dissolved in TBS, or in TBS with 10 mM $CaCl_2$, and subsequently incubated for 60 min. at room temperature, before use. Murine monoclonal IgG 22F6, that expresses LA-activity, was obtained from J. Arnout (Center for Molecular and Vascular Biology, University of Leuven, Belgium)[164,253]. 22F6 was supplied in TBS and tended to aggregate severely. Incubating 22F6 for one week in a solution of 50 mM Tris-HCl pH 7.5, 30 mM NaCl successfully dissolved these aggregates, according to analysis by sodiumdodecyl-sulphate polyacrylamide gel electrophoresis and by gel-filtration chromatography. APC, protein S and C4Bbp were a kind gift of R. van der Poel (Haemostasis and Thrombosis Laboratory, University Medical Center Utrecht). Protein-stock solutions used for binding experiments are listed in Table I.

Table I
Protein-stock solutions used for complex formation in solution

Protein	MW (kDa)	c (μM)	c (mg ml⁻¹)	c_{plasma} (μM)[‡]	V_e (ml)[†]
native β2gpI	45	287	12.9	3.3-6.6	13.6
β2gpI *1	45	400	18.0	2E-3	13.6
IgG 22F6	160	81.0	13.0	n.d.	12.6
CaM	17	772	12.9	0.018	15.4
protein S	71	13.4	1.0	0.35	12.3
APC	58	3.5	0.20	0.017	14.1
C4Bbp	570	10.0	5.7	0.30	8.0

‡ n.d. not determined; For β2gpI *1 the concentration is given in plasma of healthy individuals. For CaM the concentration in kidney is given.
† Elution volumes V_e of the free proteins after gel filtration on a Superdex 200 HR 10/30 column.

Complex formation in solution

Before qualitative analysis of β2gpI-protein complexes in solution, proteins were pre-incubated for an indicated period of time to allow for complex formation. To this end, β2gpI solutions were mixed with solutions of one of the various proteins (Table II). Complex formations were initiated by a 10 min. incubation at 37°C or by a 60 min. incubation at room temperature.

Immunoglobulin G 22F6
22F6 tended to aggregate in the presence of over 30 mM of NaCl. Complex formation between β2gpI and 22F6 was, therefore, induced in buffer 1 containing 30 mM NaCl (Table II, Exp. 1). To approximate physiological conditions β2gpI and 22F6 were also mixed in TBS (Exp. 2). In both experiments, a four-fold molar excess of β2gpI was used.

Calmodulin
Incubation of β2gpI with CaM was without the presence of Ca^{2+} (Table II, Exp. 3), or in the presence of 10 mM $CaCl_2$ (Exp. 4-9). To study whether CaM has different affinity towards β2gpI (poll A) and β2gpI *1 (pool B) we mixed CaM with β2gpI or with β2gpI *1 in a molar ratio of 2.7:1. Furthermore, the influence of NaCl concentration on complex formation between β2gpI and CaM was tested using buffers containing 15 or 150 mM NaCl (Exp. 4-,

5). Complex formation was both initiated in the presence of a molar excess of CaM (Exp. 3-7,9) or of β2gpI (Exp. 8).

Activated protein C, protein S and C4B binding protein

Previous studies showed the importance of Ca^{2+} in complex formation between β2gpI and protein S, APC or C4Bbp[83-85]. Therefore, we performed all incubations in the presence of 10 mM $CaCl_2$. β2gpI was incubated with protein S in a ten-fold (Exp. 10, 12) or in a two-fold molar excess (Exp. 11). For incubations with APC or C4Bbp a seven-fold (Exp. 13-14) and fifteen-fold molar excess of β2gpI (Exp. 15) was used, respectively. For complex formation of β2gpI with protein S or with C4Bbp, the molar ratio of β2gpI and protein S or C4Bbp resembles physiological conditions, *i.e.* 10:1 (Table I). A preliminary competitive binding study was performed to test the ability of β2gpI to disrupt previously formed protein S-C4Bbp complex (Exp. 16). Protein S and C4Bbp were pre-incubated for 10 min. before subsequent 10-min. incubation with β2gpI. Both incubations were at 37°C. Molar ratios of 1:1:1.4 for protein S, C4Bbp and β2gpI were used, respectively. As a positive control for the method of complex formation protein S was incubated with C4Bbp (Exp. 17). *In vivo* protein S binds to APC that is immobilized at a phospholipid surface. Whether protein S can bind to APC when both proteins are in solution was studied by incubation of a four-times molar excess of protein S with APC (Exp. 18).

Table II
Experimental set-up for formation of protein-protein complexes

Exp.	β2gpI[‡] (μM)	Protein 1	Conc.[‡] (μM)	Protein 2	Conc.[‡] (μM)	Incubation Temp. (°C)	Time[¶] (min.)	Buffer[†]
1	178	22F6	50	-		25	60	1
2	144	22F6	29	-		25	60	2
3	72	CaM	193	-		37	10	2
4	72	CaM	193	-		37	10	3
5	72	CaM	193	-		37	10	4
6	6.5	CaM	386	-		37	10	3
7	41	CaM	276	-		37	10	4
8	115	CaM	77	-		37	10	4
9	72	CaM	193	-		25	60	5
10	48	protein S	4.7	-		37	10	4
11	13	protein S	6.4	-		37	10	4
12	48	protein S	4.4	-		25	60	6
13	12	APC	1.6	-		37	10	4
14	12	APC	1.6	-		25	60	6
15	48	C4Bbp	3.3	-		37	10	4
16	3.2	protein S	2.4	C4Bbp	2.2	37	10/10	4
17	-	protein S	1.4	C4Bbp	4.0	37	10	4
18	-	protein S	3.5	APC	0.86	37	10	4

‡ Protein concentrations during complex formation.

¶ For Exp. 16 protein S was first incubated with C4Bbp for 10 min., followed by a 10 min. incubation with β2gpI.

† Buffers used for incubations and subsequent gel-filtration chromatography. Buffer 1, 50 mM Tris-HCl pH 7.5, 30 mM NaCl; Buffer 2, TBS; Buffer 3, 5 mM Tris-HCl pH 7.5, 15 mM NaCl, 10 mM $CaCl_2$; Buffer 4, TBS, 10 mM $CaCl_2$; Buffer 5, 15 mM Tris-HCl pH 7.5, 125 mM NaCl, 10 mM $CaCl_2$, 200 nM CaM; Buffer 6, TBS, 10 mM $CaCl_2$, 100 nM β2gpI.

Gel-filtration chromatography

Molecular-weight analyses of free proteins and qualitative analyses of protein-protein complexes by means of gel-filtration chromatography was performed with a Superdex 200 HR 10/30 column (volume 24.0 ml, void volume 7.6 ml) (Pharmacia Biotech, Uppsala, Sweden). Protein solutions were applied to the column using a 200-µl loop. All runs were performed with a flow of 1 ml min^{-1} and a recorder speed of 0.5 cm ml^{-1}. Elution of free proteins and complexes was monitored with absorption measurements at 280 nm. Runs were performed with free β2gpI (pool A), free β2gpI *1 (pool B), 22F6, CaM, protein S, APC and C4Bbp, for comparison with elution volumes V_e of complexes. After applying to the gel-filtration column low-affinity complexes will possibly rapidly dissociate due to dilution of complex and due to separation of protein-protein complexes from the free proteins,. As a consequence these low-affinity complexes, which may be initially present in the applied solution, can not be detected. Therefore, for detection of low-affinity complexes, gel-filtration experiments were performed with elution buffers that contained an excess of one of the proteins. To prevent dissociation of β2gpI-CaM complexes, 200 nM CaM was present in elution buffer 5 (Table II, Exp. 9). Binding of CaM to β2gpI *1 was also tested with elution buffer 5. To prevent dissociation of complexes of β2gpI with protein S or with APC, 100 nM β2gpI was present in buffer 6 (Exp. 12, 14). Concentrations of CaM and β2gpI in the elution buffers were based on their approximate concentrations on the Superdex 200 column during a gel-filtration run.

Table III
Qualitative analyses of protein-protein interactions

| Exp. | Peak 1[§] | | Peak 2 | |
	V_e	protein	V_e	protein
1	12.6	22F6	13.6	β2gpI
2	10.2	complex[¶]	13.6	β2gpI
3	13.6	β2gpI	15.4	CaM
4	13.6	β2gpI	15.4	CaM
5	13.6	β2gpI	15.4	CaM
6	13.6	β2gpI	15.4	CaM
7	13.6	β2gpI	15.4	CaM
8	13.6	β2gpI	15.4	CaM
9	13.6	β2gpI	15.4	CaM
10	12.4	protein S	13.4	β2gpI
11	12.4	protein S	13.4	β2gpI
12	12.8	protein S	13.5	β2gpI
13	13.4	β2gpI	13.4[†]	APC
14	13.6	β2gpI	13.6[†]	APC
15	8.0	C4Bbp	13.4	β2gpI
16	8.1	complex[‡]	13.4	β2gpI
17	8.1	complex[‡]	-	
18	12.5	protein S	14.0	APC

§ The elution volume V_e (in ml) of the peak and the protein that has been assigned to the peak are listed.

¶ Complex between β2gpI and 22F6.

† The V_e's of free β2gpI and free APC are similar and, therefore, these proteins are hardly separated on the column, resulting in a broadened peak that contains both proteins.

‡ Complex between protein S and C4Bbp.

Results

Analysis of complexes in solution

In Table I elution volumes V_e of free proteins that are used for complex formation are listed. β2gpI elutes at 13.6 ml, indicating an apparent molecular weight (MW) of approximately 60 kDa. Mass spectrometry with β2gpI revealed a MW of 45 kDa[250]. Elution of β2gpI as a protein with a higher MW is likely due to the elongated non-globular shape of the molecule[250]. C4Bbp elutes at 8.0 ml, in agreement with its MW of 570 kDa (maximum MW for fractionation on the column used is 600 kDa). Binding characteristics of β2gpI towards 22F6, CaM, protein S, APC, C4Bbp, or a mixture of protein S and C4Bbp, as observed after molecular-weight analyses with gel-filtration chromatography, are summarized in Table III and Fig. 1-3.
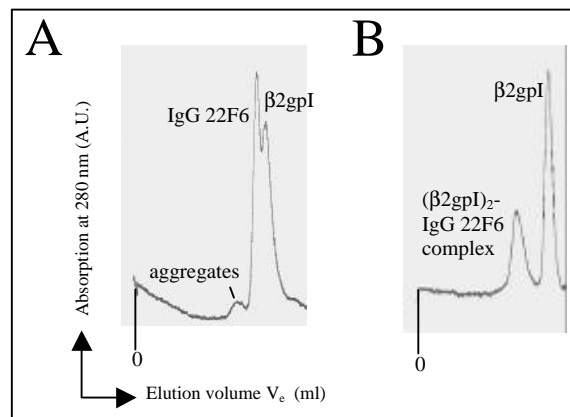
Fig. 1. Gel-filtration of β2gpI-22F6 complex. (**A**) In the presence of 30 mM NaCl 22F6 does not bind to β2gpI (Exp. 1). The peak at a V_e of 7.8 ml is assigned to aggregates of 22F6. (**B**) At 150 mM NaCl a stable complex between β2gpI and 22F6 is formed, whereas no 22F6 aggregates are present (Exp. 2).

Fig. 2. β2gpI-CaM complex is not detected with gel-filtration chromatography. Low-affinity complexes between β2gpI and CaM were not formed when CaM was continuously present at a concentration of 200 nM during gel filtration (Exp. 9). The small peak at a V_e of 7.8 ml is ascribed to β2gpI and/or CaM aggregates.

Immunoglobulin G 22F6

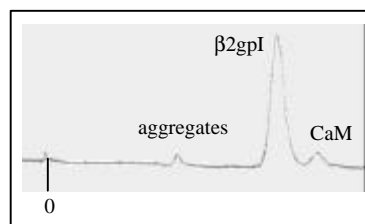β2gpI did not bind to 22F6 in the presence of 30 mM NaCl (Fig. 1A). A peak at a V_e of 7.8 ml indicated that again part of 22F6 was aggregated. At a physiological concentration of 150 mM NaCl the β2gpI-22F6 complex was formed and no aggregates were observed (Fig. 1B). The elution volume of 10.2 ml of the β2gpI-22F6 complex corresponds to a molecular weight of approximately 300 kDa, indicative for a 2:1 stoichiometry.
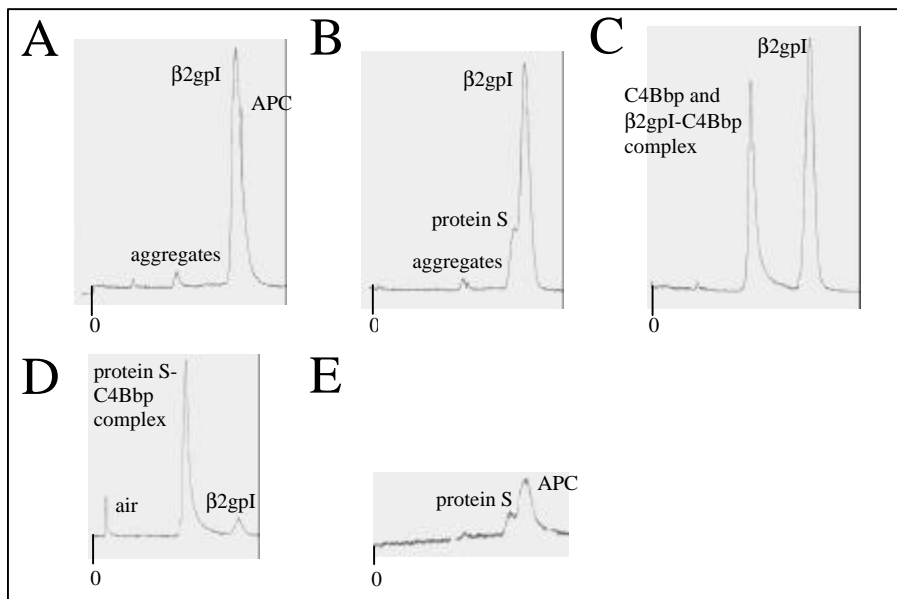

Fig. 3. Interactions of β2gpI and proteins that function in the APC-dependent anticoagulant cascade. In *A*, *B* and *E* small peaks at a V_e of 7.8 ml are present that likely originate from aggregated protein(s). (**A**) β2gpI did not complex with APC, irrespective of the continuous presence of 100 nM β2gpI during gel filtration (Exp. 14). Peaks of β2gpI and APC are not base-line separated due to similar MW's. (**B**) Neither high-affinity, nor low-affinity complexes between β2gpI and protein S were observed with gel-filtration chromatography. The chromatogram shows elution of β2gpI and protein S after mixing the proteins in a molar ratio of 10:1 (Exp. 12). (**C**) Major amount of β2gpI does not form a complex with C4Bbp (MW of 570 kDa). The peak at a V_e of 8.1 ml corresponds to elution of free C4Bbp (See Table I) but may contain a small fraction of β2gpI that putatively formed a high-affinity complex with C4Bbp (fractionation limit of the Superdex 200 column is 600 kDa) (Exp. 15). (**D**) β2gpI had no noticeable influence on pre-formed protein S-C4Bbp complex. Protein S and C4Bbp solutions were mixed prior to addition of a 1.4-times molar excess of β2gpI (Exp. 16). The protein S-C4Bbp complex elutes at a V_e of 8.1 ml, similar to free C4Bbp. (**E**) Protein S and APC do not form a high-affinity complex in solution, whereas formation of a low-affinity complex is not excluded (Exp. 18).

Calmodulin

CaM did neither bind with high affinity to β2gpI (Table II, Exp. 3-9 and Fig. 2), nor to β2gpI *1 (not shown). Lowering the NaCl concentration from 150 mM to 15 mM did not induce complex formation (Exp. 3-4). Presence of a molar excess of, either β2gpI, or CaM had no influence on complex formation. When CaM in a concentration of 200 nM was continuously

present in the buffer during gel filtration (Exp. 9), no low-affinity binding between β2gpI and CaM was detected. Very low signal of CaM at 280 nm results from the low content of aromatic amino-acid residues, *i.e.* two tyrosines are present in the CaM sequence, and the absence of disulfide bonds.

Activated protein C, protein S and C4B binding protein
Protein S readily formed a stable complex with C4Bbp (Table III, Exp. 16-17). Effective binding of protein S to C4Bbp was shown by complete absence of the protein S peak at a V_e of 12.3 ml. When β2gpI was incubated with, either APC, or protein S, or C4Bbp no high-affinity binding was observed (Exp. 10-16, Fig. 3A-C). Exp. 15 does not exclude that a minor amount of β2gpI is complexed with C4Bbp. Like the C4Bbp-protein S complex (Fig. 3D), a peak resulting from β2gpI-C4Bbp complex may be covered by the peak resulting from the excess of free C4Bbp. Low-affinity complexes between β2gpI and protein S or APC were not detected when a molar excess of β2gpI was present in the gel-filtration buffer (Exp. 12 and 14). The results of Exp. 16 show that all protein S is still bound to C4Bbp after introduction of β2gpI (Fig. 3D). In solution protein S did not bind with high affinity to APC (Exp. 18, Fig 3E), whereas putative low-affinity complex could not be detected with the system used, *i.e.* none of the two proteins was added to the elution buffer during gel filtration.

Discussion

High-affinity (β2gpI)₂-IgG 22F6 complex

β2gpI forms a high-affinity divalent complex with murine IgG 22F6, when β2gpI is immobilized[253]. Complexes tightly bound to an anionic lipid surface whereas 22F6 alone did not bind to lipids. These observations indicated that the antibody-binding site on β2gpI is located distant from the membrane-adhesion site in the fifth C-terminal SCR domain of β2gpI. 22F6 was characterized as an LA based on its capacity to prolong phospholipid-dependent clotting assays. We now demonstrated that β2gpI and 22F6 also form high-affinity complexes in solution (Fig. 1B). Apparently, β2gpI does not necessarily need to adhere to lipid layers, prior to complex formation with LA's. This suggests that thrombotic complications in the APS may not only be caused by (β2gpI)₂-auto-antibody complexes that shield catalytic lipid surfaces, which are essential for anticoagulant processes[150,229]. Additionally or alternatively, coagulation disorders may be caused by inhibited formation of β2gpI-protein ligand complexes upon formation of β2gpI-auto-antibody complexes.

β2gpI-CaM complex

Renal filtered β2gpI is partially associated with lipid layers[90]. Once excreted into kidney cells, β2gpI is actively transported back into the circulation by renal endocytic transporter megalin[93]. *In vitro*, β2gpI has been shown to interact with the cellular regulator CaM when both proteins are in solution or when CaM was immobilized (Ref. 90, 91; M. Simmelink, unpublished results). These observations may suggest that binding of CaM to β2gpI can play a role in transport of renal-filtered β2gpI back into the circulation by megalin.

Our gel-filtration chromatography experiments revealed that high-affinity β2gpI-CaM complexes are not formed in solution. Even in the continuous presence of a molar excess of CaM on the gel-filtration column, the complex between β2gpI and CaM was not

detected (Fig. 2). This suggests that CaM has at most very low affinity for β2gpI when both proteins are in solution, in contradiction with the previously reported K_d of 3 nM for complex formation in solution[91]. The low K_d, that implies very tight binding, was determined from fluorescence measurements and competitive immuno-precipitations. Apparently, these methods gave an overestimated value for the K_d. If not, the reported high affinity of CaM for β2gpI would have resulted in detectable amounts of complex in our assay. Binding of β2gpI to CaM in an ELISA set-up (M. Simmelink, unpublished data) or on a CaM-affinity column[90] may indicate that *in vivo* immobilization of β2gpI at a lipid surface is a necessary step prior to binding of CaM.

Amino-acid residue Trp53 of β2gpI has previously been indicated to be involved in interaction with CaM[91]. Furthermore, peptide KPGYVSRGGMRKFI corresponding to amino-acid residues 33-46 of β2gpI strongly inhibited binding of β2gpI to CaM, suggesting that these residues are also involved in interaction with CaM. According to Rojkjaer *et al.*, sequence 33-46 in β2gpI potentially forms a basic amphiphilic α-helix, either intrinsically, or upon binding of CaM. Such a helix would be a typical binding site for CaM. However, the crystal structure of β2gpI shows that residues 33-46 are part of a structurally rigid entity of the N-terminal SCR domain[250]. These residues take part in two β-sheets that are fully conserved amongst known SCR-domain structures. Therefore, conformational rearrangement of three β-strands, in order to facilitate formation of an α-helix upon CaM binding, seems very unlikely. Trp53 is, in addition, completely buried in the hydrophobic core of the N-terminal SCR domain and is one out of nine highly conserved residues amongst SCR domains. Exposure of Trp53 upon binding of CaM seems, therefore, also rather unlikely.

Cationic amino-acid residues of β2gpI are important in CaM binding and the local environment of at least one Trp residue is influenced by binding of β2gpI to CaM[91]. These observations strongly suggest that the extreme negatively charged surface of CaM, comprising 17 Asp and 21 Glu amino-acid residues (pdb code 1CLL, Ref. 263), may, in an alternative way, interact with the positively charged membrane-adhesion patch on the surface of the fifth SRC domain of β2gpI (12 Lys, 1 Arg, 1 His). Fully exposed Trp316 of β2gpI, that is positioned close to the positively charged patch, then, possibly accounts for the observed change in Trp fluorescence.

In our alternative model for β2gpI-CaM complex formation, the membrane-adhesion site of β2gpI coincides at least partly with the CaM-binding site. Therefore, we suppose that binding of CaM to β2gpI may interfere with adhesion of β2gpI to phospholipid layers in the kidney and/or may release membrane-bound β2gpI. Freely circulating β2gpI-CaM complexes in the kidney cells, then, may facilitate transport of β2gpI back into the circulation by megalin[93].

Binding of β2gpI to regulators of the protein C-dependent anticoagulant pathway

β2gpI has pro- and anticoagulant activity[105,123,248,249,252,264]. The ability of β2gpI to prolong or shorten coagulation time has previously been explained by a passive and aspecific mechanism in which β2gpI shields the catalytic surface for coagulation reactions by adhesion to anionic phospholipid layers[150,229]. Recent reports on binding of β2gpI to activated protein C, protein S and C4B binding protein, that function in the APC-dependent anticoagulant pathway, suggested an additional or alternative active and more specific role for β2gpI in coagulation[83-85]. M. Simmelink confirmed binding of β2gpI to protein S in an ELISA, whereas binding to C4Bbp or to APC was not observed (unpublished results). To

gain more insight into these conflicting results, we have chosen for an assay system that enabled us to directly detect β2gpI-protein complexes in solution.

With gel-filtration chromatography we did not detect high-affinity complexes (Fig. 3A) or low-affinity complexes between APC and β2gpI. Putatively, efficient and specific binding of APC to β2gpI as observed by Sim and Devine (85), only occurs when, either APC, or β2gpI is bound to a suitable lipid surface *in vivo*, thereby creating a high local concentration of one of the components in the protein-protein complex. Immobilization of β2gpI in an ELISA set-up may mimick adhesion to lipids, whereas affinity of β2gpI for APC may be too low for complex formation in solution. The *in vivo* role of β2gpI-APC complexes bound to lipid layers is yet unknown. Protein S and APC also did not form complexes in solution (Fig. 3E), suggesting that they may need to adhere to a lipid surface prior to complex formation, like we propose for formation of APC-β2gpI complexes.

The studies of Atsumi *et al.* (83), Merrill *et al.* (84) and M. Simmelink (unpublished results) suggested a regulatory role for β2gpI-protein S complex in preventing inhibition of protein S activity in APC-dependent anticoagulation by the circulating protein S-inhibitor C4Bbp. Maintenance of the level of free protein S requires high-affinity binding between β2gpI and protein S to effectively prevent formation of very stable C4Bbp-protein S complexes. When we incubated a ten-times molar excess of free β2gpI with free protein S, a molar ratio that resembles physiological conditions, no complex was formed, irrespective of the continuous presence of β2gpI during gel filtration (Exp. 10-12, Fig. 3B). In addition, β2gpI had no influence on previously formed protein S-C4Bbp complex (Fig. 3D). These results do not support a suggested role for β2gpI as an anticoagulant by regulating free protein S levels upon binding to protein S. Our experiments did, however, not exclude that a small amount of β2gpI has bound with high affinity to C4Bbp. Binding of β2gpI to C4Bbp in plasma may, in an alternative way, prevent a small fraction of protein S for complex formation with C4Bbp, that in turn may be a sufficient amount for proper functioning in the anticoagulant cascade.

--- Chapter IV ---

Inactive β$_2$-glycoprotein I carries a neutral phospholipid molecule

Barend Bouma[1], Marleen J.A. Simmelink[2], Jan Westerman[3], Philip G. de Groot[2], Gerrit J. Gerwig[4], Jan Kroon[1] and Piet Gros[1].

Bijvoet Center for Biomolecular Research, [1]Department of Crystal and Structural Chemistry, and [4]Department of Bio-organic Chemistry, Utrecht University, Padualaan 8, 3584 CH Utrecht, The Netherlands, [2]Haemostasis and Thrombosis Laboratory, University Medical Center Utrecht, PO Box 85500, 3508 GA Utrecht, The Netherlands, and [3]Institute of Biomembranes, Department of Biochemistry of Lipids, Utrecht University, Padualaan 8, 3584 CH, Utrecht, The Netherlands.

Summary

Human plasma β_2-glycoprotein I (β2gpI) adheres to anionic phospholipids and is implied in blood coagulation, in removal of apoptotic bodies from the circulation and in the auto-immune disease anti-phospholipid syndrome. An isoform of β2gpI that does not bind to anionic lipids, accumulates in man during severe oxidative stress, *i.e.* during sepsis, drowning and after streptokinase treatment of myocardial infarction. We analyzed this isoform by biophysical and crystallographic methods. With gas chromatography-mass spectrometry and with thin-layer chromatography we revealed that the isoform has phosphatidylcholine or choline plasmalogen and, to a lesser extent, sphingomyelin bound. The crystal structure of the β2gpI-lipid complex at 3.0 Å resolution indicated a binding pocket for a glycerophosphorylcholine moiety located within the adhesion site for anionic membranes. The specific binding site shows minor structural rearrangements to fit a neutral phospholipid, when compared with the structure of intact β2gpI. C-terminal amino-acid sequence analysis confirmed cleavage of scissile bond Lys317-Thr318 and revealed that sequence Phe315-Trp-Lys317, which is essential for lipid binding, was not released from the isoform, excluding additional cleavage of scissile bond Ala314-Phe315. Furthermore, sequencing showed that genetically determined mutation Trp316Ser, which abolishes membrane adhesion, was not present in the pool of β2gpI used for our analyses. Carbohydrate analysis and mass spectrometry with the β2gpI isoform and intact β2gpI revealed that similar numbers of sialic acid residues were present and that these isoforms were fully glycosylated at their four N-glycosylation sites. Therefore, reduced glycan content or putative absence of sialic acid residues do not account for abolished lipid affinity of the isoform. The crystal structure of the β2gpI-lipid complex and the biophysical data suggest that specific binding of a neutral phospholipid blocks adhesion of β2gpI to anionic lipids. The β2gpI-lipid complex with its abolished membrane-adhesion ability may play a role in specific defense mechanisms during periods of oxidative stress.

Key words: apolipoprotein H, beta2 glycoprotein I, carbohydrate analysis, choline plasmalogen, crystal structure, inactive isoform, membrane adhesion, oxidative stress, phosphatidylcholine, phospholipid binding, sphingomyelin, thin-layer chromatography

Introduction

Human β_2-glycoprotein I (β2gpI)[a] is a heavily glycosylated plasma protein that has affinity for negatively charged surfaces. β2gpI is implied in a variety of processes in which its adhesion to anionic lipids is an important aspect. It has proposed functions in pro- and anticoagulant processes[84,85,106,121,123,124,248,249]. Noteworthy, several roles for β2gpI in coagulation were suggested by *in vitro* experiments[120,128,249], whereas β2gpI deficiency seems not to influence these activities *in vivo*[30,31]. β2gpI has also been implicated in clearance of apoptotic bodies[64,131,133,265] and non-self particles[68] from the circulation. Recent determination of a specific β2gpI-independent receptor for clearance of apoptotic cells has prompted doubt on the proposed role that non-discriminatory binding of β2gpI to anionic lipids may play in clearance of apoptotic bodies[136]. β2gpI is a key antigen in the auto-immune disease anti-phospholipid syndrome (APS), defined by thrombo-embolic complications and recurrent fetal loss[116]. Additionally, β2gpI is implicated in responses to oxidative stress[32,118,119,266,267]. β2gpI mainly circulates free in blood while 4-13% of the molecules is associated with lipoproteins[62,94,268], which bind with high affinity after oxidation[266,268]. β2gpI has affinity for negatively charged lipids phosphatidylserine (PS), phosphatidic acid and cardiolipin[71], present in e.g. lipoproteins, chylomicrons[61,65,72], blood platelets[66,67], liposomes[68], and apoptotic bodies[135].

The phospholipid-binding site of β2gpI has been mapped to the fifth C-terminal short concensus repeat (SCR) domain[75]. Based on the crystal structure of human β2gpI and on additional biochemical data we proposed a membrane-adhesion model[250]. A large positively charged patch forms a membrane-adhesion site on the fifth SCR domain that provides electrostatic interactions with anionic phospholipid head-groups. The exposed membrane-insertion loop Leu313-Ala-Phe-Trp-Lys317 yields specificity for phospholipid layers. This synergistic model is supported by studies that revealed both the hydrophobic interactions and the electrostatic interactions[77,78]. Two co-factors in coagulation, factor Va and factor VIIIa regulate their binding to anionic phospholipids in a reminiscent way[269-271].

Activity of β2gpI in apoptosis, APS and blood coagulation depends on its ability to adhere to negatively charged lipid surfaces[68,111,116,123,131]. Affinity of β2gpI for these anionic phospholipids is affected by the content of sialic acid (Neu5Ac) residues of the four N-glycans[69,262] and by enzymatic cleavage of scissile bonds Ala314-Phe315 and Lys317-Thr318 in the fifth SCR domain[76,80]. Asialo-β2gpI, containing less negative charges, has lower affinity for anionic phospholipids than fully sialydated β2gpI. Scissile bonds between residues Ala314-Phe315 and between Lys317-Thr318 likely induce conformational flexibility of the membrane-insertion loop, resulting in reduced affinity of 'cleaved' β2gpI[76] for anionic membranes. Simultaneous cleavage of both scissile bonds will release the membrane anchor Trp316-Lys317, which provides specificity for anionic phospholipids. β2gpI carrying genetically determined mutation Cys306Gly[52] or Trp316Ser[52,53] also has

---

[a] Abbreviations used: APS, anti-phospholipid syndrome; β2gpI, β_2-glycoprotein I; CP, choline plasmalogen; ELISA, enzyme-linked immuno-sorbent assay; Fuc, fucose; GalNAc, *N*-acetylgalactosamine; GC-MS, gas-liquid chromatography-mass spectrometry; GlcNAc, *N*-acetylglucosamine; MALDI TOF MS, matrix-assisted laser desorption/ionization time-of-flight mass spectrometry; Man, mannose; PC, phosphatidylcholine; Neu5Ac, *N*-acetyl neuraminicacid (sialic acid); PS, phosphatidylserine; r.m.s., root-mean-square; SCR, short consensus repeat; SM, sphingomyelin; TBS, Tris-buffered saline (50 mM Tris-HCl pH 7.5, 150 mM NaCl); TLC, thin-layer chromatography.

decreased affinity for negatively charged lipids. β2gpI mutant Trp316Ser lacks the Trp that provides specificity for phospholipids to the membrane-insertion loop Leu313-Ala-Phe-Trp-Lys317. β2gpI mutant Cys306Gly lacks disulfide bond Cys287-Cys306 that is essential for conformational stability of the fifth SCR domain. Furthermore, site-directed mutagenesis studies showed the importance of residues Lys284, Lys286, Lys287, Leu313 and Phe315 in adhesion of β2gpI to anionic layers[34,79].

Recently, Horbach et al. (32) described a novel isoform of human β2gpI, designated 'β2gpI *1', which was present in plasma of patients with sepsis, after streptokinase treatment of myocardial infarction, and after rescue from drowning, i.e. patients that had been subjected to severe oxidative stress. An isoform with so far identical characteristics was formed in vitro, under influence of a proteinase and an undetermined plasma component, from β2gpI that was isolated from plasma of healthy human individuals. This isoform does not bind to anionic phospholipids and has a cleaved scissile bond at Lys317-Thr318. Furthermore, the isoform is specifically recognized by murine monoclonal antibody 13A10. In plasma of healthy individuals the level of β2gpI *1 is approximately 0.1 μg ml^{-1}, whereas the level increases ten- to hundred-fold in plasma of patients. During sepsis and in plasma of a patient rescued from drowning an increased concentration of the isoform was accompanied with a 50% decreased level of intact β2gpI. Horbach et al. (32) suggested that this decrease may result from binding of intact β2gpI to apoptotic bodies, that are abundantly generated during sepsis and subsequently cleared from the circulation. They also speculated that a decreased level of intact β2gpI may be due to accelerated formation of the new isoform during stress in vivo, that might be a prerequisite for clearance of this modified β2gpI from the circulation.

In the present study we focussed on the underlying structural differences between human intact β2gpI and the new isoform β2gpI *1, that may account for the observed differences in affinity for anionic lipid layers. With C-terminal amino-acid sequencing we checked for cleaved scissile bonds and for the potential presence of the genetically defined mutation Trp316Ser. Putative differences in carbohydrate composition were analyzed with gas-liquid chromatography (GC). Subsequent mass spectrometry (MS) was performed to identify peaks in the gas chromatogram of β2gpI *1 that could not be assigned to glycan moieties. Thin-layer chromatography (TLC) was used for analysis of lipids that were bound to β2gpI isoforms. We determined the crystal structure of the new isoform of β2gpI to define the potential location of the binding site(s) for neutral phospholipids and to establish whether conformational alterations have occurred that may cause declined lipid affinity.

Methods

Characterization of β2gpI purified from human plasma

The three β2gpI isoforms, i.e. intact β2gpI, 'cleaved' β2gpI[76], and isoform β2gpI *1 (Ref. 32) were purified as described by Horbach et al. (242) from two pools of blood plasma, each from three healthy human donors (Dutch Blood Bank, The Netherlands). Purified β2gpI was characterized with ELISA's using two antibodies: murine monoclonal antibody 13A10 that has specificity for isoform β2gpI *1, and phage-display scFv-antibody fragment F3 that has specificity for intact β2gpI (i.e. with intact Lys317-Thr318 peptide bond). N-terminal amino-acid sequences of the β2gpI isoforms were also analyzed. Intact β2gpI has one N-terminus starting with NH$_2$-Gly1, whereas cleaved β2gpI and isoform β2gpI *1 have an additional N-

terminus starting with NH$_2$-Thr318, due to enzymatic cleavage of scissile bond Lys317-Thr318. Additionally, the isoforms were checked for their lipid affinity in an ELISA set-up. Intact β2gpI shows relatively high affinity for an anionic lipid layer, cleaved β2gpI has decreased affinity, whereas β2gpI *1 can not bind to lipids.

One pool of plasma ('pool A') was used to purify intact β2gpI. However, after storage of the purified material over six months, presence of N-terminal amino-acid sequence starting with NH$_2$-Thr318 showed that half of the β2gpI molecules was cleaved at Lys317-Thr318. Significant binding of both 13A10, as well as of F3 was observed at this stage. Material of this purified batch, that contains a mixture of β2gpI isoforms, was previously used for crystal-structure determination reported by Bouma *et al.* (250). The second pool ('pool B') was used to purify the three separate forms intact β2gpI, cleaved β2gpI and β2gpI *1. The latter isoforms were initially not present but were formed during purification. N-terminal sequence analysis and ELISA's with intact β2gpI using 13A10 and F3 confirmed that this form was not cleaved at Lys317-Thr318. Solutions of purified β2gpI isoforms were stored in Tris-buffered saline (TBS).

C-terminal amino-acid sequencing

The C-terminal amino-acid sequence of β2gpI *1 was determined with automated C-terminal sequencing. It was performed by Eurosequence (Groningen, The Netherlands) with an Automated Sequenator model 477A (Applied Biosystems, CA, USA). For analysis 2.1 nmol lyophilized β2gpI *1 in TBS was used. Before lyophilization, β2gpI *1 was incubated for 60 min. at 37°C with 150 mM dithiothreitol to reduce disulfide bonds.

Carbohydrate analysis

Carbohydrate analysis was performed by GC-MS[272,273]. For the analyses, 2.8 nmol β2gpI (pool A), 3.3 nmol intact β2gpI, two times 1.5 nmol cleaved β2gpI, and 3.3 nmol and 8.8 nmol of isoform β2gpI *1, all from pool B, was used. Samples were desalted before use and 10 nmol internal standard (mannitol) was added. Each sample was lyophilized and dried over P$_2$O$_5$. Methanolysis was performed with 0.5 ml of 1.0 M methanolic-HCl for 24 h at 85°C. After cooling to room temperature, solutions were neutralized with solid silver carbonate. Acetic anhydride (20 µl) was added for re-*N*-acetylation (24 h at room temperature). After centrifugation (3 min. at 2500 rpm), supernatants were collected. The residue of silver salts was washed twice with 0.5 ml of dry methanol. Pooled supernatants were evaporated under reduced pressure. The residue was dried over P$_2$O$_5$. Finally, samples were trimethylsilylated for 30 min. at room temperature with 50 µl of a mixture of pyridine, hexamethyldisilazane and chlorotrimethylsilane (volume ratio of 5:1:1). Quantitative analysis of trimethylsilylated-(methylester)methyl glycosides was carried out by GC-MS using a Fisons Instruments GC 8060 / MD 800 System (Interscience, Ontario, Canada). The GC column was a CP-Sil 5 CB of 25 m x 0.25 mm (Varian Chrompack Benelux, Bergen op Zoom, The Netherlands) and the temperature program was 140 to 240°C at 4° min.$^{-1}$. Molar ratios of fucose (Fuc), xylose (Xyl), mannose (Man), galactose (Gal), glucose (Glc), *N*-acetylgalactosamine (GalNAc), *N*-acetylglucosamine (GlcNAc) and Neu5Ac were calculated. The molar ratio of Man residues was normalized to 3, based on the presence of three Man units in the most common N-glycan core structure attached to plasma glycoproteins, *i.e.* (Man-)(Man-)Man-GlcNAc-GlcNAc-Asn (Fig. 1). Whether the core glycan structures are di-, tri- and tetra-antennary branched can be deduced from the relative contents of GlcNAc, Man, and Gal units in a preparation of

β2gpI. Peaks in the gas chromatogram of β2gpI *1 that could not be assigned to sugar residues were subsequently analyzed with MS (Fisons Instruments GC 8060 / MD 800 System, Interscience, Ontario, Canada).

Molecular masses of the mixture of β2gpI isoforms from pool A and of cleaved β2gpI and β2gpI *1 from pool B were measured with matrix-assisted laser desorption/ionization time-of-flight mass spectrometry (MALDI TOF MS; Ref. 274, 275). The average glycan content of the β2gpI isoforms can be deduced from the measurements and from the calculated molecular mass of β2gpI based on amino-acid residues only (36.3 kDa)[40].

A

Neu5Ac-Gal-GlcNAc-Man
|
Man-GlcNAc-GlcNAc-Asn
| |
Neu5Ac-Gal-GlcNAc-Man   Fuc

B

Neu5Ac-Gal-GlcNAc-Man
|
Man-GlcNAc-GlcNAc-Asn
| |
Neu5Ac-Gal-GlcNAc-Man   Fuc
|
Neu5Ac-Gal-GlcNAc

Titel:
(asn143.eps)
Gemaakt door:
Adobe Illustrator(R) 8.0
Voorbeeld:
Deze EPS-figuur is niet opgeslagen
met een ingesloten voorbeeld.
Commentaar:
Dit EPS-bestand kan worden afgedrukt
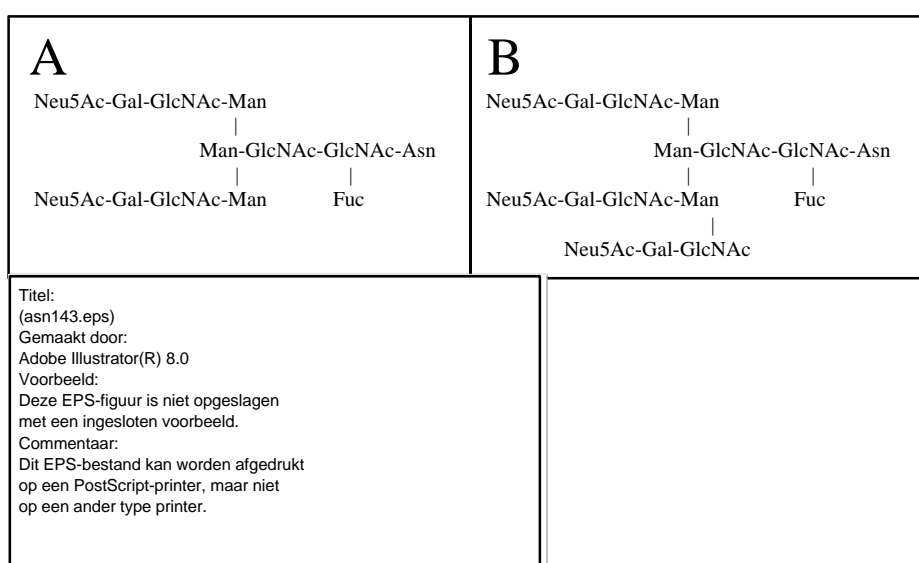op een PostScript-printer, maar niet
op een ander type printer.

Fig. 1. Isoforms of β2gpI have, on average, three di-antennary N-linked carbohydrate structures attached and one tri-antennary structure. These N-glycans are partially fucosylated and partially desialylated, with on average one or two sialic acid residues cleaved off from the four antennae. (**A**) Di-antennary N-linked carbohydrate structure. (**B**) Tri-antennary N-glycan. (**C**) Electron-density accounting for the N-glycan attached to Asn143 of β2gpI *1. The 2|F$_o$|-|F$_c$| map at 3.0 Å resolution is contoured at 0.7 σ. The partially visible N-glycan forms bridging crystal contacts between Gly1' and Thr130" of two separate symmetry-related molecules.

Lipid analysis

Aliquots of 10 nmol β2gpI (pool A), 9.3 nmol intact β2gpI and 10 nmol and 5 nmol β2gpI *1 from pool B were used for qualitative lipid analysis by TLC. Lipid extraction was performed according to the protocol described by Bligh and Dyer (276). After extraction lipids were dried under a nitrogen flow, dissolved in 50 μl of chloroform, and loaded on silica gel HPTLC-Fertig plates (Merck, Darmstadt, Germany). Reference lipids lyso-phosphatidylcholine (l-PC), sphingomyelin (SM), PS, PC, phosphatidylglycerol and phosphatidylethanolamine were from Sigma Aldrich (Zwijndrecht, The Netherlands). The mobile phase was chloroform-water-methanol (65:4:25 v/v/v). After approximately 30 min.

of migration plates were stained with iodo vapor, ninhydrin (Merck, Darmstadt, Germany), phosphor reagent Molybdenum Blue (Sigma Chemical Co., St. Louis, MO, USA) and by heating in the presence of sulfuric acid.

Crystallization and X-ray data collection

Crystallization trials with isoform β2gpI *1 were performed with protein concentrated to 9 mg ml^{-1}. The hanging-drop vapor-diffusion method at 4°C was used with set-ups of 2 μl protein solution and 2 μl reservoir solution over 750 μl reservoir solution. The crystallization condition was as described before (Ref. 259; pdb code 1QUB), *i.e.* 1.5 M $(NH_4)_2HPO_4$, 0.1 M NaOAc pH 5.6. Crystals with a pyramidal shape grew within 10 days in space group $C222_1$, like 1QUB, and had a size of approximately 0.3x0.4x0.4 mm^3. Unit-cell dimensions were also similar to those reported for β2gpI 1QUB and the crystals contained one β2gpI molecule in the asymmetric unit. X-ray diffraction data were collected using a crystal that was equilibrated for 20 sec. in 1.65 M $(NH_4)_2SO_4$, 35% v/v glycerol, 20 mM HEPES pH 7.5, and that was subsequently frozen in a gaseous nitrogen stream at 100 K. X-ray data were collected on beam line ID14-EH1 (European Synchrotron Radiation Facility (ESRF), Grenoble, France) using a MarCCD detector. Data collection was aided by use of STRATEGY[244]. Data were processed and scaled using DENZO and SCALEPACK[26]. See Table I for data-collection statistics.

At an early stage, a data set was collected from another crystal of β2gpI *1, on beam line ID14-EH3 (ESRF, Grenoble, France). This first data set was subjected to radiation damage. Comparison of data sets collected at ID14-EH1 and -EH3, with respect to effects of non-specific and specific radiation damage on data quality and on the refined structure of β2gpI *1, is described in the *Appendix* to this chapter.

Table I
Diffraction-data statistics and structure-refinement statistics

Data statistics[†]		Refinement statistics	
Resolution (Å)	36.0 – 3.0	Resolution (Å)	36.0 – 3.0
Mosaicity (°)	0.71	R-factor/R_{free}	0.238/0.260
Space group	$C222_1$	r.m.s.d. bond distances (Å)	0.008
Unit cell: *a b c* (Å)	159.0 165.9 115.0	r.m.s.d. angles (°)	1.4
Redundancy	4.9	Average B-factor (Å^2)[¥]	60
No. unique reflections	30,789	Solvent content (%)	86
$<I>/<σ(I)>$	20.5 (6.0)	No. non-hydrogen atoms	2,709
Completeness (%)	99.4 (99.2)	No. protein residues	318
R_{merge} (%)	5.6 (21.4)	No. sugar residues[‡]	15
		No. lipid molecules[¶]	1
		No. sulfate ions	4
		No. solvent molecules	5

† Numbers in parentheses indicate statistics for the highest resolution shell (3.11-3.00 Å). Diffraction data were collected on beam line ID14-EH1 of the ESRF (Grenoble, France).

¥ Average B-factor for all atoms in the model.

‡ Forty to sixty sugar residues are expected, based on MALDI-TOF MS.

¶ A glycerophosphorylcholine moiety is built into the structure. Acyl chains of the PC, CP or SM molecule were not observed in the electron density.

Crystal-structure refinement and interpretation

Rigid-body refinement, positional refinement and B-factor refinement, using the model of β2gpI 1QUB[250] was performed with CNS[9]. The initial model consisted of amino-acid residues 1-310 and 318-326 and seven carbohydrate moieties. Carbohydrate antennae were subsequently lengthened according to extended electron density in difference maps. Four sulfate ions and a glycerophosphorylcholine moiety were built into the structure. Water molecules were defined in difference maps, and B-factors and positions were refined with CNS. The search criteria for water molecules were a peak height > 4.0 σ, a distance of 2.5-3.3 Å to the hydrogen acceptor or donor, and a B-factor smaller than 60 Å^2. Rebuilding of carbohydrates, the glycerophosphorylcholine moiety and parts of the protein structure was aided by O[16]. Refinement used the maximum-likelihood algorithm[29] and during refinement cross validation was used. Bulk solvent correction was applied as calculated by CNS. The model quality was checked with WHATIF[17] and PROCHECK[18]. Electrostatic potentials were calculated with GRASP[246]. Fig. 1C, 4A and 4B were generated with BOBSCRIPT[277] and RASTER3D[203]. Fig. 3A was generated using MOLSCRIPT[202] and RASTER3D. Fig. 3B and 4C were generated using MOLSCRIPT.

Results

C-terminal amino-acid sequencing of isoform β2gpI *1

C-terminal amino-acid sequencing of isoform β2gpI *1 yielded a single sequence of COOH-Lys317-Trp-Phe-Ala314. Cys326, corresponding to the C-terminus of the native sequence[40], was not observed, because cysteine residues are hardly detected by the sequenator used and presence of a Pro residue at position 325 terminates the sequencing process, altogether.

Carbohydrate analysis

Molar ratios of carbohydrate-building blocks of the mixture of β2gpI isoforms from pool A and intact β2gpI, cleaved β2gpI and isoform β2gpI *1 (pool B) were determined with GC (See Table II). Molar ratios of Fuc, Man, Gal and GlcNAc residues were very similar for intact β2gpI, cleaved β2gpI and β2gpI *1. The content of Fuc residues indicates that on average one Fuc residue is attached to approximately 20% of the β2gpI molecules. The relative amounts of Man, Gal and GlcNAc residues indicate the presence of on average three di-antennary carbohydrate structures (Fig. 1A) and one tri- or tri'-antennary structure (Fig. 1B), in accordance with previous findings[43]. The sialic acid residue content varied among the three β2gpI isoforms from pool B, and correspond to the presence of nine, seven and eight Neu5Ac residues for intact β2gpI, cleaved β2gpI and β2gpI *1, respectively. This observed difference is, however, not significant. Carbohydrate antennae are intrinsically susceptible for chemical cleavage of Neu5Ac residues. Variation in the degree of Neu5Ac cleavage among the isoforms is potentially due to differences in treatment with respect to purification and storage. The sialic acid residue content of the mixture of β2gpI isoforms isolated from pool A was similar to the average content of Neu5Ac residues of the separate isoforms of pool B, and corresponds to the presence of eight or nine Neu5Ac residues. GalNAc was absent in all preparations of the β2gpI isoforms, indicating that O-linked carbohydrate antennae[278] were not attached. Xyl and Glc residues are a common contamination, originating from column or filter material that was used during purification[242]. Apart from peaks originating from carbohydrate residues, additional peaks in the gas chromatogram

were observed in the preparation of the isoform β2gpI *1, which were absent for the other isoforms. Subsequent MS analysis identified these peaks as C16:0-, C18:0-, C18:1-, C18:2-acyl chains and putatively alkene $C_{16}H_{32}$.

MALDI TOF MS analysis of β2gpI isoforms revealed a mean molecular mass of 45 (± 2) kDa for cleaved β2gpI (pool B), isoform β2gpI *1 (pool B) and the mixture of isoforms (pool A). This mass is similar to the molecular mass of approximately 43 kDa obtained with gel electrophoresis[32]. Based on the MS analysis β2gpI contains approximately 9 kDa (~20% w/w) N-glycans. Furthermore, the carbohydrate analysis revealed an (maximum) N-glycan content of 18% w/w. The glycan mass is in agreement with the presence of partially fucosylated and desialylated carbohydrates of which three are di-antennary structures (MW 1.8-2.6 kDa) and one is tri-antennary branched (MW 2.2-3.3 kDa), which is in correspondence with the relative amounts of carbohydrate units.

Table II
Carbohydrate analysis

mono-saccharide	molar ratios[†]			
	β2gpI (pool A)[¶]	intact β2gpI (pool B)	cleaved β2gpI (pool B)	β2gpI *1 (pool B)
Man[‡]	3	3	3	3
Fuc	0.2	0.2	0.2	0.1
GlcNAc	4.2	4.4	4.4	4.4
Gal	2.0	2.2	2.0	2.1
Neu5Ac[¥]	2.2	2.4	1.7	2.0
GalNAc[#]	0.0	0.0	0.0	0.0
Xyl[$]	0.3	0.1	0.3	0.2
Glc	0.4	0.2	0.6	1.0

† Carbohydrate contents are in molar ratios. Molar ratios for β2gpI (pool A), cleaved β2gpI and β2gpI *1 (pool B) are averages over two, two and three analyses, respectively. In β2gpI *1 C16:0, C18:0, C18:1, C18:2 acyl-chains and putatively alkene $C_{16}H_{32}$ were additionally present.

¶ β2gpI purified from plasma pool A consisted of a mixture of isoforms. The isoforms were purified separately from plasma pool B.

‡ The molar ratio of Man was normalized to 3, based on the presence of three Man residues in the most common N-glycan core in plasma glycoproteins. The relative contents of Man, GlcNAc and Gal are indicative for the presence of, on average, three di-antennary carbohydrate structures and one tri-antennary structure[43].

¥ Differences in sialic acid residue content among β2gpI isoforms purified from pool B are not significant. N-glycans are highly susceptible for cleavage of the peripheral Neu5Ac residues. Differences in the degree of Neu5Ac cleavage among the isoforms likely originate from differences in purification and storage.

The absence of GalNAc indicates that O-glycans are not linked to the β2gpI isoforms[278].

$ Xyl and Glc are a contamination originating from column and filter material used during purification of β2gpI.

Lipid extraction and thin-layer chromatography with β2gpI isoforms

Lipid extraction followed by thin-layer chromatography revealed two large spots for isoform β2gpI *1 that co-migrated with PC and SM standards (Fig. 2). Spot 1 is far more abundant in β2gpI *1 than spot 2, according to the relative intensities of the two spots using iodo staining or spraying with phosphor reagent. Two weak spots were observed for the mixture of β2gpI isoforms from pool A, that co-migrated with the two spots of β2gpI *1 and with PC and SM standards. R_f values of the two spots and of reference phospholipids are given in Table III. Both spot 1 and spot 2 were visible after staining with iodo vapor, with Molybdenum Blue, and after baking in the presence of H_2SO_4, indicating that the spots originate from

Fig. 2. Thin-layer chromatogram. Phospholipids were extracted from a mixture of β2gpI isoforms purified from plasma pool A and from β2gpI *1 purified from plasma pool B. Lipids were chromatographed in chloroform-water-methanol (65:4:25 v/v/v) and visualized with iodo vapor. Lane 1, lipids extracted from the mixture of β2gpI isoforms; 2, β2gpI *1; 3, PE/PG/PC; 4, PS; 5, PC/l-PC; 6, β2gpI *1; 7, SM. Spot 1 from the mixture of β2gpI isoforms and β2gpI *1 co-migrates with the PC standard, indicative for the presence of PC and choline plasmalogen, spot 2 co-migrates with SM.

Table III
*TLC with phospholipids bound to **b**2gpI*

Lipids in β2gpI[¶]	R_f[†]	Standards[‡]	R_f
Spot 1	11	lyso-PC	8
Spot 2	19	SM	11
		PS	15
		PC	19
		PG	27
		PE	42

¶ TLC analysis with β2gpI *1from plasma pool B and the mixture of β2gpI isoforms from pool A revealed that these preparations have the same lipids bound. Lipids were abundant in β2gpI *1, whereas only traces of lipids were observed for the mixture of β2gpI isoforms. Phospholipids were not detected in intact β2gpI.
† R_f is the migrated distance of the lipid spot on the TLC plate divided by the migrated distance of the mobile phase.
‡ The R_f values of lyso-PC, PS, PC, PG and PE standards are averages over two, four, four, two and two analyses, respectively. SM was analyzed once. PC co-migrates with choline plasmalogens, which were putatively present.

phospholipids containing unsaturated acyl chains. The spots were not stained with ninhydrin, excluding the presence of lipids that contain amino groups. PC and choline plasmalogens (CP), which are PC analogues that contain an alk-1-enyl group instead of an alkyl moiety at their *sn*-1 position[279], co-migrate during one-dimensional TLC[280,281]. Therefore, spot 1, which co-migrates with a PC standard, may in fact contain PC and/or choline plasmalogens. No spots co-migrating with phospholipids were observed for intact β2gpI from pool B (not shown). Cleaved β2gpI was not analyzed with TLC due to limited amount of protein.

Crystal structure determination and analysis of β2gpI *1

The crystal structure of isoform β2gpI *1 was determined using the model of β2gpI 1QUB[250] as a starting point for refinement. The structure has been refined to a final R-factor of 23.8% and a free R-factor of 26.0% (5% of the data) using diffraction data to 3.0 Å resolution. The structure displays good model geometry with 84% of the residues in most favored regions of the Ramachandran plot and 16% in generously allowed regions. Statistics for the refined model are given in Table I.

The overall structure of β2gpI *1 is identical to previously reported structures (Ref. 250, 251; pdb code 1QUB, 1C1Z), showing the typical fish-hook like appearance (Fig. 3A). We do not observe residues 310-317 in the electron density for β2gpI *1. This encompasses the membrane-insertion loop 313-317 that provides specificity for anionic layers[79,250]. Enzymatic cleavage of this solvent-exposed loop at scissile bond Lys317-Thr318 likely results in mobility or disorder. Position of terminal Thr318, next to the cleavage site, is defined by the electron density and appears fixed by a crystal contact with Glu259 of a symmetry-related molecule. Electron density for the side chain of amino-acid residues Lys59, Arg135, Lys138, Lys177, Lys250, Lys251, Lys284 and Lys286 is incomplete. Additional density near Thr204/Tyr206 and near Tyr207 reveal that sulfate ions form hydrogen bonds with hydroxyl groups of these amino-acid residues instead of being covalent bound, as was suggested previously[250]. Two additional sulfate ions are built into the structure near Arg191/His216 and near Lys208/Glu228, of which the latter two residues form an intra-molecular salt bridge. B-factors of the four sulfate ions are relatively high and suggest partial occupation or disorder.

Electron density near Asn143, Asn164, Asn174 and Asn234 allowed for building of fifteen carbohydrate residues at the four N-glycosylation sites, *i.e.* β-D-GlcNAc-(1→2)-α-D-Man-(1→3)-β-D-Man-(1→4)-β-D-GlcNAc-(1→4)-β-D-GlcNAc-(1→N)-Asn143, β-D-GlcNAc-(1→4)-β-D-GlcNAc-(1→N)-Asn164, α-D-Man-(1→6)-[α-D-Man-(1→3)]-β-D-Man-(1→4)-β-D-GlcNAc-(1→4)-β-D-GlcNAc-(1→N)-Asn174, and β-D-Man-(1→4)-β-D-GlcNAc-(1→4)-β-D-GlcNAc-(1→N)-Asn234. In comparison, only seven and eleven carbohydrate residues were incorporated in the β2gpI models 1QUB and 1C1Z, respectively. Weak electron density near Thr130" and Gly1' of two symmetry-related molecule originates from an extension of the N-linked glycan linked to Asn143 of a third symmetry-related molecule (Fig. 1C). Electron density indicative of Fuc residues linked to GlcNAc-Asn was not observed at any of the four N-glycosylation sites.

Weak non-continuous electron density was observed in a pocket in the fifth SCR domain of β2gpI *1 (Fig. 4). The pocket is located in the center of the positively charged patch, that forms the adhesion site for anionic layers, and is positioned next to the (cleaved) membrane-insertion loop Leu313-Lys317 (Fig. 3A, 4C). The bottom of this pocket is formed by Phe280, Phe307, the carbonyl oxygen of Lys308, and Asp319. The sides of the pocket are lined by Ala252, Thr253, Gln264, Glu265 and Ser321. Its rim is formed by Lys251 and Lys262, that are part of the membrane-adhesion site. The observed electron density inside this pocket was putatively assigned to a glycerophosphorylcholine moiety of a phospholipid molecule. The choline moiety is buried deeply inside the pocket, near aromatic residues Phe280 and Phe307 and negatively charged Asp319. The phosphate is located close to residues Thr253 and Gln264 and is putatively hydrogen-bonded to $O_{\gamma1}$ of Thr253 and $N_{\epsilon2}$ of Gln264. The glycerol moiety of the phospholipid is located at the surface of the molecule and is putatively hydrogen-bonded to $O_{\epsilon2}$ of Glu265. Acyl chains of the lipid molecule are not visible in the electron density.

Fig. 3. Structural representation of β2gpI *1. (**A**) Ribbon drawing of β2gpI *1 with SCR domains labeled I-V. The glycerophosphorylcholine moiety of the bound neutral phospholipid is located in a pocket in the fifth domain. The four N-linked glycans are indicated with ball-and-stick models. Residues 310-317 are not observed in the electron density. (**B**) Stereo drawing of the structural overlay of C_α-atoms of the fifth SCR domain of β2gpI *1 (in gray, this work) and intact β2gpI 1C1Z (in black, Ref. 251). C_α-atoms of amino-acid residues 245-309 and 318-326 are used in the superposition. The overall fold of the fifth SCR domain is well conserved among the two models, despite the location of a lipid molecule in the interior of the domain in β2gpI *1. This isoform is cleaved at scissile bond Lys317-Thr318 likely resulting in high mobility of loop 310-317. The three disulfide bonds present in the domain are represented with ball-and-stick models in the model of intact β2gpI.

Fig. 4. A neutral phospholipid molecule is specifically bound in a pocket within the anionic membrane-adhesion site of β2gpI *1. (**A**) Electron-density inside the specific binding pocket for a neutral phospholipid, calculated with phases of the refined model, including the glycerophosphorylcholine moiety. The $2|F_o|-|F_c|$ map at 3.0 Å resolution is contoured at 0.7 σ. Electron density accounting for the glycerophosphorylcholine moiety is weak and non-continuous, likely due to mobility of the phospholipid and a low occupancy. (**B**) Difference electron-density inside the pocket calculated with phases of the refined model omitting the glycerophosphorylcholine. The $|F_o|-|F_c|$ map at 3.0 Å resolution is contoured at 2.5 σ. The refined model of the glycerophosphorylcholine moiety is shown for clarity. (**C**) Stereo drawing showing the residues of β2gpI *1 involved in glycerophosphorylcholine binding. Side chains of amino-acid residues of β2gpI *1 that interact with the glycerophosphorylcholine moiety are shown in gray and the lipid is represented with a ball-and-stick model.

The final model of β2gpI *1 comprises amino-acid residues 1-309, 318-326, nine GlcNAc residues, six Man residues, four sulfate ions and one glycerophosphorylcholine moiety.

Comparison of β2gpI crystal structures

For the whole β2gpI *1 molecule root-mean-square (r.m.s.) coordinate differences of C_α-atoms are 0.31 and 0.65 Å when compared with the crystal structures of β2gpI 1QUB and β2gpI 1C1Z, respectively. For individual domains r.m.s. coordinate differences after superimposing C_α-atoms are approximately 0.15-0.25 Å. Significant differences between structures of β2gpI are restricted to the region of the membrane-insertion loop 313-317, which is observed in 1C1Z, but which was not visible in β2gpI *1 and 1QUB (Fig. 3B). β2gpI *1 and β2gpI 1QUB differ slightly in the position of residues His310 and Thr318 that precede and follow the membrane-insertion loop, respectively. Electron density accounting for His310 is not observed for β2gpI *1 and the position of Thr318 differ between the two structures. Differences between structures of β2gpI *1 and of intact β2gpI 1C1Z are restricted to the position of residues Gly1-Arg2, and to loop 310-317. In the crystal structure of intact β2gpI 1C1Z this loop was not cleaved at Lys317-Thr318 and its position was deduced from the electron density (Fig. 5). His310 forms an intra-molecular salt bridge with Asp319 in 1C1Z. In β2gpI *1 residues 310-317 could not be located in the structure and the salt bridge between His310 and Asp319 is, as a consequence, not observed. Structures 1QUB and 1C1Z of β2gpI have different positions of His310, but in both structures this residue forms a salt bridge with Asp319.

Structures of β2gpI *1 and of β2gpI 1QUB show weak non-continuous electron density in the pocket that is located within the positively charged membrane-adhesion patch. Structure factors of intact β2gpI 1C1Z[251] were not made available by the authors upon request and, therefore, we could not include analysis of the electron density in the pocket of intact β2gpI 1C1Z in our comparison.

Electrostatic surface potentials of the membrane-adhesion site at the fifth SCR domain, calculated from the β2gpI *1 and 1QUB models, are very similar, showing a large positively charged patch (Fig. 5). In contrast, the electrostatic surface potential calculated from the 1C1Z model shows a much smaller patch (Fig. 5B). The loop Lys282-Asn-Lys-Glu-Lys-Lys287 and residues Lys308 and Lys324 yield a local potential that is common among the three structures. Residues Lys246, Lys250, Lys251, Arg260, Lys262 and Lys266 enlarge the large positively charged patch in β2gpI *1 and β2gpI 1QUB. The absence or presence of the mainly hydrophobic loop Ser311-Ser-Leu-Ala-Phe-Trp-Lys317, which encompasses the intact membrane-insertion loop 313-317, accounts for the observed differences.

Discussion

With the current study we aimed at characterizing human β2gpI *1 that has lost its ability to adhere to anionic membranes. β2gpI *1 is formed *in vitro* during purification of β2gpI from plasma of healthy human individuals under influence of an undetermined proteinase and an unknown plasma component[32]. Based on abolished binding to negatively charged phospholipids, specific recognition by antibody 13A10 and cleavage at scissile bond Lys317-Thr318, Horbach *et al.* (32) reported similarity between the *in vitro* formed β2gpI *1 and an isoform that was detected in patients who suffered from life-threatening oxidative stress. We,

now, used β2gpI *1 that was formed *in vitro* for further biophysical and crystallographic analyses.

C-terminal amino-acid sequence analysis confirmed that β2gpI *1 is cleaved at Lys317-Thr318, and revealed that it is not additionally cleaved at Ala314-Phe315. Cleavage at scissile bond Ala314-Phe315 would release residues Trp316-Lys317, that form the specific anchor for anionic membranes[250], and residue Phe315, that is, in addition, essential for binding[79]. The determined C-terminal sequence COOH-Lys317-Trp-Phe-Ala314 also implicates presence of a Trp at position 316, excluding the genetically determined mutation Trp316Ser, which is present in part of the population. Heterozygotes carrying this mutation show decreased binding of β2gpI to lipid layers, whereas lipid binding is inhibited in homozygotes[52,53]. Thus, these data show that abolished membrane-adhesion ability of β2gpI *1 is neither due to enzymatic release of sequence Phe315-Trp-Lys317, nor due to the presence of a Ser residue at position 316.

Carbohydrate analysis revealed that β2gpI *1, cleaved β2gpI and intact β2gpI from pool B and a mixture of these β2gpI isoforms from pool A contain very similar relative amounts of the N-glycan building blocks Man, Gal, Fuc, GlcNAc, and Neu5Ac. In addition, our analysis indicated that none of the β2gpI isoforms has O-glycans attached, in contrast to previous results reported by Gambino *et al.* (44, 45). The relative amounts of Man, Gal and GlcNAc units indicated that on average three di-antennary glycan structures and one tri-antennary structure (See Fig. 1) are attached to the four N-glycosylation sites Asn143, Asn164, Asn174 and Asn234 of β2gpI. MALDI TOF MS analysis revealed an identical average N-glycan content of approximately 20% w/w for β2gpI isoforms, in agreement with the total carbohydrate content of 18% w/w determined with GC-MS. Horbach *et al.* (32) speculated that affinity of β2gpI for anionic lipids may be regulated by the degree of glycosylation. However, the total glycan mass of 9 kDa indicated that each of the four N-glycosylation sites of cleaved β2gpI and isoform β2gpI *1 was fully occupied with carbohydrate antennae. Hagihara *et al.* (69) and Brighton *et al.* (262) have shown that complete cleavage of peripheral sialic acid residues decreases affinity of β2gpI for anionic lipids. Our carbohydrate analyses revealed that sialic acid residues are cleaved off to some extent but that eight out of nine Neu5Ac are still present in the preparation of β2gpI *1 (Table II). Thus, our data show that reduced affinity of β2gpI *1 for lipid layers neither results from variation in N-glycan content, nor from cleavage of Neu5Ac residues.

GC-MS analysis with carbohydrate preparations from β2gpI *1 pointed to the presence of C16 and C18 acyl chains, likely originating from lipids or fat molecules. Alkene $C_{16}H_{32}$ may originate from the alk-1-enyl group of CP or from part of the sphingosine group of an SM molecule. TLC analysis confirmed the presence of PC/CP and SM in the β2gpI *1 preparation. In addition, with TLC these lipids were identified in the mixture of β2gpI isoforms (pool A), that was used previously for the crystal structure determination reported by Bouma *et al.* (250). In difference maps calculated with β2gpI *1 and β2gpI 1QUB weak and non-continuous electron density was observed in a pocket in the fifth SCR domain (Fig. 4B). The pocket is located within the positively charged patch that forms the adhesion site for anionic membranes (Fig. 5A), and next to the anionic-membrane insertion loop Leu313-Ala-Phe-Trp-Lys317 (Fig. 3A, 5C). Density inside the pocket could account for a glycerophosphorylcholine moiety. This indicates that the pocket is a potential binding site for one neutral phospholipid molecule, *i.e.* SM, CP or PC. This binding site provides no specificity for the two acyl chains of the neutral lipid, which point away from the protein

surface. Aromatic residues Phe280 and Phe307 and negatively charged Asp319 are positioned inside the pocket and provide specificity for the choline moiety in a way reminiscent to commonly observed protein-choline interactions[282,283]. Similar phosphatidyl-choline binding is observed for the Fab fragment of antibody McPC603 (Ref. 284; pdb code 2MCP), *Staphylococcal* LukF (Ref. 285; pdb code 3LKF) and human C-reactive protein (Ref. 286; pdb code 1BO9). Apparently, β2gpI specifically binds a neutral phospholipid, whereas it has a well-characterized specificity for lipid layers containing anionic PS or CL[71,76]. Adhesion of β2gpI to these anionic membranes is extensively discussed in literature[34,69,71,76-80,116,250], whereas the mechanism that regulates binding of a neutral lipid is not yet known. Work of Horbach *et al.* (32) indicated that cleavage of scissile bond Lys317-Thr318 is a necessary prerequisite for uptake of a lipid molecule. Here we have shown that the neutral phospholipid molecule is bound within the non-specific binding site for anionic lipid layers.

A membrane-adhesion model has been proposed for β2gpI based on the crystal structure and available biochemical data[250]. In this model a large positively charged patched located at the fifth SCR domain has charge interactions with head groups of anionic phospholipids. The mainly hydrophobic membrane-insertion loop Leu313-Ala-Phe-Trp-Lys317, containing a typical Trp-Lys membrane anchor, provides specificity for lipid layers. Crystal structures of β2gpI *1 (this work) and intact β2gpI[251] add new insights contributing to a more detailed lipid adhesion model. The electrostatic surface potentials calculated with the models of β2gpI *1, β2gpI 1QUB and intact β2gpI (Fig. 5 A-C) suggest a potential three-step membrane-adhesion model. Free in solution, a primary positively charged patch located at the C-terminal top of domain V is fully exposed (Fig. 5B) and can interact with any negatively charged surface present in the circulation. Binding to anionic lipids exposed on blood platelets, lipoproteins or apoptotic cells possibly induces membrane insertion of loop Leu313-Ala-Phe-Trp-Lys317, providing specificity for phospholipid layers. Wang *et al.* (162) reported an increase in α-helical content after lipid adhesion of β2gpI. Possibly, interaction of the primary patch with phospholipids not only orients the membrane anchor prior to insertion, but additionally induces conformational changes in β2gpI in favor of membrane insertion. After insertion of loop 313-317, mimicked by deletion of the loop in the β2gpI *1 and β2gpI 1QUB models, a secondary positively charged patch becomes exposed for additional charge interactions with negatively charged head groups of anionic phospholipids (Fig. 5A, C). This will provide further specificity of β2gpI towards phospholipid membranes. Apparently, the positive electrostatic surface potential of the secondary patch remains shielded by the mainly hydrophobic loop 313-317 in solution or when β2gpI adheres non-specifically to any negatively charged surface other than provided by anionic lipids, e.g. when it binds to DNA and heparin (Fig. 5B).

Our data indicate that specific uptake of a neutral phospholipid blocks adhesion of β2gpI to anionic lipids. In this inactive state the glycerophosphorylcholine moiety is positioned inside the pocket between the primary and secondary membrane-adhesion patches, whereas the two acyl chains point away from the protein surface (Fig. 3A, 5A). These long hydrophobic acyl chains may inhibit adhesion to lipid layers by interacting with the mainly hydrophobic membrane-insertion loop Leu313-Ala-Phe-Trp-Lys317, by steric hindrance, or by shielding the positive electrostatic surface potential of the primary patch, analogous to observed shielding of the secondary membrane-adhesion patch by the insertion loop 313-317 (Fig. 5B).

β2gpI *1 is present in plasma of patients who suffered from oxidative stress. Severe complications induced by this oxidative stress are, among others, *i.* undesired uptake of oxidized lipoproteins by macrophages[119], and *ii.* auto-immune responses against oxidized lipoproteins[118,119], abundantly present apoptotic cells[131,142,142,265] and β2gpI[266,267,287,288]. Two defense mechanisms are known that prevent damage induced by oxidized lipoproteins. Firstly, (choline) plasmalogens in lipoproteins are oxidized and act as antioxidant[279,289]. Secondly, oxidized lipoproteins are prevented from uptake through the binding of β2gpI to cardiolipin[72,75] and to adducts of oxidized lipids and proteins[267,268,290] present in the lipoproteins paricles. Our findings show that β2gpI *1 has a neutral phospholipid bound. This suggests new potential functions for β2gpI *1 in reversal of oxidative stress; *i.* uptake of CL may be directly involved in removal of oxidized CL from the lipoproteins, *ii.* reduced affinity of β2gpI *1 for anionic lipids prevents formation of highly immunogenic complexes of its precursor β2gpI with apoptotic bodies or oxidized lipoproteins, and *iii.* uptake of neutral lipids by β2gpI may induce clearance of apoptotic bodies by enlargement of their anionic receptor-recognition site[135,136].
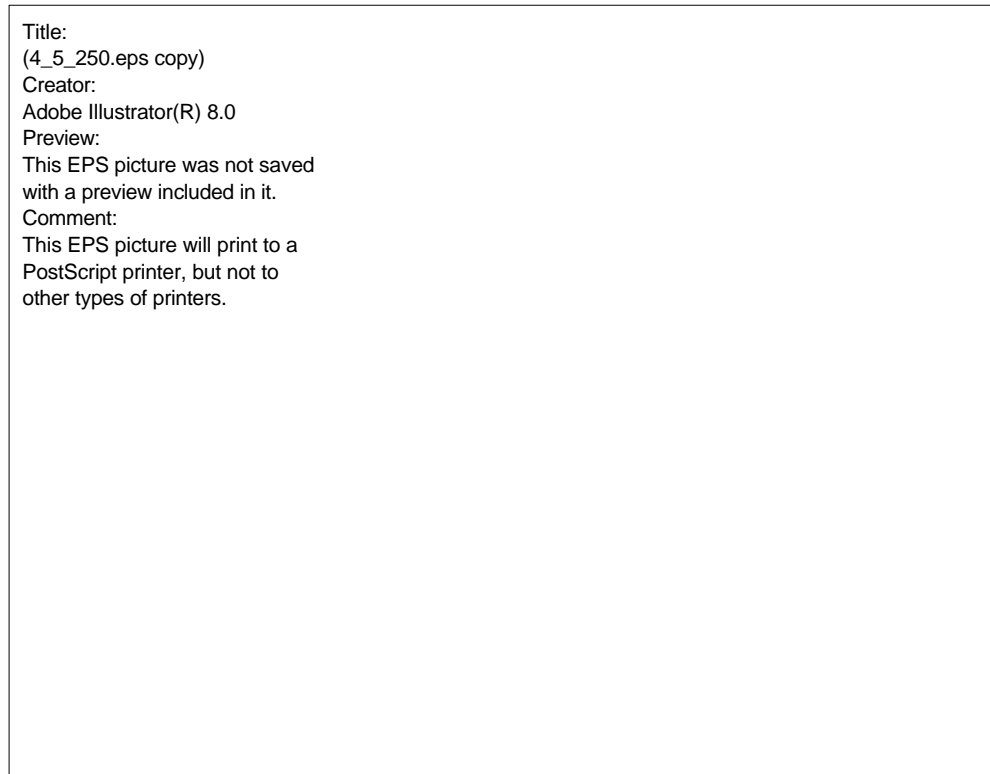
Acknowledgements

Fig. 5. Electrostatic surface potential at the positively charged membrane-adhesion patch, calculated with three models of β2gpI. Positive charge is encoded in blue, negative charge is in red, neutral patches are in white. (**A**) Primary and secondary positively charged membrane-adhesion patches on the fifth SCR domain of β2gpI *1 (This work). Loop 310-317 was not visible in the electron density and is not implied in the model. The bound glycerophosphorylcholine moiety is positioned deeply in the interior of the pocket, located in the center of the positively charged patch. Residue Asp319, that interacts with the choline moiety and that is located at the bottom of the neutral-lipid binding pocket is indicated. (**B**) Membrane-adhesion site of intact β2gpI 1C1Z[251]. The position of loop 311-317 was indicated by the electron density, most likely aided by an intact scissile bond Lys317-Thr318. The primary positively charged membrane-adhesion site is exposed in solution and is available for charged interactions with negatively charged surfaces. The secondary patch is largely shielded likely by the presence of the exposed and mainly hydrophobic membrane-insertion loop Leu313-Ala-Phe-Trp-Lys 317. The electrostatic surface potential calculated with the model of intact β2gpI omitting residues 311-317 (not shown), resembles the potential calculated for β2gpI 1QUB and β2gpI *1 (Fig. A and C), and may mimic the expanded membrane-adhesion patch involved in protein-lipid interactions in the membrane-bound state. (**C**) Membrane-adhesion site of β2gpI 1QUB[250]. Loop 311-317 was disordered or mobile in the structure and is not implied in the model. Residues that contribute to the primary and secondary adhesion patches are indicated. (**D**) Ribbon drawing of SCR domain V of intact β2gpI. The orientation of the domain is similar to the orientations in figures A-C.

--- Appendix to Chapter IV ---

Analysis of the influence of structural radiation damage on β_2-glycoprotein I

Brief introduction to radiation damage

X-ray diffraction experiments suffer from radiation damage. Important indicators for radiation damage are, *i.* a decrease in resolution limit, *ii.* an increasing overall B-factor, and *iii.* an increasing mosaicity. Cryo-cooling largely suppresses the globular effects of radiation damage; in particular yielding a significant prolonged life time of the crystals during data collection[20,21]. Recently however, Weik *et al.* (22), Burmeister (24) and Ravelli and McSweeny (23) reported insights into highly specific effects of X-rays on the structure of protein molecules. In particular, these effects are observed when crystals are irradiated with very intense X-ray beams of third generation synchrotrons, e.g. using the beam lines of ID14 at the European Synchrotron Radiation Facility (ESRF, Grenoble, France)[a]. The occurrence of specific structural radiation damage calls for careful consideration of data-collection strategy and subsequent structure determination, validation and interpretation.

In a protein structure, effects of specific structural radiation damage can be recognized by diminished electron density at the expected position of S-S, C=O, OH and S-C groups and by relatively high corresponding B-factors. These observations indicate breaking of disulfide bonds, decarboxylation of aspartate and glutamate residues, and release of hydroxyl and methylthio groups of tyrosines and methionines, respectively.

Ravelli and McSweeny (23) suggested that several published crystal structures are likely affected by radiation damage, without being noticed. In *Chapter II* the crystal structure of human β_2-glycoprotein I (β2gpI) is presented (pdb code 1QUB, Ref. 250). X-ray data used for refinement of the β2gpI model were collected on beam line ID14-EH4 (ESRF). Reconsideration of the disulfide bonds in β2gpI model 1QUB revealed that all 22 cystines were possibly affected to some extent by the intense X-ray beam, as indicated by relatively high B-factors for S_γ-atoms with respect to those for C_β-atoms. In addition, positions of carboxyl groups of Glu285 and Glu309 were poorly defined by the electron density, indicating that they may also be affected by the intense beam. These observations prompted us to further investigate data sets measured from two crystals of an isoform of β2gpI and the models obtained with these data, in reference to the markers that identify specific structural radiation damage. A method is suggested and described for refinement of partially affected disulfide bonds. Effects of local and specific radiation damage on the global fold of the β2gpI structures and on local structural details were considered. The effects and the degree of radiation damage should be taken into account when comparing models.

Data sets from β2gpI *1 crystals

In *Chapter IV* we described the crystal structure of an isoform of β2gpI, designated 'β2gpI *1'. Diffraction data from two crystals of β2gpI *1 were collected on ESRF beam line ID14-EH1, referred to as 'crystal 1' (See *Chapter IV*) and on ID14-EH3, designated 'crystal 2'. Details on data collection are shown in Table I. The intensity ratio between beam lines ID14-EH1 and ID14-EH3 is approximately 3:1. Crystal 1 had a ~15 times bigger volume than crystal 2. For both data sets slit sizes used were smaller than the crystal sizes, thus only part of the crystals was irradiated. Crystal 1 was exposed for in total 1,080 sec. to the beam of

---

[a] Abbreviations used: β2gpI, β_2-glycoprotein I; ESRF, European synchrotron radiation facility; ID14-EH#, insertion device 14-experimental hutch number #; PDB, protein data bank; r.m.s., root-mean-square; SCR, short concensus repeat.

EH1, crystal 2 was exposed for in total 3,690 sec. to the beam of EH3. Diffraction data were processed and scaled using DENZO and SCALEPACK[26] and similar statistics were observed for the two crystals (See Table I in *Chapter IV* and Table II).

Table I

Settings for data collection

	β2gpI *1 crystal 1	β2gpI *1 crystal 2
Beam line[†]	ID14-EH1	ID14-EH3
Relative intensity	~3	1
Wavelength (Å)	0.934	0.931
Slits (μm x μm)	200 x 200	100 x 100
Oscillation range (°)	1	1
Oscillation step (°)	1	1
Exposure time per image (sec.)	6	30
No. of images	180	123
No. of images used for structure refinement	140	110
Temperature (K)	100	100
Crystal volume (μm^3)	~36	~2.2
Change of cell volume (%)	+0.6	+1.2
Relative global B-factor (Å^2)[¶]	2.9 (1.0)	10.6 (8.5)

[†] Data sets were collected at the ESRF (Grenoble, France).

[¶] Relative global B-factors are given for the last recorded image. For the first image the overall B-factor is set to 0. Numbers between parentheses give the relative global B-factor for the last recorded image that is used for structure refinement.

Data set collected on ID14-EH1 from crystal 1

The data set collected on beam line ID14-EH1 from crystal 1 comprised 180 images. The first 140 images were used for structure refinement. The relative global B-factor varied non-monotonously (Fig. 1A). The length of the *a*-axis varied discontinuously (Fig. 1B). An initial decrease of the B-factor (images 1-80) was accompanied by lengthening of the *a*-axis, whereas a subsequent slight increase of the B-factor (images 80-180) was accompanied by shortening of the *a*-axis. The observed effects represented in Fig. 1A and B are influenced by the inaccuracies in their determination due to the limited amount of data used in processing a single image. Additionally, the anisotropy of the crystal shape may also be of influence. Variations in the length of the *b*- and *c*-axis were relatively small during the course of data collection (Fig. 1C, D). The increase in cell volume was 0.6% from image 1 to 180 and 0.4% for images 1-140 (Fig. 1E). The high-resolution limit did not noticeably drop during data collection.

Data set collected on ID14-EH3 from crystal 2

In total, 123 images were recorded from crystal 2 of which the first 110 were used for structure refinement. See Table II for the diffraction-data statistics. Crystal 2 proved to be subjected to severe radiation damage. During data collection non-specific radiation damage was indicated within the data set by an increase of the relative global B-factor to 10.6 Å^2 for the last image (Fig. 1A, Table I). Simultaneously, the length of the *a*-axis and the *c*-axis increased gradually by 0.8% and 0.5%, respectively (Fig. 1B, D). Alternatively, the length of the *b*-axis increased by 0.3% up to image 65 and then decreased again by 0.3% (Fig. 1C). The increase in cell volume was more than 1% for images 1-123 (Fig. 1E). The high-resolution limit slightly dropped with 0.1 Å.
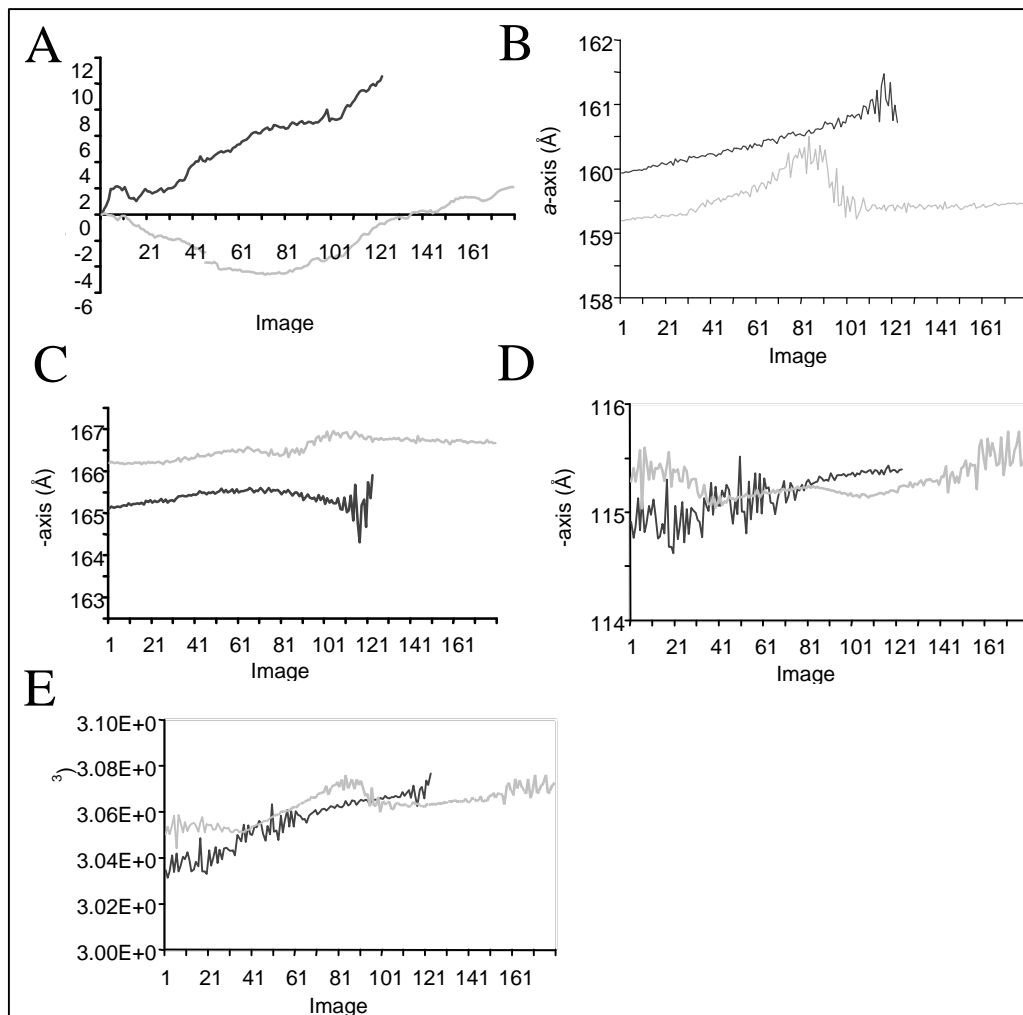
Fig. 1. Global non-specific radiation damage and specific structural radiation damage for diffraction data of β2gpI *1 collected on beam line ID14-EH1 from crystal 1 and on ID14-EH3 from crystal 2. Curves for data collected on ID14-EH1 (ESRF, Grenoble, France) are in gray, curves for data collected on ID14-EH3 are in black. (**A**) Relative global B-factor in Å[2], as printed per image in the SCALEPACK output[26] (**B**) Length of the *a*-axis during the course of the data collection. (**C**) Length of the *b*-axis. (**D**) Length of the *c*-axis. (**E**) Total cell volume during the course of data collection. Cell volumes are calculated with diffraction data from individual images.

Structure refinement

Two models of β2gpI *1 were refined using diffraction data from crystal 1 (ID14-EH1) and crystal 2 (ID14-EH3) and using the structure of β2gpI reported by Bouma *et al.* (250) as a starting point (See *Chapter IV*). Rigid-body refinement, positional refinement and atomic B-factor refinement were performed with CNS[9]. Refinement statistics for the two independent models are similar and are shown in Table I in *Chapter IV* and in Table II, respectively. After refinement of the models markers for the occurrence of specific structural radiation damage were investigated.

Table II

Data-collection and structure-refinement statistics for diffraction data collected on beam line ID14-EH3 from crystal 2

Diffraction-data statistics[†]		Refinement statistics[§]	
Resolution (Å)	38.4 – 3.0	Resolution (Å)	38.4 – 3.0
Mosaicity (°)	0.7	R-factor/R$_{free}$	0.248/0.272
Space group	C222$_1$	r.m.s.d. bond distances (Å)	0.008
Unit cell: *a b c* (Å)	160.5 165.7 115.5	r.m.s.d. angles (°)	1.4
Redundancy	3.9	Average B-factor (Å^2)[¥]	59
No. unique reflections	29,965	Solvent content (%)	88
$<I>/<\sigma(I)>$	16.6 (3.0)	No. non-hydrogen atoms	2,701
Completeness (%)	96.3 (94.5)	No. protein residues	319
R$_{merge}$ (%)	6.3 (43.3)	No. sugar residues[‡]	12
		No. sulfate ions	2
		No. lipid molecules[¶]	1

† Numbers in parentheses indicate statistics for the highest resolution shell (3.11-3.00 Å). Data were collected on ESRF beam line ID14-EH3. See *Chapter IV* for comparison of the statistics with those of data collected on ID14-EH1 from crystal 1.

§ Disulfide bonds were not specified in the model and, instead cysteines were refined. The van der Waals radius of the S$_\gamma$-atoms was set to 0.

¥ Average atomic B-factor for all atoms in the model.

‡ Forty to sixty sugar residues are expected, based on MALDI-TOF mass spectrometry.

¶ A glycerophosphorylcholine moiety, which is part of, either phosphatidylcholine, sphingomyelin, or choline plasmalogen, was built in the structure.

Methionines and tyrosines
For both models the four methionine residues and 14 tyrosine residues present were not affected by radiation, as judged from the electron density and from atomic B-factors for S-C and O-H groups.

Aspartates and glutamates
Complete and unaltered electron density at positions of side chains of the 14 Asp and 20 Glu amino-acid residues was observed for crystal 1. Complete electron density at the side-chain positions of 13 Asp and 11 Glu residues in the model from crystal 2 indicated that most of these residues were not severely affected by the intense X-ray beam. Weak electron density for the carboxyl groups of Asp9 and Glu108, Glu154, Glu180, Glu225, Glu259, Glu265, Glu292 and Glu302, however, indicated that the carboxyl group of these residues was, either partially cleaved off , or disordered or mobile. The carboxyl group of solvent exposed Glu114 was apparently cleaved off completely, according to the absence of electron density (Fig. 2A). Noteworthy, the position of a water molecule that likely forms a hydrogen bond

with atom $O_{\varepsilon 1}$ or $O_{\varepsilon 2}$ of Glu114 is still indicated in the electron-density map. This water molecule was also visible in the crystal structure of β2gpI reported by Bouma *et al.* (250).

```
Title:
(a_2.eps)
Creator:
Adobe Illustrator(R) 8.0
Preview:
This EPS picture was not saved
with a preview included in it.
Comment:
This EPS picture will print to a
PostScript printer, but not to
other types of printers.
```
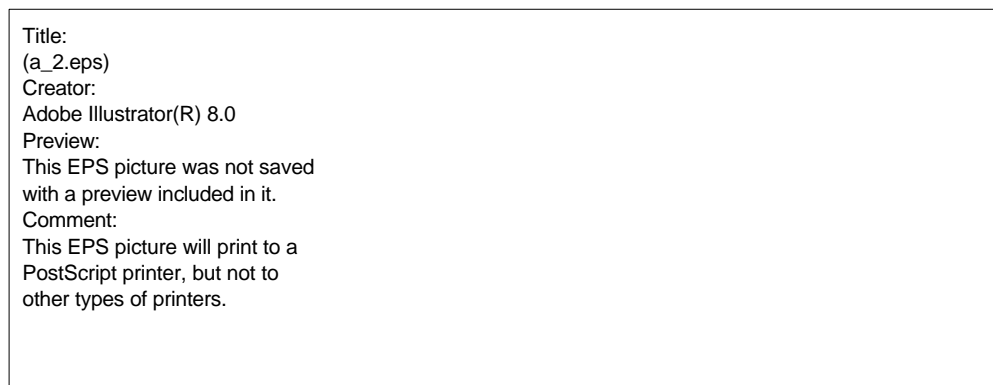
Fig. 2. Weak electron density for solvent exposed cystines in disulfide bond 281-306 and glutamate 114 indicated that β2gpI *1 (crystal 2) suffered from severe specific structural radiation damage. The figure is generated with BOBSCRIPT[277] and RASTER3D[203]. (**A**) Electron density contoured at 1 σ accounting for the carboxyl group of Glu114 of β2gpI *1, (crystal 2, left). The density indicates that the carboxy group is at least partially cleaved off. The position of a water molecule that putatively forms a hydrogen bond with atom $O_{\varepsilon 1}$ or $O_{\varepsilon 2}$ of Glu114, is still manifest. For comparison Glu114 of the structure derived from data collected on ID14-EH1 from crystal 1 is shown (right). (**B**) Electron density for the strongly affected disulfide bond Cys281-Cys306 in β2gpI *1 (crystal 2, ID14-EH3, left). The S_{γ}-S_{γ} distance is 3.31 Å. For comparison the less affected disulfide bond Cys281-Cys306 in the structure derived from data collected on ID14-EH1 from crystal 1 is shown (right).

Cystines

The fish-hook shaped β2gpI molecule consists of five short consensus repeat (SCR) domains arranged in tandem. Half of the fifth C-terminal domain has an aberrant fold, whereas the other half has a fold similar to domain I-IV (Fig. 3). The standard SCR domains contain two disulfide bonds (Fig. 3). Nine of the ten disulfide bonds in β2gpI *1 are located in the core of the domains surrounded by hydrophobic side chains, whereas in domain V disulfide bond 281-306 is highly solvent exposed and partially surrounded by charged side chains. The aberrant domain V contains an additional third disulfide bond 288-326. This disulfide bond is fully solvent exposed (Fig. 3) and partially surrounded by charged amino-acid side chains.

For crystal 1 complete electron density was observed for all eleven disulfide bonds in a $2|F_o|-|F_c|$ map. Negative electron density is observed for S_{γ} of Cys281 in an $|F_o|-|F_c|$ difference map. Atomic B-factors were slightly increased (+2 to +9 Å^2) with respect to C_{β}-atoms for 14 out of 22 cystine S_{γ}-atoms. These observations indicated an early stage of specific and localized structural radiation damage. Weik *et al.* (22) and Ravelli and McSweeney (23) addressed severe damage of disulfide bonds, expressed as the lost definition of the S_{γ}-atom in the electron density, by refining alanine residues instead of cystines. In our case this procedure was at forehand not recommendable because disulfide bonds appeared predominantly intact in this structure. To take into account that disulfide

bonds were potentially partially broken we replaced all cystines by cysteines with the van der Waals radius of S_γ-atoms set to 0. After positional refinement S_γ-S_γ distances were all still close to 2.05 Å with somewhat larger distances observed for Cys155-Cys181, Cys245-Cys296 and Cys281-Cys306 (Table III). Atomic B-factors for the S_γ-atoms did not differ significantly from those when positions of S_γ-atoms were restrained during refinement of specified disulfide bonds. The R-factor increased from 0.238 to 0.246, the free R-factor increased from 0.260 to 0.270, when refining cysteines. These results for crystal 1 suggested that breaking of disulfide bonds had not yet occurred to a large extent for most of the bonds. Similar positions of the S_γ-atoms for eight out of the eleven disulfide bonds present indicated that cysteine refinement (van der Waals radius of S_γ-atoms set to 0) does not influence disulfide bonds which are not or hardly effected by radiation damage. Moreover, for β2gpI *1 (crystal 1) the observed increase in free R-factor validates restrained refinement of the S_γ-atoms in disulfide bonds, as performed previously with this model (*Chapter IV*).

During early stages of refinement of the model obtained with crystal 2 disulfide bonds were specified and, therefore, positions of S_γ-atoms were restrained. In the structure, disulfide bonds of β2gpI *1 proved to be affected by specific structural radiation damage. Negative peaks in $|F_o|$-$|F_c|$ difference-density maps were observed near each of the eleven disulfide bonds. Electron density in $2|F_o|$-$|F_c|$ maps at the positions of disulfide bonds 91-118, 155-181, 186-229, 245-296 was weak compared to maps calculated with the model from crystal 1, and electron density for disulfide bonds 281-306 (Fig. 2B) and 288-326 in domain V was very weak. B-factors for the S_γ-atoms were slightly increased (+2 to +14 Å^2) compared to B-factors for the C_β-atoms. These observations indicated that at least the six bonds that show weak electron density were partially broken. Replacement of cystines by alanines and subsequent positional and atomic B-factor refinement resulted in positive peaks in $|F_o|$-$|F_c|$ difference density maps at each of the 22 expected positions of the S_γ-atoms. The R-factor increased from 0.248 to 0.269, the free R-factor increased from 0.272 to 0.290. These observations indicated that disulfide bonds were not completely broken. After refinement with cysteines instead of cystines and with the van der Waals radius of S_γ-atoms set to 0, the R- and free R-factor were not influenced. Occurrence of specific damage was, however, clearly indicated by (large) movements of all S_γ-atoms except for disulfide bond Cys65-Cys105 (Table III). Despite new positions for the S_γ-atoms, the electron density in the regions of the disulfide bonds was not significantly altered in the $2|F_o|$-$|F_c|$ maps at 3.0 Å resolution.

Comparison of the eleven disulfide bonds of severely damaged crystal 2 showed that these bonds have varying susceptibilities to radiation (Table III). In summary, largest movements of S_γ-atoms were observed for solvent exposed disulfide bonds 281-306 and 288-326 in domain V accompanied with relatively weak electron density at the expected position of the bonds. This observation indicates that these two disulfide bonds are relatively highly susceptible to radiation. This may be correlated with their high solvent accessibility or possibly by the surrounding charged side chains. Cys65-Cys105 in SCR domain II is the only disulfide bond that stays intact when S_γ-atoms were not restrained in disulfide bonds. The electron density is virtually unaltered at the position of this bond. This indicates that Cys65-Cys105 is the least susceptible disulfide bond of β2gpI *1. The remaining eight disulfide bonds were to various degrees affected by radiation damage. In contrast to the high solvent accessibility of the two most susceptible disulfide bonds in domain V, the other nine disulfide bonds are all located inside the hydrophobic core of the SCR domains and are

surrounded by hydrophobic side chains. Therefore, observed differences in susceptibility for radiation among these disulfide links may depend on different aspects of the micro-environment of the bonds. The limiting resolution of the diffraction data (3 Å) hamper further detailed consideration of those micro-environments.
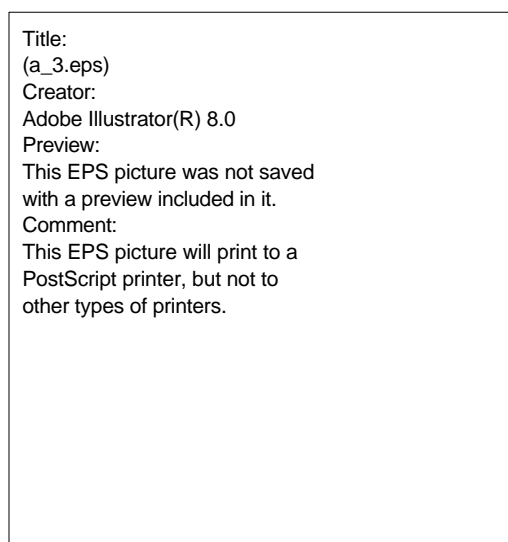

Fig. 3. Location of disulfide bonds in the short consensus repeat domains of β2gpI *1. C_α-trace representation of SCR domain I of β2gpI *1, that is representative for the fold of domains II-IV (left), and C_α-trace representation of domain V (right). One half of domain V has a fold reminiscent to the fold of domains I-IV, whereas the other half has an aberrant fold. Fully exposed disulfide bond Cys288-Cys326 is unique to domain V. Solvent exposed disulfide bonds Cys281-Cys306 and Cys288-Cys326 are most susceptible to radiation among the eleven bonds of β2gpI. Glu309 and Thr318 indicate the position of loop 310-317 that is not observed in the electron density. Disulfide bonds are indicated by ball-and-stick models and are labeled with their residue numbers. The figure is generated with MOLSCRIPT[202] and RASTER3D.

Comparison of available models of β2gpI

A similar range of root-mean-square (r.m.s.) coordinate differences are observed after superimposing C_α-atoms of the five individual SCR domains of the two β2gpI *1 models (Table IV), despite varying degrees of specific structural radiation damage. In addition, superposition of the C_α-atoms of each of the SCR domains of the two β2gpI *1 models and of β2gpI models 1QUB and 1C1Z reported by Bouma *et al.* (250) and Schwarzenbacher *et al.* (251) respectively, revealed a similar range of r.m.s. coordinate differences. This demonstrated that the global conformation of β2gpI *1 is not influenced by specific local radiation damage. The relatively large r.m.s. coordinate differences of 0.3 Å after superimposing C_α-atoms of the fifth SCR domain of the two β2gpI *1 models (Table IV) resulted mainly from deviating positions of C_α-atoms of residues Cys245 and Cys306, and of residues Glu309 and Thr318. In both structures Glu309 and Thr318 precede and follow a highly flexible or disordered loop of β2gpI (See *Chapter II* and *Chapter IV*), which likely

resulted in intrinsic mobility of these two flanking residues. The slight difference in positions of C$_\alpha$-atoms of Cys245 and Cys306 is due to the fact that crystal 2 was more damaged than crystal 1. Positions of C$_\alpha$-atoms of amino-acid residues flanking these cysteines are very similar among the two models, further indicating that the effects of specific structural radiation damage were very locally restricted.

Table III

*Relative susceptibility to radiation of disulfide bonds in **b**2gpI*
*1 as indicated by S$_g$-S$_g$ distances and electron density

Disulfide bonds	S$_\gamma$-S$_\gamma$ distance (Å)[†]		Electron density in the region of disulfide bonds[‡]
Cys-Cys	Crystal 1	Crystal 2	
4-47	2.23	2.45	Virtually unaltered
32-60	2.12	2.57	Virtually unaltered
65-105	2.18	2.16	Virtually unaltered
91-118	2.23	3.09	Weak
123-169	2.09	2.35	Virtually unaltered
155-181	2.39	2.93	Weak
186-229	2.19	2.52	Weak
215-241	2.22	2.50	Virtually unaltered
245-296	2.40	2.85	Weak
281-306	2.59	3.31	Very weak
288-326	2.24	3.32	Very weak

[†] During refinement disulfide bonds were not specified and the van der Waals radius of S$_\gamma$-atoms in cysteines was set to 0. The S$_\gamma$-S$_\gamma$ distance in a non-affected disulfide bond is 2.05 Å. Data from crystal 1 are collected at ESRF beam line ID14-EH1 (Grenoble, France), data from crystal 2 are collected at ID14-EH3.
[‡] The classification is based on a comparison of the observed electron density near the disulfide bonds of crystal 1 with density accounting for the bonds in crystal 2 in a 2|F$_o$|-|F$_c$| map.

Table IV

Superposition of C$_a$-atoms of individual SCR
*domains using two **b**2gpI *1 models*

SCR domain	No. amino-acid residues	r.m.s. coordinate difference (Å)[†]
I	61	0.249
II	58	0.192
III	63	0.139
IV	58	0.179
V	76	0.307

[†] C$_\alpha$-atoms of each of the SCR domains of the model refined using data collected on ESRF beam line ID14-EH3 from crystal 2 are superimposed on the C$_\alpha$-atoms of the equivalent SCR domains of the model refined using data collected on ESRF beam line ID14-EH1 from crystal 1.

Conclusion

In this *Appendix* a new refinement protocol is used for structures with partially broken disulfide bonds upon irradiation with intense X-ray beams. During refinement cysteines with a van der Waals radius of 0 were incorporated in the model instead of cystines. After positional and atomic B-factor refinement the procedure was validated by investigation of changes in S_γ-S_γ distances, of peaks in $|F_o|$-$|F_c|$ difference maps, of relative values of the B-factors for C_α, C_β and S_γ-atoms, and of $2|F_o|$-$|F_c|$ electron density accounting for the partially broken disulfide bonds. Applying the refinement method to crystal 1 revealed that all disulfide bonds were affected to a minor extent. The procedure was also applied to crystal 2 obtained with data from ID14-EH3. For five out of six disulfide bonds for which weak electron density was present, relatively large movements of the S_γ-atoms were observed, whereas no large movements were observed for disulfide bonds with virtually unaltered electron density (Table III). These observations proved that the refinement method was useful for our model containing partially broken disulfide bonds (crystal 2). For this model the moved positions of S_γ-atoms of the refined cysteines and weak electron density for several partially broken disulfide bonds allowed for a first classification of the eleven disulfide bonds of β2gpI *1 with respect to their susceptibility to radiation. Comparison suggested that solvent exposed disulfide bonds partly surrounded by charged side chains of amino-acid residues were more susceptible than buried disulfide bonds surrounded by hydrophobic side chains. A detailed analysis of the micro-environment of disulfide bonds requires high-resolution diffraction data and is necessary for identification of parameters that determine the apparent differences in susceptibility.

Comparison of the severely affected model of β2gpI *1 with available models of β2gpI showed that specific structural radiation damage (at 100 K) is localized to a few types of amino-acid residues, *i.e.* acidic residues and cystines. No changes in global conformation of β2gpI *1 were observed. Thus, the structural implications presented in *Chapter IV* were not compromised by specific radiation damage.

Acknowledgements

--- Chapter V ---

Structure of a von Willebrand factor A3-domain – Fab complex points to a location for the collagen-binding site

Barend Bouma[1*], Eric G. Huizinga[1,2*], Marion E. Schiphorst[2], Jan J. Sixma[2], Jan Kroon[1] and Piet Gros[1]

[1]Bijvoet Center for Biomolecular Research, Department of Crystal and Structural Chemistry, Utrecht University, Padualaan 8, 3584 CH, Utrecht, The Netherlands, and [2]Haemostasis and Thrombosis Laboratory, University Medical Center Utrecht, PO Box 85500, 3508 GA, Utrecht, The Netherlands.

* The first two authors contributed equally to this work.

Summary

Von Willebrand factor (vWf) is a multimeric glycoprotein that mediates platelet adhesion and thrombus formation at sites of vascular injury. vWf functions as a molecular bridge that binds to collagen that is exposed by the damaged vessel wall, and to glycoprotein Ib at the platelet surface. The major collagen-binding site of vWf is contained within the A3 domain, but its precise location is not known. To localize the collagen-binding site, we determined the crystal structure of A3 in complex with a Fab fragment of antibody RU5 that inhibits binding of vWf to collagen. The structure was solved at 2.0 Å resolution by molecular replacement, aided by the anomalous signal of seleno-methionines in A3. The epitope of RU5 involves residues 962-966, 981-997 and 1022-1026 that are part of α-helix 2 and loops $\alpha1\beta2$, $\beta3\alpha2$ and $\alpha3\beta4$, located at the 'bottom' side of A3, but opposite to the N- and C-terminus. Comparison with other structures of A3 shows that RU5 binding does not induce long-range conformational changes. Instead, RU5 most likely blocks collagen binding by steric hindrance, which implies that the collagen-binding site is located at or close to the epitope of RU5 near the bottom side of A3. Surprisingly, the collagen-binding site of vWf-A3 is located distant from the top face of the domain where collagen-binding sites are found in homologous integrin I-domains. Apparently, vWf-A3 and integrin I-domains bind collagen in fundamentally different ways. Coordinates are in the Protein Data Bank (accession code 1FE8).

Key words: A domain, A3 domain, collagen binding, conformational changes, crystal structure, Fab fragment of antibody RU5, I domain, integrin, mutations, von Willebrand factor

72

Introduction

Platelet adhesion to damaged vessel walls is the first step in the formation of an occluding platelet plug, which leads to the arrest of bleeding during normal haemostasis. Platelet adhesion can also cause thrombotic complications such as the occlusion of aetherosclerotic arteries[183]. The multimeric glycoprotein von Willebrand factor (vWf)[a] plays an essential role in platelet adhesion under conditions of high shear stress[166,167]. In this process vWf serves as a molecular bridge that links collagen exposed by the damaged vessel wall to glycoprotein Ib (gpIb) located on the platelet surface. Collagen types that act as binding sites for vWf include collagen I and III in perivascular connective tissue and collagen type VI in the sub-endothelial matrix[167,168].

Mature vWf consists of a 2,050 residue monomer that contains multiple copies of so called A, B, C and D-type domains and one CK (cystine knot) domain arranged in the order D'-D3-A1-A2-A3-D4-B1-B2-B3-C1-C2-CK[167,183]. Disulfide-bond formation between N-terminal D3 domains and between C-terminal CK domains generates vWf multimers that consist of up to 80 monomers. The A1 domain contains the binding site for gpIb[291]. The A3 domain (residues 920-1111) contains the major binding site for collagen types I and III[180]. The multimeric structure of vWf is essential for high-affinity collagen binding. Multimeric vWf binds collagen with an apparent K_d of 1-7 nM[201], while a recombinant A3 domain has a much higher K_d of 2 μM[292]. Deletion of the A2 and D4 domains, that flank the A3 domain, or deletion of the A1 domain does not decrease collagen binding of multimeric vWf[180,201]. These data show that a monomeric A3 domain contains a fully active collagen-binding site, the only requirement for tight binding to collagen being the presence of multiple A3 domains within one vWf multimer.

Integrin I-type domains are homologous to vWf A-type domains[293,294]. I-domains of integrin α-chains α1, α2, α10 and α11 all possess collagen-binding sites. A crystal structure of the α$_2$ I-domain reveals binding of a collagen-like peptide to a groove in the surface of the 'top' face of the domain[200]. This groove contains a so-called metal ion-dependent adhesion site (MIDAS) motif[198,295] which engages a glutamate residue of collagen.

The location of the collagen-binding site in the vWf A3 domain is not known. Crystal structures of A3 do not display a collagen-binding groove in the top face, instead the surface of A3 is rather smooth[193,194]. Although the MIDAS motif is partly conserved, binding of A3 to collagen does not require a metal ion[296] and no metal ion is observed in crystal structures of A3. Moreover, point mutations in the MIDAS motif of A3 (D934A, D934A/S936A, S938R, S1005V, D1039Q, D1039A) do not disrupt collagen binding[193,201] showing that the motif is not involved in collagen binding, at all. Site-directed mutagenesis studies of other residues in the top face of A3 have yielded conflicting results. Cruz *et al.* (297) reported in abstract form that amino-acid substitutions D1069R, R1074D, R1090D and E1092R resulted in a 50% reduction in binding of monomeric A3 to collagen. Van der Plas *et al.* (201), however, observed normal collagen binding of fully processed multimeric vWf

---

[a] Abbreviations used: a.u., asymmetric unit; CDR, complementarity determining region; C$_{H1}$, constant domain H1 of an immunoglobulin heavy chain; CK, cystine knot; C$_L$, constant domain of an immunoglobulin light chain; DLS, dynamic light scattering; Fuc, fucose; GlcNAc, *N*-acetylglucosamine; gpIb, platelet glycoprotein Ib; IEF, iso-electric focussing; MPD, 2-methyl-2,4-pentanediol; MW, molecular weight; n.c.s., non-crystallographic symmetry; PBS, phosphate-buffered saline; PCR, polymerase-chain reaction; r.m.s., root-mean-square; SDS PAGE, sodium dodecylsulfate poly-acrylamide gel electrophoresis; Se-Met, seleno-methionine; V$_e$, elution volume; V$_H$, variable domain of an immunoglobulin heavy chain; V$_L$, variable domain of an immunoglobulin light chain; vWf, von Willebrand factor.

containing mutations D1069A, D1069R or R1074A. In the same study, mutations V1040A/V1042A, D1046A and D1066A also displayed normal collagen binding, suggesting that the collagen-binding site of vWf-A3 is not located in its top face.

The crystallographic study presented here was conducted to provide new clues on the location of the collagen-binding site of the vWf-A3 domain. We determined the structure of the A3 domain in complex with a Fab fragment of antibody RU5, which inhibits binding of vWf-A3 to collagen. The crystal structure of A3-RU5 now provides strong evidence for an alternative location of the collagen-binding site, located distant from the top face of A3.

Experimental procedures

Protein purification

Recombinant seleno-methionine (Se-Met) A3, comprising residues 920 to 1111 of human von Willebrand factor, was produced in *Escherichia coli* strain B834 and subsequently folded and purified as described before[194]. The histidine tag was removed by thrombin digestion. (Se-Met) A3 appeared as one band with a molecular weight (MW) of 22 kDa after sodium dodecylsulfate poly-acrylamide gel electrophoresis (SDS PAGE). On an iso-electric focussing gel (IEF), four bands with similar intensities were visible with a pI ranging from 4.6 to 5.2.

For production of monoclonal antibody RU5 (IgG$_{2a, \kappa}$) hybridoma cells were injected in mice and ascites fluid was collected (Eurogentec, Seraing, Belgium). The ascites fluid was diluted with an equal volume of loading buffer (phosphate-buffered saline pH 7.3, PBS) before purification of IgG on a 5 ml protein G-Sepharose column (Pierce, Rockford IL, USA). Elution buffer was 0.1 M glycine pH 2.7. Fab fragments were generated, using an ImmunoPure Fab Kit according to the manufacturers recommendations (Pierce, Rockford IL, USA). In short, IgG was incubated with papain-coated beads for 6 h at 37ºC, and Fc fragments and uncut IgG were removed on a Protein A-Sepharose column. RU5 Fab was further purified with A3-affinity chromatography. For that end, 10 mg of A3[194] was irreversibly bound via its N-terminal histidine tag to cobalt(III)-iminodiacetate chelating Sepharose (Pharmacia Biotech, Uppsala, Sweden), according to a procedure described by Hale (298). A 2.5 ml column was equilibrated with PBS before use. Solution containing Fab fragments was loaded and the column was washed with 10 ml of PBS, 10 ml of a 2 M NaCl solution, and 10 ml of PBS, respectively. Bound RU5 Fab fragments were eluted with 7.5 ml of a 50 mM tri-ethylamine solution (pH 10.0). Some aggregates were removed on a Superdex 75 HR 10/30 gel-filtration column (Pharmacia, Uppsala, Sweden). Running buffer was 10 mM Tris-HCl pH 8.0, 25 mM NaCl. RU5 Fab was concentrated to 10 mg ml^{-1} using Centriplus and Centricon concentrators with a molecular-weight cut-off of 30 kDa (Amicon, Beverly MA, USA). After SDS PAGE, RU5 Fab appeared as one band with an MW of 55 kDa. On IEF gel RU5 Fab appeared as eight bands with a pI ranging from 4.5 to 5.9.

Complex formation of (Se-Met) A3 and RU5

For isolation of A3-RU5 complexes, Fab was mixed with a twofold molar excess of (Se-Met) A3. Solutions containing 10 mg ml^{-1} of RU5 and 10 mg ml^{-1} of (Se-Met) A3 in 10 mM Tris-HCl pH 8.0, 25 mM NaCl were used for 5 min. incubations at room temperature. Complexes of A3-RU5 were separated from the excess of A3 on a Superdex 75 10/30 gel-filtration column (Pharmacia, Uppsala, Sweden) using 10 mM Tris-HCl pH 8.0, 25 mM NaCl as running buffer. The complex eluted separately from the excess of A3 at an elution volume of

9.1 ml (A3 eluted at 11.8 ml). No peak that could account for free RU5 was visible in the elution pattern indicating that all Fab was complexed (free RU5 eluted at 9.5 ml). The complex was concentrated to 10 or 15 mg ml^{-1} prior to crystallization, using Micro-concentrators with a molecular-weight cut-off of 30 kDa (Microsep, Northborough MA, USA). Dynamic-light scattering (DLS) measurements on a Dynapro-801 DLS Instrument (Protein Solutions, Charlottesville VA, USA) indicated the presence of 69-kDa particles in agreement with the expected molecular weight of about 72 kDa of the complex between A3 and RU5.

Determination of RU5 heavy-chain and light-chain variable domain sequences

The amino-acid sequence of the variable domain of the heavy chain (V_H) of RU5 was deduced from a cDNA nucleotide sequence. Cloning and sequencing was carried out using established procedures. Total mRNA was extracted from $4*10^6$ RU5 hybridoma cells with RNAzol using the RNA-isolation protocol of the supplier (Campro Scientific, Veenendaal, The Netherlands). First-strand cDNA was synthesized from mRNA using Superscript II reverse transcriptase (Gibco, Rockville MD, USA). During first-strand cDNA synthesis, 3.2 U μl^{-1} of RNase-inhibitor RNaseOUT (Gibco, Rockville MD, USA) was added. cDNA encoding the V_H domain was amplified by polymerase chain reaction (PCR) with Pwo DNA polymerase (Boehringer, Mannheim, Germany). A 5' variable-region concensus primer 'V$_H$-back' was used together with a forward primer 'V$_H$-for' that hydridizes with a consensus sequence in the J_H region (Ref. 299; Table I). The PCR product was extended with a 3'-A overhang with Taq DNA polymerase (Promega, Madison WI, USA). The PCR product with 3'-A overhang was cloned into the pCR2.1-TOPO Vector according to the manufacturer's protocol (Invitrogen, Leek, The Netherlands). Nucleotide sequences of three clones were determined using the di-deoxy method (Hubrecht Laboratories, Utrecht, The Netherlands) (Fig. 1A)[b].

For determination of the sequence of the variable domain (V_L) of the RU5 κ-light chain, the same procedure was used as for the V_H domain. For cloning of the V_L gene, one variable region concensus primer 'V$_L$-back' and two variable region concensus primers 'V$_L$-for' were used (Table I). However, determination of the sequence was hampered by the abundance of mRNA encoding the light chain of the non-producing myeloma fusion partner in the cytoplasm of the RU5 hybridoma cell, which is a known feature when using the myeloma cell line P363Ag8.653 (Ref. 300).

Table I
Primers for amplification of RU5 V_H and V_L domains[†]

B3c V$_H$-for 5'-d(CGG ATG GCC AGG T(C/G)(A/C) AGC TGC AG(C/G) AGT C(A/T)G G)
B4 V$_H$-back 5'-d(CCA GGG GCC AGT GGA TAG ACA AGC TTG GGT GTC GTT TT)

PD3 V$_L$-for 5'-d(CAG GAA ACA GCT ATG ACC GAG CTC GTG ATC ACC CAG TCT CC)
PD4 V$_L$-for 5'-d(TGT AAA ACG ACG GCC AGT TCT AGA TGG TGG GAA GAT GGA)
PD1 V$_L$-back 5'-d(GAT ATT GTG ATG ACC CAG TCT (C/G)T)

† See Ref. 299

[b] The nucleotide sequence for the variable domain V_H of the monoclonal antibody RU5 has been deposited in the GenBank database under GenBank Accession Number AF286587.

Crystallization

Initial crystallization trials were performed using various sparse-matrix crystal screens with solutions containing 10 mg ml^{-1} of A3-RU5 complex, both at room temperature and at 4°C. No crystals were obtained with the very soluble complex. Additional screening with a complex concentration of 15 mg ml^{-1} also gave no crystals and hardly any precipitates. The few conditions in which the complex precipitated as white powder, however, predominantly contained iso-propanol and had pH's around 5. These leads were used for subsequent grid screens with various precipitants and buffers/pH's. Crystalline thin four-sided or six-sided plates were obtained in 27% v/v iso-propanol, 100 mM cacodylic acid pH 5.5, at 4°C using a solution containing 15 mg ml^{-1} of A3-Fab. Further refinement of this initial condition resulted in crystals grown in 13% iso-propanol, 22% v/v 2-methyl-2,4-pentanediol (MPD), 100 mM cacodylic acid pH 5.3 that were suitable for X-ray data collection. The crystal used for structure determination had a size of 0.1x0.1x0.2 mm^3 and was equilibrated in a cryo-protectant solution consisting of 8% iso-propanol, 30% MPD, 100 mM cacodylic acid pH 5.3, and subsequently stored in liquid nitrogen.

Titel:
(5_1.eps)
Gemaakt door:
Adobe Illustrator(R) 8.0
Voorbeeld:
Deze EPS-figuur is niet opgeslagen
met een ingesloten voorbeeld.
Commentaar:
Dit EPS-bestand kan worden afgedrukt
op een PostScript-printer, maar niet
op een ander type printer.

Fig. 1. Amino-acid sequences of RU5 V_L and V_H domains. CDRs (underlined) were defined according to Kabat *et al.* (301). Strict sequential numbering (#) is used throughout the text. Numbering according to the convention of Kabat *et al.* (301) (#K) is also shown. (**A**) The amino-acid sequence of V_H was deduced from cDNA. Residues 1 to 7 could not be deduced precisely due to the use of a primer complementary to the 5' coding region. Asn56 in CDR$_{H2}$ (shaded) is N-glycosylated. The nucleotide sequence for the variable domain V_H of the monoclonal antibody RU5 has been deposited in the GenBank database under GenBank Accession Number AF286587. (**B**) The sequence of the V_L domain was deduced from electron density. The sequence was adjusted according to a consensus sequence based on a multiple sequence alignment of 110 Fabs.

Data Collection

The crystal of the A3-RU5 complex belonged to space group C2 with unit cell dimensions of $a = 121.8$ Å, $b = 183.4$ Å, $c = 131.8$ Å and $\beta = 116.2°$. A self-rotation function, calculated with POLARRFN[245] and the unit-cell volume suggested the presence of three A3-RU5 complexes in the asymmetric unit (a.u.). X-ray diffraction data were collected on beam line BW7B of the synchrotron-radiation facility of the EMBL outstation (Hamburg, Germany) with a Mar345 imaging plate (Mar, Evanston IL, USA). Data reduction, merging and scaling were performed with DENZO and SCALEPACK[26]. Diffraction-data statistics can be found in Table II. Diffraction of the A3-RU5 crystal was anisotropic. This anisotropy effected data completeness between 2.5 and 2.0 Å resolution, which dropped to 51.5% for the highest

resolution shell (Table II). For structure determination, anisotropic B-factors were applied with SCALEIT and SFTOOLS[245] to correct for the observed anisotropy.

Table II

Diffraction-data statistics

Wavelength (Å)	0.8469
Resolution (Å)	29.9-2.56/2.03[‡]
Space group	C2
a, b, c (Å)	121.80, 183.55, 131.84
α, β, γ (°)	90.0, 116.21, 90.0
Solvent content (%)	63
V_M (Å^3 Da^{-1})	3.3
Mosaicity (°)	0.22
Redundancy	4.2
No. of unique reflections	143,255
$<I>/<\sigma(I)>$	20.4 (2.4)[†]
Completeness (%)	85.9 (51.5)[‡]
R_{merge} (%)[¶]	6.1 (40.4)

‡ Data completeness is 100% between 29.9-2.56 Å resolution and drops to 51.5% between 2.56-2.03 Å resolution, due to anisotropic diffraction.

† Numbers in parentheses indicate statistics for the highest resolution shell (2.10-2.03 Å).

¶ $R_{merge} = \sum_h \sum_i |I_{hi} - <I_h>| / \sum_h \sum_i |I_{hi}|$

Structure determination and refinement

Initially, we tried to solve the structure of the complex of vWf- (Se-Met) A3 and RU5 Fab by conventional molecular replacement using the programs AMoRe[302] and CNS[9]. As search model native A3[194] and a number of different Fab structures[12] were used. Molecular replacement failed, most likely due to the large number of molecules present in the a.u.

The A3 domain contains five methionine residues. One of these derives from the pET-15b vector and remains attached to the N-terminus of the molecule after removal of the histidine-tag by thrombin[194]. This methionine is disordered in the structure of native A3. Determination of the positions of at least three out of the four remaining Se atoms uniquely defines the position and orientation of an A3 molecule. Therefore, we attempted to use the weak anomalous signal ($<\Delta f_{ano}/\sigma(F)> = 1.18$) in the diffraction data that arose from the presence of (Se-Met) A3.

The program RSPS[303] was used to identify Se sites from an anomalous Patterson map calculated with data between 30 and 2.5 Å resolution. A consistent set of seven Se sites was found. All Harker peaks had values of 3 σ above mean and the majority of cross vectors had values above 1 σ. Next, we attempted to attribute each Se site to a specific methionine residue on the basis of inter-atomic distances. It was assumed that distances between Se atoms within A3 in the A3-Fab complex were similar to the known distances between methionine sulphur atoms in the structure of native A3. The distances between Se atoms within two pairs of sites were consistent with the distance between the sulphur atoms of Met947 and Met998. Other distances between these four Se sites indicated that they were located in two molecules related by two-fold non-crystallographic symmetry (n.c.s.).

In the structure of native A3 sulphur atoms of Met947 and Met998 have B-factors of 7.3 and 8.1 Å^2, respectively. The sulphur atoms of Met1022 and Met1097 have higher B-values of 10.3 and 14.7 Å^2, respectively. The higher mobility of the Se atoms in Met1022 and Met1097 leads to a reduced height of the corresponding Harker peaks most probably causing RSPS to fail in identifying these Se sites. A systematic analysis of cross vectors to

the four known Se sites was performed, based on the expected cross vectors for sulphur sites of methionines in A3. Only cross-vectors with a length close to one of the expected inter-atomic distances were considered. In total, 352 possible Se sites were generated. Two of these sites met the distance criteria for the Se atom in Met1097 and also obeyed the two-fold n.c.s. The Harker peaks of these sites are indeed low being 0.7 σ and –1.7 σ. Identification of six Se sites allowed for positioning of two A3 molecules in the a.u. With hindsight it turns out that the selenium atom of Met1022 is shifted by approximately 6 Å relative to the sulphur atom of Met1022 in the structure of native A3, hampering a straight forward assignment of all Se peaks within an A3 molecule using the described procedure.

Next, a rotation function was calculated with the program AMoRe using the Fab-fragment of protein data bank entry 2MPA as a search model[12,304]. The 50 highest-ranking solutions from the rotation function were subjected to Patterson correlation refinement[305] using CNS. During Patterson correlation refinement the orientations and relative positions of the four individual immunoglobulin domains were optimised. Cross-translation functions were calculated with CNS. Solutions 1, 7 and 25 from the rotation function produced the lowest R-factors in the translation search, namely 51.7%, 51.9% and 52.3%, respectively. Other solutions from the rotation function gave R-factors in the translation function between 53.1 and 54.3%. When a translation function was calculated without the prior placement of the two A3 domains no correct translation vectors were obtained. In combination with the two A3 domains the three Fab molecules that produced the lowest R-factors were successfully positioned in the a.u. A model consisting of two A3 domains and the three Fab-fragments was subjected to rigid body refinement resulting in a free R-factor of 45.4%. Next, a third A3 molecule was generated on the basis of n.c.s. observed for two of the Fab-fragments. The a.u. finally contained three A3-RU5 complexes. Rigid body refinement of this model gave a free R-factor of 42.8%.

Further refinement of the initial model was carried out with CNS[9]. Cycles of rebuilding using O[16] and positional and B-factor refinement using CNS, were performed until convergence. Cross validation was used throughout refinement, using a 5% test set of reflections. Refinement used the maximum-likelihood algorithm[29] and bulk-solvent correction was applied as calculated by CNS. During structure refinement, diffraction data between 29.9 and 2.0 Å resolution were anisotropically scaled with CNS. During the first cycles of refinement, n.c.s. restraints were used for the three A3-RU5 complexes. Based on the behaviour of the free R-factor, these restraints were omitted during final stages of refinement. Sequences of the constant domain of the light chain (C_L) and of the constant domain of the heavy chain (C_{H1}) of RU5 were taken from $IgG_{2a, \kappa}$ monoclonal antibody 4-4-20 (Ref. 306, 307). Residues 1 to 110 of the V_L domain of RU5 were built in the structure based on electron density, aided by the consensus sequence of Fabs after alignment of 110 sequences (Fig. 1B). At Asn56 of the V_H domain, located within complementarity determining region H2 (CDR_{H2}) of RU5, additional electron density indicated the presence of an N-linked glycan. *N*-acetylglucosamine and fucose residues were built into the structure, according to the electron density. Water molecules were defined in a difference electron-density map, placed in the structure, and subsequently, B-factors and positions were refined with CNS. The search criteria for water molecules were a peak height of 2.8 σ, a distance of 2.5-3.4 Å to the hydrogen donor or acceptor and a B-factor smaller than 65 $Å^2$. A cacodylate ion ($[(CH_3)_2AsO_2]^-$) was built into the structure based on a strong peak in the difference map. Coordinates of cacodylate were taken from pdb code 1BEH[308] and conformational and non-bonded energy parameters of phosphate, arsenicum and CH_3 moieties from CNS were used

during refinement of the position of the cacodylate ion. Coordinates are in the Protein Data Bank (accession code 1QUB).

Results

Structure determination and refinement

The crystal structure of a complex between the vWf (Se-Met) A3-domain and a Fab-fragment of RU5, an antibody that inhibits binding of vWf to collagen, was determined by molecular replacement. Structure determination was aided by the anomalous signal from selenium atoms in (Se-Met) A3, which was used to find the positions of two out of the three A3 molecules in the a.u. The structure has been refined to an R-factor of 22.7% and a free R-factor of 26.4% using diffraction data to a maximal resolution of 2.0 Å (Table III). R-factors are somewhat higher than could be expected for a 2.0 Å resolution structure. This is possibly caused by, *i.* anisotropy of the diffraction that reduced data completeness between 2.0 and 2.6 Å (Table II), and *ii.* the fact that the sequence of the RU5 V_L domain was deduced from electron density and, therefore, may contain errors. The structure displays good model geometry with 88.8% of the residues in the most favored region of the Ramachandran plot and 10.8% in the additionally allowed region. Residue Thr51 of RU5 V_L domains occurs in the disallowed region of the Ramachandran plot, but its electron density is convincing.

The a.u. consists of three A3-RU5 complexes that are denoted *A*, *B* and *C*. The overall structure of the (Se-Met) A3 molecule is the same as the structure of native A3[193,194]. It consists of a central six-stranded β-sheet on both sides flanked by α-helices. The final model comprises amino-acid residues 921-1110 of A3 molecules in complex *A* and *B* and residues 920-1110 of the A3 molecule in complex *C*. Positions of the N- and C-termini of A3, including disulfide bond Cys923-Cys1109 that connects these termini, are poorly defined. The model of RU5 consists of residues 1 to 211 of the light chains and residues 1 to 129 and 136 to 216 of the heavy chains. Residues 130-135 of the heavy chains display very weak electron density and are excluded from the model. Disorder of this loop is a commonly observed feature in Fab structures[309]. Asn56 of the V_H domain is N-glycosylated. Electron density near Asn56 accounted for a GlcNAc(-Fuc)-GlcNAc moiety in complexes *A* and *B* and only a GlcNAc-Fuc moiety in complex *C*. B-factors of these moieties are relatively high, *i.e.* approximately 60 Å^2, compared to an average overall B-factor of 38 Å^2. The model contains one cacodylate ion from the crystallization solution.

Table III
Refinement statistics

Resolution (Å)	29.9 - 2.03
R-factor	0.227
R_{free}	0.264
r.m.s.d. bond distances (Å)	0.007
r.m.s.d. angles (°)	1.41
Average overall B-factor (Å^2)	38
No. of protein atoms[†]	13,889
No. of carbohydrate atoms	100
No. of cacodylate ions	1
No. of solvent molecules	878

† An asymmetric unit contains three A3-RU5 complexes.

Crystal packing and differences between complexes

In the a.u. A3-RU5 complexes *B* and *C* form a tightly interacting anti-parallel dimer and are related by two-fold n.c.s. A3-RU5 complex *A* forms a similar anti-parallel dimer with a crystallographically related complex *A'*. Complexes within dimers *B-C* and *A-A'* have large contact areas of 932 Å^2 and 1,454 Å^2, respectively (GRASP; Ref. 246). These large interaction-surface areas suggest that the dimer of A3-RU5 complexes may also be stable in solution. DLS measurements, however, clearly indicated that the A3-RU5 complex does not form dimers in solution. Therefore, dimers observed in the crystal are a result of crystal packing.

Superposition of C$_\alpha$-atoms of the three A3-RU5 complexes gives large root-mean-square (r.m.s.) coordinate differences ranging from 0.7 to 0.9 Å. When superpositions are limited to A3 molecules with bound V$_H$ and V$_L$ domains r.m.s. coordinate differences of 0.5-0.6 Å are obtained. Visual inspection of these superpositions (Fig. 2) shows that the A3-RU5 interaction region is well conserved, whereas regions of A3 and the variable domains located further away from the interaction region superimpose less well. More detailed inspection of the A3-RU5 binding region reveals that all side chain conformations are very similar (not shown). In conclusion, the A3-RU5 interaction region is well conserved among the three complexes in the a.u.

Title:
(5_2.eps)
Creator:
Adobe Illustrator(R) 8.0
Preview:
This EPS picture was not saved
with a preview included in it.
Comment:
This EPS picture will print to a
PostScript printer, but not to
other types of printers.
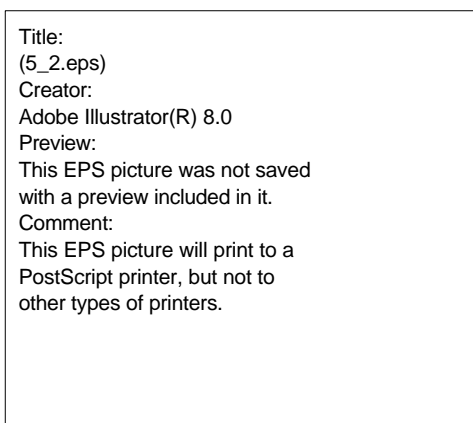
Fig. 2. Structural overlay of C$_\alpha$-traces of the three A3-RU5 Fab complexes in the asymmetric unit. For calculation of the best superposition C$_\alpha$-atoms of A3 and variable domains of RU5 were used. The A3-RU5 interaction region is well conserved amongst the three complexes, while relatively large differences are shown in orientations of the RU5 constant domains with respect to its variable domains and A3.
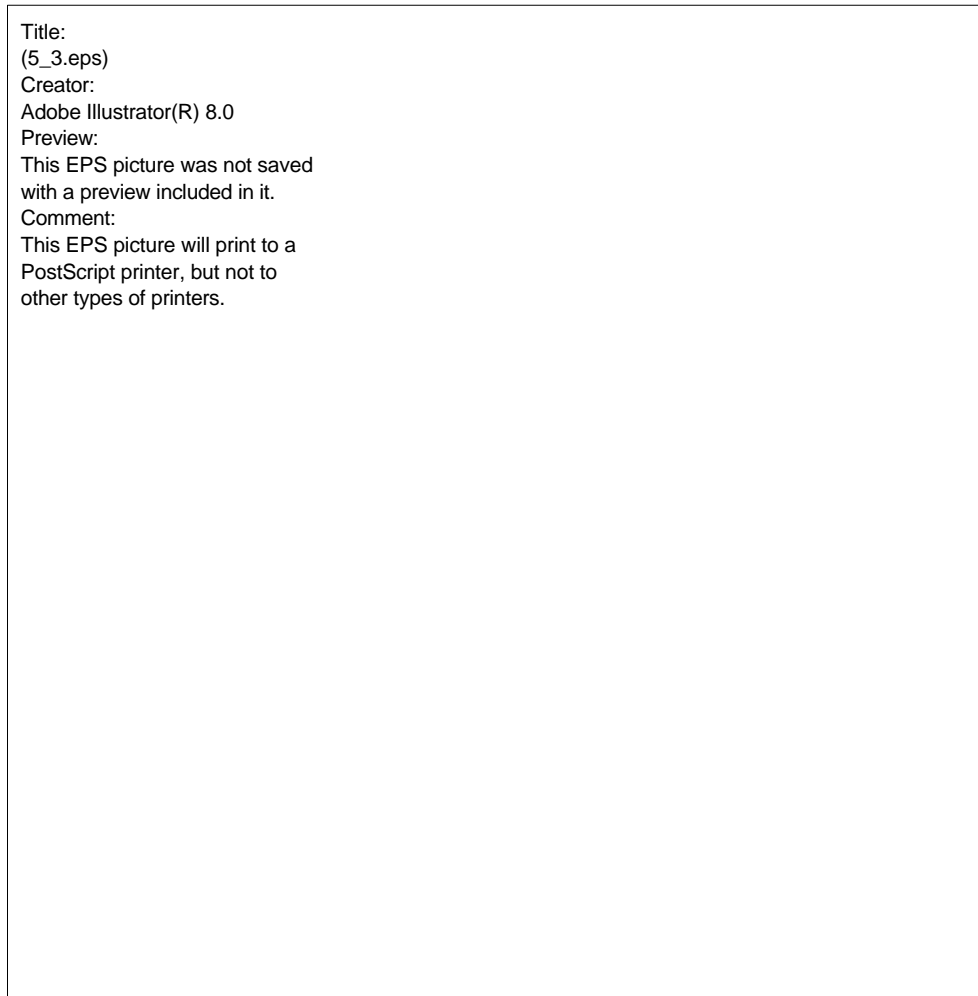
Title:
(5_3.eps)
Creator:
Adobe Illustrator(R) 8.0
Preview:
This EPS picture was not saved
with a preview included in it.
Comment:
This EPS picture will print to a
PostScript printer, but not to
other types of printers.

Fig. 3. Ribbon diagram of A3 and RU5 variable domains. Residues of A3 that are part of the epitope of RU5 are indicated by green spheres. Regions of RU5 CDRs that interact with A3 are color-coded in light-blue. Regions of A3 that show different conformations among four crystal structures are shown in purple trace. Residues that have been mutated in previous studies (See discussion) are located in the top face of A3, opposite to the RU5-binding site, and are indicated by black spheres. Disulfide bond Cys923-Cys1109 is shown in ball-and-stick. The α-helices and β-strands of A3 are depicted in blue and red, respectively. For clarity, α-helix 2 is not shown by a ribbon, but in 'coil' representation. The V_H domain of RU5 is in brown, the V_L domain is in green. Diagram was generated with MOLSCRIPT[202] and RASTER3D[203].

The epitope of RU5

A3 interacts with RU5 through a non-linear epitope comprising residues in loop α1β2, loop β3α2 followed by helix α2 and loop α3β4 (Table IV). All three loops that are engaged in the epitope are located in the bottom face of A3 (Fig. 3). The N- and C-termini of A3 that are also located in the bottom face do not interact with RU5. This observation is in agreement with the fact that RU5 was raised against complete vWf in which the termini connect A3 to flanking A2 and D4 domains. Residues of RU5 that interact with loops α1β2 and α3β4 are located in CDR_{L1} and CDR_{L2}. All six CDRs interact with residues in the contiguous segment formed by loop β3α2 and helix α2. The A3-RU5 interactions involve five hydrogen bonds and one salt bridge. Interestingly, the fucose residue attached to residue Asn56 in CDR_{H2} of complex *A* interacts with Lys988-Ala989 of A3. The carbohydrate residues attached to Asn56 in complex *B* and *C* do not interact with A3. The buried surface area of A3 molecules in the complex is approximately 1,200 Å^2, which is about 7% of the total surface area of A3.

Conformational changes in A3

To analyze whether binding of RU5 causes conformational changes in A3 we compared models of A3 in the A3-RU5 complex with two structures of free A3[193,194]. The two structures of free A3 were determined from different crystal forms with unrelated crystal packing interactions. In both crystal forms two molecules are present in the a.u. Since the A3-RU5 complex was obtained with (Se-Met) A3 we also included the structure of free (Se-Met) A3 (E.G. Huizinga, unpublished results) in the analysis to detect possible structural differences caused by Se-Met. R.m.s. coordinate differences after pair-wise superposing C_α-atoms of all eight models range from 0.24 to 0.81 Å. Large differences are restricted to three loops, located within the RU5-binding site, and to two loops that are located distant from the epitope (Fig. 3, Table IV). The three conformational diverse loops that are located in the RU5 epitope are shown in Fig. 4A.

Residues Gly961-Pro-Arg963 in loop α1β2 have a unique conformation in the A3-RU5 complex. The peptide bond between Pro962 and Arg963 is flipped with respect to the conformations observed in free A3. As a result the side chain of Pro962 in the complex is positioned somewhat further away from the A3 surface.

Residues Asn983-Val-Val-Pro-Glu987 in loop β3α2 have considerable conformational freedom as is evident from the conformation observed in A3 model *B* of Bienkowska *et al.* (193), which differs dramatically from the conformations observed in the other models. Considering the seven more similar loops, the orientation of the side chain of Asn983 shows the most pronounced variation, while residues 984-987 are rather similar. RU5 interacts with all residues in this loop but the conformations observed in the RU5-A3 complex are not systematically different from the conformations observed in free A3.

Two conformational extremes exist for residues Thr1019-Ser-Glu-Met-His-Gly-Ala1025 in loop α3β4, the position of Met1022 being the most prominent difference. In all three A3-RU5 complexes and in one of the crystal forms of free A3[193] Met1022 points away from the A3 surface. In the other crystal form of free A3[194] the side chain of Met1022 packs against the surface of the molecule and its C_α-atom is shifted by approximately 4 Å. The same conformation is observed in free (Se-Met) A3 and, therefore, the selenium atom in Se-Met1022 does not trigger the observed differences. The conformation of loop α3β4 in the complex is not induced by the presence of RU5 since similar conformations of this loop are observed in free A3[193]. In all available A3 structures at least part of loops β3α2 and/or α3β4 contribute to crystal packing.

Table IV

The epitope of RU5 and loops that show conformational variation

Residues in the RU5 epitope[‡]	
Structural element	Residues
Loop α1β2	Pro962-Arg963
	Gln966
Loop β3α2	Pro981-Trp-Asn-Val-Val-Pro-Glu987
Helix α2	Lys988-Ala-His990
	Ser993-Leu994
	Asp996-Val997
Loop α3β4	Met1022-His-Gly1024
	Arg1026
Residues with variable conformations[†]	
Structural element	Residues
Loop β1α1	Ser938-Phe-Pro940
Loop α1β2	Gly961-<u>Pro-Arg963</u>
Loop β3α2	<u>Asn983-Val-Val-Pro-Glu987</u>
Loop α3β4	Thr1019-Ser-Glu-<u>Met-His-Gly</u>-Ala1025
Loop α5β6	Gly1078-Pro-Ala-Gly-Asp-Ser1083

‡ Residues listed are positioned within 4.0 Å distance from RU5.
† Residues that are also part of the epitope of RU5 are underlined.

Distant from the RU5 epitope in the top face of A3, conformational variation is observed for residues Ser938-Phe-Pro940 in loop β1α1 (Fig. 4B). Ser938 is part of the vestigial MIDAS motif. In RU5-A3 complex *C* Phe939 is solvent exposed as is observed in all models of free A3. In complexes *A* and *B*, however, Phe939 is buried in the hydrophobic core of A3. The solvent exposed conformation of Phe939 has relatively high B-factors, whereas the buried conformation has low B-factors. In complexes *A* and *B*, the buried conformation of Phe939 coincides with crystal contacts between residues 940-942 of A3 and symmetry related RU5 V_H domains. In contrast, A3 in complex *C* lacks these crystal contacts. The position of Pro940 in complex *C* and in structures of free A3, would not allow for the crystal packing observed for complexes *A* and *B*.

Residues Gly1078-Pro-Ala-Gly-Asp-Ser1083 in loop α5β6 adopt a range of conformations (Fig. 4C). This loop is located in a side face of A3 distant from the epitope of RU5. In A3 domain *B* of the structure of Bienkowska *et al.* (193) loop α5β6 has a very

Title:
(5_4.eps)
Creator:
Adobe Illustrator(R) 8.0
Preview:
This EPS picture was not saved
with a preview included in it.
Comment:
This EPS picture will print to a
PostScript printer, but not to
other types of printers.

Fig. 4. The conformation of five loops varies among different crystal structures of A3. Models compared include free A3 (pdb code 1atz and 1ao3), free (Se-Met) A3 and A3 from the A3-RU5 complex. (**A**) Stereo picture of loops $\alpha1\beta2$ (residues 961-963), $\beta3\alpha2$ (983-987) and $\alpha3\beta4$ (1019-1025). Residues of A3 in A3-RU5 complex *A* are shown in thick line. A3 domain *A* from the structure of Huizinga *et al.* (194) is shown in gray. (**B**) Stereo diagram of residues Ser938-Phe-Pro940 in the top face of A3. Buried and exposed conformations of Phe939 are labeled. (**C**) Stereo diagram of loop $\alpha5\beta6$ (residues 1078-1083). The aberrant A3 domain *B* from the structure of Bienkowska *et al.* (193) is shown in thick line.

different conformation. This aberrant conformation coincides with crystal contacts unique to molecule *B*. No crystal contacts are present in the other structures. The conformations observed in the RU5-A3 complex are not systematically different from the conformations observed in free A3.

Discussion

The current study was aimed at locating the collagen-binding site in the vWf-A3 domain. For this purpose, we solved the crystal structure of the A3 domain in complex with a Fab fragment of RU5, that inhibits collagen binding of A3. The structure of the complex shows that RU5 binds to residues within A3 sequences 962-966, 981-997 and 1022-1026. These residues are located in α-helix 2 and in loops α1β2, β3α2 and α3β4 at the bottom of the A3 domain (See Fig. 3).

Inhibition of collagen binding by RU5 could be caused by two distinct mechanisms. Firstly, RU5 could block collagen binding through steric hindrance. Secondly, RU5 could act by inducing a conformational change in A3 that disrupts the collagen-binding site. Long-range conformational changes induced upon ligand binding do occur in the structurally related I domains of integrins $\alpha_M\beta_2$[198,206,207,310] and $\alpha_2\beta_1$[200], and have been proposed for the vWf-A1 domain[195,196]. Identification of the actual mechanism of inhibition is relevant for localizing the collagen-binding site of A3. In case of steric hindrance the binding site is expected to lie at or close to the epitope of RU5, while for a mechanism involving a conformational change the collagen-binding site could also be located distant from the epitope.

A detailed structural comparison revealed significant, but local, conformational differences between A3 in the crystal structure of the A3-RU5 complex and in crystal structures of free A3. Differences of similar magnitude are also observed among different structures of free A3. Differences are restricted to five loops. Three of these loops are located in the RU5 epitope, *i.e.* loops α1β2, β3α2 and α3β4. Loop α1β2 has a unique conformation in the A3-RU5 complex, indicating that its conformation is induced by RU5. Conformations of loops β3α2 and α3β4 in A3-RU5 are, however, also observed in some of the structures of free A3, suggesting that their conformation is not induced by RU5. The same argument holds for loop α5β6, that is located distant from the RU5 epitope. In the top face of A3 close to the vestigial MIDAS motif structural variation is observed for residues Ser938-Phe-Pro940 in loop β1α1 (Fig. 3). In A3-RU5 complexes *A* and *B* the side chain of Phe939 is buried, whereas in complex *C* and in all structures of free A3 its side chain is solvent exposed (See Fig. 4b). From the fact that both the exposed and buried conformations of Phe939 are observed in the three A3-RU5 complexes we conclude that the conformation of loop β1α1 is not influenced by binding of RU5.

In conclusion, analysis of conformational variation in structures of A3 shows that RU5 does not induce long range conformational changes. This excludes a mechanism in which collagen binding is inhibited by induction of conformational changes in the collagen-binding site. Thus, most likely RU5 blocks collagen binding of A3 by steric hindrance, which implies that the collagen-binding site is located in the vicinity of the epitope of RU5.

Previously, the collagen-binding site of A3 was proposed to be located in its top face[194,297] like it is in the homologous I domains of integrins $\alpha_1\beta_1$ and $\alpha_2\beta_1$[200,311-313]. Point mutations introduced in the top face in free A3[297] and in full-length vWf[201] gave conflicting results. Our crystal structure now shows that the collagen-binding site is not located in the

top face of A3. Therefore, collagen binding by vWf-A3 appears to be completely different from the collagen-binding mechanism of the I domains of integrins $\alpha_1\beta_1$ and $\alpha_2\beta_1$.

Previously, solvent exposure of residue Phe939 was proposed to be important for the structural stability of the A3 domain, as an alternative for metal-ion binding in the vestigial MIDAS motif[193]. It was suggested that solvent exposure of Phe939 opens an essential water channel to the buried Asp934. Phe939 in A3-RU5 complexes *A* and *B* is, now buried, similar to the conformation of homologues residues in I-domains of integrins α_2, α_M and α_L[197,198,200]. This shows that the solvent exposed conformation is not essential for stability.

As was argued above, RU5 blocks collagen binding by steric hindrance. This does not require that the epitope of RU5, which comprises 7% of the A3 surface area, overlaps with the actual collagen binding site. Therefore, in addition to the epitope of RU5 located in α-helix 2 and loops $\alpha1\beta2$, $\beta3\alpha2$ and $\alpha3\beta4$, also residues that lie somewhat further away from the epitope could play a role in collagen-binding (Fig. 3). If residues are considered that are positioned up to 10 Å away from RU5, the location of the collagen-binding site is confined to 32% of the total surface area of A3. This area includes residues from helices $\alpha1$ and $\alpha3$. Previously, regions comprising residues 948-998 (Ref. 314) and 1018-1114 (Ref. 292) of vWf-A3 were implicated in the major collagen-binding site of vWf. These two regions indeed overlap with regions of A3 that are indicated by the A3-RU5 crystal structure as potential contributors to the collagen-binding site.

In conclusion, the structure of the A3-RU5 complex shows that the collagen-binding site of A3 is most likely located in the bottom or side face of A3 in the vicinity of α-helices 1, 2 and 3, and loops $\alpha1\beta2$, $\beta3\alpha2$ and $\alpha3\beta4$, and not in the top face as was previously proposed. The structure of A3-RU5 provides an excellent starting point for further exploration of the collagen-binding site by means of site-directed mutagenesis.

Acknowledgements

--- References ---

1. Watson, J.D. and Crick, F.H.C. (1953) Genetic implications of the structure of deoxyribonucleic acid. *Nature* **171**, 964-967.
2. Perutz, M.F., Rossmann, M.G., Cullis, A.F., Muirhead, H. and Will, G. (1960) Structure of heamoglobin: A three dimensional fourier synthesis at 5.5 Å resolution, obtained by X-ray analysis. *Nature* **185**, 416-422.
3. Kendrew, J.C., Dickerson, R.E., Strandberg, B.E., Hart, R.G., Davies, D.R., Philips, D.C. and Shore, V.C. (1960) Structure of myoglobin: A three dimensional fourier synthesis at 2 Å resolution. *Nature* **185**, 422-427.
4. Ban, N., Nissen, P., Hansen, J., Moore, P.B. and Steitz, T.A. (2000) The structure of the 50S ribosomal subuni at 2.7 Å resolution and its functional consequences. Abstract of paper presented at the EMBO Millennium Symposium on Structural Biology, EMBL-Heidelberg, March 26-29.
5. Lindley, P.F. (1999) Macromolecular crystallography with a third-generation synchrotron source. *Acta Crystallogr. D* **55**, 1654-1662.
6. Zanini, F., Lausi, A. and Savoia, A. (1999) The beamlines of ELETTRA and their application to structural biology. *Genetica* **106**, 171-180.
7. Hendrickson, W.A. (1991) Determination of macromolecular structures from anomalous diffraction of synchrotron radiation. *Science* **254**, 51-58.
8. Walsh, M.A., Evans, G., Sanishvili, R., Dementieva, I. and Joachimiak, A. (1999) MAD data collection -current trends. *Acta Crystallogr. D* **55**, 1726-1732.
9. Brünger, A.T., Adams, P.D., Clore, G.M., DeLano, W.L., Gros, P., Grosse-Kunstleve, R.W., Jiang, J-.S., Kuszewski, J., Nilges, M., Pannu, N.S., Read, R.J., Rice, L.M., Simonson, T. and Warren, G.L. (1998) Crystallography and NMR system: A new software suite for macromolecular structure determination. *Acta Crystallogr. D* **54**, 905-921.
10. Terwilliger, T.C. and Berendzen, J. (1999) Automated MAD and MIR structure solution. *Acta Crystallogr. D* **55**, 849-861.
11. Bergfors, T.M. (1999) Protein crystallization technologies, strategies and tips. A laboratory manual. International University Line, California, USA.
12. Berman, H.M., Westbrook, J., Feng, Z., Gilliland, G., Bhat, T.N., Weissig, H., Shindyalov, I.N. and Bourne, P.E. (2000) The Protein Data Bank. *Nucleic Acid Research* **28**, 235-242.
13. Wüthrich, K. (1995) NMR – This other method for protein and nucleic acid structure determination. *Acta Crystallogr. D* **51**, 249-270.
14. Lamzin, V.S. and Wilson, K.S. (1993) Automated refinement of protein models. *Acta Crystallogr. D.* **49**, 129-149.
15. Perrakis, A., Sixma, T.K., Wilson, K.S. and Lamzin, V.S. (1997) wARP: Improvement and extension of crystallographic phases by weighted averaging of multiple-refined dummy atomic models. *Acta Crystallogr. D* **53**, 448-455.
16. Jones, T.A., Zou, J.Y., Cowan, S.W. and Kjeldgaard, M. (1991) Improved methods for the building of protein models in electron density maps and the location of errors in these models. *Acta Crystallogr. A* **47**, 110-119.
17. Vriend, G. (1990) WHAT IF: A molecular modelling and drug design program. *J. Mol. Graph.* **8**, 52-56.
18. Laskowski, R.A., MacArthur, M.W., Moss, D.S. and Thornton, J.M. (1993) PROCHECK-a program to check the stereochemical quality of protein structures. *J. Appl. Crystallogr.* **26**, 283-191.
19. Cusack, S., Belrhali, H., Bram, A., Burghammer, M., Perrakis, A. and Riekel, C. (1998) Small is beautiful: protein micro crystallography. *Nature Struct. Biol. synchrotron supplement*, 634-637.
20. Garman, E.F. and Schneider, T.R. (1997) Macromolecular cryocrystallography. *J. Appl. Cryst.* **30**, 211-237.
21. Garman, E.F. (1999) Cool data: quantity AND quality. *Acta Crystallogr. D* **55**, 1641-1653.
22. Weik, M., Ravelli, R.B.G., Kryger, G., McSweeney, S.M., Raves, M.L., Harel, M., Gros, P., Silman, I., Kroon, J. and Sussman, J.L. (2000) Specific chemical and structural damage to proteins produced by synchrotron radiation. *Proc. Natl. Acad. Sci. USA*. **97**, 623-628.
23. Ravelli, R.B.G. and McSweeney, S.M. (2000) The 'fingerprint' that X-rays can leave on structures. *Structure* **8**, 315-328.
24. Burmeister, W.P. (2000) Structural changes in a cryo-cooled protein crystal owing to radiation damage. *Acta Crystallogr. D* **56,** 328-341.
25. Nave, C. (1999) Matching X-ray source, optics and detectors to protein crystallography. *Acta Crystallogr. D* **55**, 1663-1668.
26. Otwinowski, Z. and Minor, W. (1996) Processing of X-ray diffraction data collected in oscillation mode. *Methods Enzymol.* **276**, 307-326.
27. Ealick, S.E. (1997) Now we're cooking: new successes for shake-and-bake. *Structure* **5**, 469-472.
28. Weeks, C.M. and Miller, R. (1999) The design and implementation of SnB v2.0. *J. Appl. Cryst.* **32**, 120-124.
29. Pannu, N.S. and Read, R.J. (1996) Improved structure refinement through Maximum Likelihood. *Acta Crystallogr. A* **52**, 659-668.
30. Hoeg, J.M., Segal, P., Gregg, R.E., Chang, Y.S., Lindgren, F.T., Adamson, G.L., Frank, M., Brickman, C. and Brewer, Jr., H.B. (1985) Characterization of plasma lipids and lipoproteins in patients with β2-Glycoprotein I (apolipoprotein H) deficiency. *Atherosclerosis* **55**, 25-34.
31. Bancsi, L.F.J.M.M., van der Linden, I.K. and Bertina, R.M. (1992) β2-glycoprotein I deficiency and the risk of thrombosis. *Thromb. Haemost.* **67**, 649-653.
32. Horbach, D.A., van Oort, E., Lisman, T., Meijers, J,C.M., Derksen, R.H.W.M. and de Groot, P.G. (1999) β2 glycoprotein I is proteolytically cleaved *in vivo* upon activation of fibrinolysis. *Thromb. Haemost.* **81**, 87-95.
33. Sorice, M., Circella, A., Griggi, T., Garofalo, T., Nicodemo, G., Pittoni, V., Pontier, G.M., Lendi, L. and Valesini, G. (1996) Anticardiolipin and anti-β2-GPI are two distinct populations of autoantibodies. *Thromb. Haemost.* **75**, 303-308.
34. Sheng, Y., Sali, A., Herzog, H., Lahnstein, J. and Krilis, S.A. (1996) Site-directed mutagenesis of recombinant human β2 glycoprotein I identifies a cluster of lysine residues that are critical for phospholipid binding and anti-cardiolipin antibody activity. *J. Immunol.* **157**, 3744-3751.

35. Galazka, M., Keil, L.B., Kohles, J.D., Li, J., Kelty, S.P., Petersheim, M. and DeBari, V.A. (1998) A stable, multi-subunit complex of β2-Glycoprotein I. *Thromb. Res.* **90**, 131-137.

36. Caronti, B., Calderaro, C., Alessandri, C., Conti, F., Tinghino, R., Palladini, G. and Valesini, G. (1999) β2 Glycoprotein I (β2-GPI) mRNA is expressed by several cell types involved in anti-phospholipid syndrome-related tissue damage. *Clin. Exp. Immunol.* **115**, 214-219.

37. Caronti, B., Calderaro, C., Alessandri, C., Conti, F., Tinghino, R., Palladini, G. and Valesini, G. (1998) Serum anti-β2 Glycoprotein I antibodies from patients with antiphospholipid antibody syndrome bind central nervous system cells. *J. Autoimmunity* **11**, 425-429.

38. Steinkasserer, A., Estaller, C., Weiss, E.H. and Sim., R.B. (1991) Complete nucleotide and deduced amino acid sequence of human β_2 glycoprotein I. *Biochem. J.* **277**, 387-391.

39. Chamley, L.W., Allen, J.L. and Johnson, P.M. (1997) Synthesis of β2-Glycoprotein 1 by the human placenta. *Placenta* **18**, 403-410.

40. Kristensen, T., Schousboe, I., Boel, E., Mulvihill, E.M., Rosendahl Hansen, R., Bach Møller, K., Hundahl Møller, N.P. and Sottrup-Jensen, L. (1991) Molecular cloning and mammalian expression of human β_2-Glycoprotein I cDNA. *FEBS Letters* **289**, 183-186.

41. Lozier, J., Takahashi, N. and Putnam, F.W. (1984) Complete amino acid sequence of human plasma β_2 Glycoprotein I. *Proc. Natl. Acad. Sci. USA* **81**, 3640-3644.

42. Kato, H. and Enjyoji, K. (1991) Amino acid sequence and location of the disulfide bonds in bovine β2 Glycoprotein I: the presence of five sushi domains. *Biochemistry* **30**, 11687-11694.

43. Walsh, M.T., Watzlawick, H., Putnam, F.W., Schmid, K. and Brossmer, R. (1990) Effect of the carbohydrate moiety on the secondary structure of β_2-Glycoprotein I. Implications for the biosynthesis and folding of glycoproteins. *Biochemistry* **29**, 6250-6357.

44. Gambino, R., Ruiu, G., Pagano, G. and Cassader, M. (1997) Qualitative analysis of the carbohydrate composition of apolipoprotein H. *J. Prot. Chem.* **16**, 205-212.

45. Gambino, R., Ruiu, G., Pagano, G. and Cassader, M. (1999) Study of the glycosylation of apolipoprotein H. *Chem. Phys. Lipids* **103**, 161-174.

46. Schousboe, I. (1983) Characterization of subfractions of β_2 glycoprotein I: evidence for sialic acid microheterogeneity. *Int. J. Biochem.* **15**, 35-44.

47. Gries, A., Nimpf, J., Wurm, H., Kostner, G.M. and Kenner, T. (1989) Characterization of isoelectric subspecies of asialo β2 Glycoprotein I. *Biochem. J.* **260**, 531-534.

48. Finlayson, J.S. and Mushinski, J.F. (1967) Separation of subfractions of human β2-Glycoprotein I. *Biochim. Biophys. Acta* **147**, 413-420.

49. Kamboh, M.I., Ferell, R.E. and Seperhrnia, B. (1988) Genetic studies of human apolipoproteins. IV. Structural heterogeneity of apolipoprotein H (β2-Glycoprotein I) *Am. J. Hum. Genet.* **42**, 452-457.

50. Richter, A. and Cleve, H. (1988) Genetic variations of human serum β_2 glycoprotein I demonstrated by isoelectric focusing. *Electrophoresis* **9**, 317-322.

51. Hirose, N., Williams, R., Alberts, A.R., Furie, R.A., Chartash, E.K., Jain, R.I., Sison, C., Lahita, R.G., Merrill, J.T., Cucurull, E., Gharavi, A.E., Sammaritano, L.R., Salmon, J.E., Hashimoto, S., Sawada, T., Chu, C.C., Gregersen, P.K. and Chiorazzi, N. (1999) A role for the polymorphism at position 247 of the β2-Glycoprotein I gene in the generation of anti-β2-Glycoprotein I antibodies in the antiphospholipid syndrome. *Arthritis Rheum.* **42**, 1655-1661.

52. Sanghera, D.K., Wagenknecht, D.R., McIntyre, J.A. and Kamboh, M.I. (1997) Identification of structural mutations in the fifth domain of apolipoprotein H (β_2-glycoprotein I) which affect phospholipid binding. *Hum. Mol. Gen.* **6**, 311-316.

53. Horbach, D.A., van Oort, E., Tempelman, M.J., Derksen, R.H.W.M. and de Groot, P.G. (1998) The prevalence of a non phospholipid-binding form of β_2-glycoprotein I in human plasma. *Thromb. Haemost.* **80**, 791-798.

54. Bork, P., Downing, K.A., Kieffer, B. and Campbell, I.D. (1996) Structure and distribution of modules in extracellular proteins. *Q. Rev. Biophys.* **29**, 119-167.

55. Norman, D.G., Barlow, P.N., Baron, M. Day, A.J., Sim, R.B. and Campbell, I.D. (1991) Three dimensional structure of a complement control protein module in solution. *J. Mol. Biol.* **219**, 717-725.

56. Barlow, P.N., Norman, D.G., Steinkasser, A., Horne, T.J., Pearce, J., Driscoll, P.C., Sim, R.B. and Campbell, I.D. (1992) Solution structure of the fifth repeat of factor H: a second example of the complement control protein module. *Biochemistry* **31**, 3626-3634.

57. Barlow, P.N., Steinkasser, A., Norman, D.G., Kieffer, B., Wiles, A.P. Sim, R.B. and Campbell, I.D. (1993) Solution structure of a pair of complement modules by nuclear magnetic resonance. *J. Mol. Biol.* **232**, 268-284.

58. Wiles, A.P., Shaw, G., Bright, J., Perczel, A., Campbell, I.D. and Barlow, P.N. (1997) NMR studies of a viral protein that mimicks the regulators of complement activation. *J. Mol. Biol.* **272**, 253-265.

59. Casasnovas, J.M., Larvie, M. and Stehle, T. (1999) Crystal structure of two CD46 domains reveals an extended measles virus-binding surface. *EMBO J.* **18**, 2911-2922.

60. Gaboriaud, C., Rossi, V., Bally, I., Arlaud, G.J. and Fontecilla-Camps, J.C. (2000) Crystal structure of the catalytic domain of human complement C1s: a serine protease with a handle. *EMBO J.* **19**, 1755-1765.

61. Polz, E., Wurm, H. and Kostner, G.M. (1980) Investigations on β_2 glycoprotein I in the rat: isolation from serum and demonstration in lipoprotein density fractions. *Int. J. Biochem.* **11**, 265-270.

62. Gambino, R., Ruiu, G., Pagano, G. and Cassader, M. (1999) The binding of apolipoprotein H (β_2-glycoprotein I) to lipoproteins. *Prostaglandins Other Lipid Mediat.* **57**, 351-359.

63. Balasubramanian, K., Chandra, J. and Schroit (1997) Immune clearance of phosphatidylserine-expressing cells by phagocytes. The role of β_2-glycoprotein I in macrophage recognition. *J. Biol. Chem.* **272**, 31113-31117.

64. Balasubramanian, K. and Schroit, A.J. (1998) Characterization of phosphatidylserine dependent β_2-Glycoprotein I macrophage interactions. *J. Biol. Chem.* **273**, 29272-29277.

65. Polz, E. and Kostner, G.M. (1979) The binding of beta2-glycoprotein to human serum lipoproteins. *FEBS Letters* **102**, 183-186.

66. Schousboe, I. (1980) Binding of β₂ glycoprotein I to platelets: effect of adenylate cyclase activity. *Thromb. Research* **19**, 225-237.

67. Nimpf, J., Wurm, H. and Kostner, G.M. (1985) Interaction of β₂ glycoprotein I with human blood platelets: influence upon the ADP-induced aggregation. *Thromb. Haemost.* **54**, 397-401.

68. Chonn, A., Semple, S.C. and Cullis, P.R. (1995) β2 Glycoprotein I is a major protein associated with very rapidly cleared liposomes in vivo, suggesting a significant role in the immune clearance of "non-self" particles. *J. Biol. Chem.* **270**, 25845-25849.

69. Hagihara, Y., Goto, Y., Kato, H. and Yoshimura, T. (1995) Structure and function of β2-glycoprotein I: with special reference to the interaction with phospholipid. *Lupus* **4** Suppl. 1, S3-S5.

70. Wurm, H., Beubler, E., Holasek, A. and Kostner, G. (1982) Studies on the possible function of β2-Glycoprotein I: influence in the triglyceride metabolism in the rat. *Metabolism* **31**, 484-486.

71. Harper, M.F., Hayes, P.M., Lentz, B.R. and Roubey, R.A.S. (1998) Characterization of β₂-Glycoprotein I binding to phospholipid membranes. *Thromb. Haemost.* **80**, 610-614.

72. Deguchi, H., Fernández, J.A., Hackeng, T.M., Banka, C.L. and Griffin, J.H. (2000) Cardiolipin is a normal component of human plasma lipoproteins. *Proc. Natl. Acad. Sci. USA* **97**, 1743-1748.

73. Steinkasserer, A., Barlow, P.N., Willis, A.C., Kertesz, Z., Campbell, I.D., Sim, R.B. and Norman, D.G. (1992) Activity, disulfide mapping and structural modelling of the fifth domain of human β₂-glycoprotein I. *FEBS Letters* **313**, 193-197.

74. Lauer, S.A., Hempel, U., Gries, A. and Frank, K.-H. (1993) Amino acid sequence of the region of β₂ glycoprotein 1 (gp1) which mediates binding of autoantibodies to the cardiolipin-gp1 complex in humans. *Immunology* **80**, 22-28.

75. Igarashi, M., Matsuura, E., Igarashi, Y., Nagae, H., Ichikawa, K., Triplett, D.A. and Koike, T. (1996) Human β₂ glycoprotein I as an anticardiolipin cofactor determined using deleted mutants expressed by a baculovirus system. *Blood* **87**, 3263-3270.

76. Hunt, J. and Krilis, S. (1994) The fifth domain of β₂-glycoprotein I contains a phospholipid binding site (Cys281-Cys288) and a region recognized by anticardiolipin antibodies. *J. Immunol.* **152**, 653-659.

77. Wang, S.X., Cai, G.P. and Sui, S. (1998) The insertion of human apolipoprotein H into phospholipid membranes: a monolayer study. *Biochem. J.* **335**, 225-232.

78. Wang, S.X., Cai, G.P. and Sui, S. (1999) Intrinsic fluorescence study of the interaction of human apolipoprotein H with phospholipid vesicles. *Biochemistry* **38**, 9477-9484.

79. Mehdi, H., Naqvi, A. and Kamboh, M.I. (2000) A hydrophobic sequence at position 313-316 (Leu-Ala-Phe-Trp) in the fifth domain of apolipoprotein H (β₂-glycoprotein I) is crucial for cardiolipin binding. *Eur. J. Biochem.* **267**, 1770-1776.

80. Hunt, J.E., Simpson, R.J. and Krilis, S.A. (1993) Identification of a region of β₂-glycoprotein I critical for lipid binding and anti-cardiolipin antibody cofactor activity. *Proc. Natl. Acad. Sci. USA* **90**, 2141-2145.

81. Hagihara, Y., Enjyoji, K., Omasa, T., Katakura, Y., Suga, K., Igarashi, M., Matsuura, E., Kato, H., Yoshomura, T. and Goto, Y. (1997) Structure and function of the recombinant fifth domain of human β2-glycoprotein I: effects of specific cleavage between Lys77 and Thr78. *J. Biochem.* **121**, 128-137.

82. Ohkura, N., Hagihara, Y., Yoshimura, T., Goto, Y. and Kato, H. (1998) Plasmin can reduce the function of human β₂ glycoprotein I by cleaving domain V into a nicked form. *Blood* **91**, 4173-4179.

83. Atsumi, T., Khamashta, M.A., Ames, P.R.J., Ichikawa, K., Koike, T. and Hughes, G.R.V. (1996) Effect of β₂ glycoprotein I and human monoclonal anticardiolipin antibody on the protein S/C4b-binding protein system. *Lupus* **6** 358-364.

84. Merrill, J.T., Zhang, H.W., Shen, C., Butman, B.T., Jeffries, E.P., Lahita, R.G. and Myones, B.L. (1999) Enhancement of protein S anticoagulant function by β₂-glycoprotein I, a major target antigen of antiphospholipid antibodies. *Thromb. Haemost.* **81** 748-757.

85. Sim, D.S. and Devine, D.V. (1999) Activated protein C binding to β2-glycoprotein I is modulated by the level of protein S and C4b-binding protein and is disrupted by antiphospholipid antibodies. Abstract XVIIth Congress of the International Society on Thrombosis and Haemostatis, Washington DC, USA, Aug. 1999.

86. Esmon, C.T., Vigano-D'Angelo, S., D'Angelo, A. and Comp, P.C. (1987) Anticoagulation proteins C and S. *Adv. Exp. Med. Biol.* **214**, 47-54.

87. Dahlbäck, B. (1991) Protein S and C4b-binding protein; components involved in the regulation of the protein C anticoagulant system. *Thromb. Haemost.* **66**, 49-61.

88. Thorelli, E. (1999) Mechanisms that regulate the anticoagulant function of coagulation factor V. *Scand. J. Clin. Lab. Invest. Suppl.* **229**, 19-26.

89. Gaffney, P.J., Edgell, T.A. and Whitton, C.M. (1999) The haemostatic balance – Astrup revisited. *Haemostasis* **29**, 58-71.

90. Klaerke, D.A., Rojkjaer, R., Christensen, L. and Schousboe, I. Identification of β₂ glycoprotein I as a membrane associated protein in kidney: purification by calmodulin affinity chromatography. *Biochim. Biophys. Acta* **1339** (1997) 203-216.

91. Rojkjaer, R., Klaerke, D.A. and Schousboe, I. (1997) Characterization of the interaction between beta2 glycoprotein I and calmodulin, and identification of a binding sequence in beta2-glycoprotein I. *Biochim. Biophys. Acta* **1339**, 217-225.

92. Finn, B.E. and Forsén (1995) The evolving model of calmodulin structure, function and activation. *Structure* **3**, 7-11.

93. Moestrup, S.K., Schousboe, I., Jacobsen, C., Leheste, J.-R., Christensen, E.L. and Wilnow, T.E. (1998) β₂ Glycoprotein I (Apolipoprotein H) and β₂-Glycoprotein I-Phospholipid complex harbor a recognition site for the endocytic receptor Megalin. *J. Clin. Invest.* **102**, 902-909.

94. Köchl, S., Fresser, F., Lobentanz, E., Baier, G. and Utermann, G. (1997) Novel interaction of apolipoprotein(a) with β₂ glycoprotein I mediated by the Kringle IV domain. *Blood* **90**, 1482-1489.

95. Ma, K., Simantov, R., Zhang, J.C., Silverstein, R., Hajjor, K.A. and McCrae, K.R. (2000) High affinity binding of β₂ Glycoprotein I to human endothelial cells is mediated by annexin II. *J. Biol. Chem.* **275**, 15541-15548.

96. Zhang, L., Jacobsson, K., Ström, K., Lindberg, M. and Frykberg, L. (1999) *Staphylococcus aureus* expresses a cell surface protein that binds both IgG and β2-Glycoprotein I. *Microbiology* **145**, 177-183.

97. Stefas, E., Rucheton, M., Graafland, H., Moynier, M., Sompeyrac, C., Bahraoui, E.M. and Veas, F. (1997) Human plasmatic apolipoprotein H binds human immunodeficiency virus type 1 and type 2 proteins. *AIDS Res. Human Retrov.* **13**, 97-104.

98. Mehdi, H., Kaplan, M.J., Anlar, F.Y., Yang, X., Bayer, R., Sutherland, K. and Peeples, M.E. (1994) Hepatitis B virus surface antigen binds to apolipoprotein H. *J. Virology* **68**, 2415-2424.

99. Neurath, A.R. and Strick, N. (1994) The putative cell receptors for Hepatitis B virus (HBV), annexin V, apolipoprotein H, bind to lipid components of HBV. *Virology* **204**, 475-477.

100. Schultze, H.E., Heide, K. and Haupt, H. (1961) Über ein bisher unbekanntes nidermolekulares β_2-Globulin des Humanserums. *Naturwissenschaften* **48**, 719-724.

101. Burstein, M. and Scholnik, H.R. (1972) Precipitation of chylomicrons and very low density lipoproteins from human serum with sodium lauryl sulfate. *Life Sci.* **11**, 177-184.

102. Cassader, M., Ruiu, G., Gambino, R., Veglia, F. and Pagano, G. (1997) Apolipoprotein H levels in diabetic subjects: correlation with cholesterol levels. *Metabolism* **46**, 522-525.

103. Vlachoyiannopoulos, P.G., Krilis, S.A., Hunt, J.E., Manoussakis, M.N. and Moutsopoulos, H.M. (1992) Patients with anticardiolipin antibodies with and without antiphospholipid syndrome: their clinical features and β2-Glycoprotein I plasma levels. *Eur. J. Clin. Invest.* **22**, 482-487.

104. Inanç, M., Radway-Bright, E.L. and Isenberg, D.A. (1997) β2-Glycoprotein I and anti-β2-Glycoprotein I antibodies: where are we now? *Br. J. Rheumatol.* **36**, 1247-1257.

105. Schousboe, I. (1985) Beta2-glycoprotein I: a plasma inhibitor of the contact activation of the intrinsic blood coagulation pathway. *Blood* **66**, 1086-1091.

106. Brighton, T.A., Hogg, P.J., Dai, Y-P., Murray, B.H., Chong, B.H. and Chesterman, C.N. (1996) β_2 glycoprotein I in thrombosis: evidence for a role as a natural anticoagulant. *Br. J. Haematol.* **93**, 185-194.

107. Rand, J.H., Wu, X.X., Andree, H.A., Lockwood, C.J., Guller, S., Scher, J. and Harpel, P.C. (1997) Pregnancy loss in the antiphospholipid-antibody syndrome – a possible thrombogenic mechanism. *N. Engl. J. Med.* **337**, 154-160.

108. Vogt, E., Ng, A.-K. and Rote, N.S. (1997) Antiphosphatidylserine antibody removes annexin-V and facilitates the binding of prothrombin at the surface of a choriocarcinoma model of trophoblast differentiation. *Am. J. Obstet. Gynecol.* **177**, 964-972.

109. Kutteh, W.H., Rote, N.S. and Silver, R. (1999) Antiphospholipid antibodies and reproduction: the antiphospholipid antibody syndrome. *Am. J. Reprod. Immunol.* **41**, 133-152.

110. Roubey, R.A.S., Eisenberg, R.A., Harper, M.F. and Winfield, J.B. (1995) "Anticardiolipin" autoantibodies recognize β_2 glycoprotein I in the absence of phospholipid. *J. Immunol.* **154**, 954-960.

111. Kandiah, D.A. and Krilis, S.A. (1994) β2-Glycoprotein I. *Lupus* **3**, 207-212.

112. Bick, R.L. and Baker, W.F. (1994) Antiphospholipid and thrombosis syndromes. *Sem. Thromb. Hemos.* **20**, 3-15.

113. Mangia, A., Margaglione, M., Cascavilla, I., Gentile, R., Cappucci, G., Facciorusso, D., Grandone, E., Di Minno, G., Rizzetto, M. and Andriulli, A. (1999) Anticardiolipin antibodies in patients with liver disease. *Am. J. Gastroenterol.* **94**, 2983-2987.

114. Matsuura, E., Igarashi, Y., Fujimoto, M., Ichikawa, K., Suzuki, T., Sumida, T., Yasuda, T. and Koike, T. (1992) Heterogeneity of anticardiolipin antibodies defined by the anticardiolipin cofactor. *J. Immunol.* **148**, 3885-3891.

115. Cabiedes, J., Cabral, A.R. and Alarcón-Segovia (1995) Clinical manifestations of the antiphospholipid syndrome in patients with systemic lupus erythematosus associate more strongly with anti-β2-glycoprotein I than with antiphospholipid antibodies. *J. Rheumatol.* **22**, 1899-1906.

116. Ichikawa, K., Tsutsumi, A., Matsuura, E. and Koike, T. (1999) Antiphospholipid syndrome. *Intern. Med.* **38**, 170-173.

117. Shan, H., Goldman, J., Cunto, G., Manuppello, J., Chaiken, I., Cines, D.B. and Silberstein, L.E. (1998) Heterogeneity of anti phospholipid and anti-endothelial cell antibodies. *J. Autoimmun.* **11**, 651-660.

118. Wu, R., Nityanand, S., Berglund, L., Lithell, H., Holm, G. and Lefvert, A.K. (1997) Antibodies against cardiolipin and oxidatively modified LDL in 50-year-old men predict myocardial infarction. *Arterioscler. Thromb. Vasc. Biol.* **17**, 3159-3163.

119. Erkkilä, A.T., Närvänen, O., Lehto, S., Uusitupa, M.I.J., Ylä-Herttuala, S. (2000) Autoantibodies against oxidized low density lipoprotein and cardiolipin in patients with coronary heart disease. *Arterioscler. Thromb. Vasc. Biol.* **20**, 204-209.

120. Keeling, D.M., Wilson, A.J.G., Mackie, I.J., Isenberg, D.A. and Machin, S.J. (1993) Role of β_2 glycoprotein I and anti phospholipid antibodies in activation of protein C *in vitro*. *J. Clin. Pathol.* **46**, 908-91

121. Mori, T., Takeya, H., Nishioka, J., Gabazza, E.C. and Suzuki, K. (1996) Beta2-glycoprotein I modulates the anticoagulant activity of activated protein C on the phospholipid surface. *Thromb. Haemost.* **75**, 49-55.

122. Thiagarajan, P., Le, A. and Benedict, C.R. (1999) β2-Glycoprotein I promotes the binding of anionic phospholipid vesicles by macrophages. *Arterioscler. Thromb. Vasc. Biol.* **19**, 2807-2811.

123. Nimpf, J., Bevers, E.M., Bomans, P.H.H., Till, U., Wurm, H., Kostner, G.M. and Zwaal, R.F.A. (1986) Prothrombinase activity of human platelets is inhibited by beta2-glycoprotein-I. *Biochim. Biophys. Acta* **884**, 142-149.

124. Nimpf, J., Wurm, H. and Kostner, G.M. (1987) β_2 glycoprotein I (apo-H) inhibits the release reaction of human platelets during ADP-induced aggregation. *Atherosclerosis* **63**, 109-114.

125. Schousboe, I. (1988) In vitro activation of the contact activation system (Hageman factor system) in plasma by acidic phospholipids and the inhibitory effect of β_2 glycoprotein I on this activation. *Int. J. Biochem.* **20**, 309-315.

126. Shi, W., Chong, B.H., Hogg, P.J. and Chesterman, C.N. (1993) Anticardiolipin antibodies block the inhibition by β_2 glycoprotein I of the factor Xa generating activity of platelets. *Thromb. Haemost.* **70**, 342-345.

127. Schousboe, I. and Rasmussen, M.S. (1995) Synchronized inhibition of the phospholipid mediated autoactivation of factor XII in plasma by β_2 glycoprotein I and anti-β_2 glycoprotein I. *Thromb. Haemost.* **73**, 798-804.

128. McNally, T., Mackie, I.J., Isenberg, D.A. and Machin, S.J. (1996) β_2 glycoprotein I inhibits factor XII activation on triglyceride rich lipoproteins: the effect of antibodies from plasma of patients with antiphospholipid syndrome. *Thromb. Haemost.* **76**, 220-225.

129. Pierangeli, S.S., Dean, J., Goldsmith, G.H., Branch, D.W., Gharavi, A. and Harris, E.N. (1996) Studies on the interaction of placental anticoagulant protein I, β_2 glycoprotein I, and antiphospholipid antibodies in the prothrombinase reaction and in the solid phase anticardiolipin assays. *J. Lab. Clin. Med.* **128**, 194-201.

130. Ieko, M., Yasukouchi, T, Sawada, K., -I. and Koike, T. (1998) The influence of β2-Glycoprotein I on tissue factor activity. *Seminars Thromb. Hemost.* **24**, 211-215.

131. Price, B.E., Rauch, J., Shia, M.A., Walsh, M.T., Lieberthal, W., Gilligan, H.M., O'Laughlin, T., Koh, J.S. and Levine, J.S. (1996) Antiphospholipid autoantibodies bind to apoptotic, but not viable, Thymocytes in a β_2-Glycoprotein I-dependent manner. *J. Immunol.* **157**, 2201-2208.

132. Dombroski, D., Balasubramanian, K. and Schroit, A.J. (2000) Phosphatidylserine expression on cell surfaces promotes antibody-dependent aggregation and thrombosis in β2-Glycoprotein I-immune mice. *J. Autoimmunity* **14**, 221-229.

133. Manfredi, A.A., Rovere, P., Heltai, S., Galati, G., Nebbia, G., Tincani, A., Balestrieri, G. and Sabbadini, M.G. (1998) Apoptotic cell clearance in systematic lupus erythematosus II. Role of β₂-Glycoprotein I. *Arthritis Rheumatism* **41**, 215-223.

134. Fadok, V.A., Voelker, D.R., Campbell, P.A., Coehn, J.J., Bratton, D.L. and Henson, P.M. (1992) Exposure of phosphatidylserine on the surface of apoptotic lymphocytes triggers specific recognition and removal by macrophages. *J. Immunol.* **148**, 2207-2216.

135. Fadok, V.A., Bratton, D.L., Frasch, S.C., Warner, M.L. and Henson, P.M. (1998) The role of phosphatidylserine in recognition of apoptotic cells by phagocytes. *Cell Death Differ.* **5**, 551-562.

136. Fadok, V.A., Bratton, D.L., Rose, D.M., Pearson, A., Ezekewitz, R.A.B. and henson, P.M. (2000) A receptor for phosphatidylserine-specific clearance of apoptotic cells. *Nature* **405**, 85-90.

137. Roubey, R.A.S., Pratt, C.W., Buyon, J.P. and Winfield, J.B. (1992) Lupus Anticoagulant activity of autoimmune antiphospholipid antibodies is dependent upon β₂ glycoprotein I. *J. Clin. Invest.* **90**, 1100-1104.

138. Oosting, J.D., Derksen, R.H.W.M., Entjes, H.T.I., Bouma, B.N. and de Groot, Ph.G. (1992) Lupus Anticoagulant activity is frequently dependent on the presence of β₂ glycoprotein I. *Thromb. Haemost.* **67**, 499-502.

139. Pengo, V., Biasiolo, A., Brocco, T., Tonetto, S. and Ruffatti, A. (1996) Autoantibodies to phospholipid-binding plasma proteins in patients with thrombosis and phospholipid-reactive antibodies. *Thromb. Haemost.* **75**, 721-724.

140. Biasolo, A., Rampazzo, P., Brocco, T., Barbero, F., Rosato, A. and Pengo, V. (1999) [anti-β₂-glycoprotein I - β₂ glycoprotein I] immune complexes in patients with antiphospholipid syndrome and other autoimmune diseases. *Lupus* **8**, 121-126.

141. Tsutsumi, A., Ichikawa, K., Matsuura, E., Sawada, K.I. and Koike, T. (2000) Heterogeneous behavior of anti beta2 glycoprotein I antibodies on various commercially available immunoassay plates coated with beta2 glycoprotein I. *J. Rheumatol.* **27**, 391-396.

142. Levine, J.S., Subang, R., Koh, J.S. and Rauch, J. (1998) Induction of antiphospholipid autoantibodies by β2 glycoprotein I bound to apoptotic Thymocytes. *J. Autoimmun.* **11**, 413-424.

143. Levine, J.S., Koh, J.S., Subang, R. and Rauch, J. (1999) Apoptotic cells as immunogen and antigen in the antiphospholipid syndrome. *Exp. Mol. Pathol.* **66**, 82-98.

144. Gharavi, E.E., Chaimovich, H., Cucurull, E., Celli, C.M., Tang, H., Wilson, W.A. and Gharavi, A.E. (1999a) Induction of antiphospholipid antibodies by immunization with synthetic viral and bacterial peptides. *Lupus* **8**, 449-455.

145. Gharavi, A.E., Pierangeli, S.S., Colden-Stanfield, M., Wei Liu, X., Espinola, R.G. and Harris, E.N. (1999b) GDKV induced antiphospholipid antibodies enhance thrombosis and activate endothelial cells *in vivo* and *in vitro*. *J. Immunol.* **163**, 2922-2927.

146. Asherson, R.A. and Shoenfeld, Y. (2000) The role of infection in the pathogenesis of catastrophic antiphospholipid syndrome – molecular mimicry? *J. Rheumatol.* **27**, 12-14.

147. Galli, M., Comfurius, P., Maassen, C., Hemker, H.C., de Baets, M.H., van Breda-Vriesman, P.J.C., Barbui, T., Zwaal, R.F.A. and Bevers, E.M. (1990) Anticardiolipin antibodies (ACA) directed not to cardiolipin but to a plasma protein cofactor. *Lancet* **335**, 1544 1547.

148. McNeil, H.O., Simpson, R.J., Chesterman, C.N. and Krilis, S.A. (1990) Anti-phospholipid antibodies are directed against a complex antigen that includes a lipid binding inhibitor of coagulation: β₂-glycoprotein I (apolipoprotein H). *Proc. Natl. Acad. Sci. USA* **87**, 4120-4124.

149. Koike, T. and Matsuura, E. (1991) What is the "true" antigen for anticardiolipin antibodies? *Lancet* **337**, 671-672.

150. Takeya, H., Mori, T., Gabazza, E.C., Kuroda, K., Deguchi, H., Matsuura, E., Ichikawa, K., Koike, T. and Suzuki, K. (1997) Anti-β2-Glycoprotein I (β2GPI) monoclonal antibodies with lupus anticoagulant-like activity enhance the β2GPI binding to phospholipids. *J. Clin. Invest.* **99**, 2260-2268.

151. Iverson, G.M., Victoria, E.J. and Marquis, D.M. (1998) Anti-β2 glycoprotein I (β2GPI) autoantibodies recognize an epitope on the first domain of β2GPI. *Proc. Natl. Acad. Sci. USA* **95**, 15542-15546.

152. George, J., Gilburd, B., Hojnik, M., Levy, Y., Langevitz, P., Matsuura, E., Koike, T. and Shoenfeld, Y. (1998) Target recognition of β₂-Glycoprotein I (β₂GPI)-dependent anticardiolipin antibodies: evidence for involvement of the fourth domain of β₂GPI in antibody binding. *J. Immunol.* **160**, 3917-3923.

153. Blank, M., Shoenfeld, Y., Cabilly, S., Heldman, Y., Fridkin, M. and Katchalski-Katzir, E. (1999) Prevention of experimental antiphospholipid syndrome and endothelial cell activation by synthetic peptides. *Proc. Natl. Acad. Sci. USA* **96**, 5164-5168.

154. Wang, M.X., Kandiah, D.A., Ichikawa, K., Khamashta, M., Hughes, G., Koike, T., Roubey, R. and Krilis, S.A. (1995) Epitope specificity of monoclonal anti-β₂ glycoprotein I antibodies derived from patients with the antiphospholipid syndrome. *J. Immunol.* **155**, 1629-1636.

155. Cheng-De, Y., Shun-Le, C., Nan, S., Ming, Q. and Feng, X. (1998) Detection of anti-recombinant β2 Glycoprotein 1 and anti-recombinant β2-Glycoprotein 1 fifth-domain antibodies in sera from patients with systemic lupus erythematosus. *Rheumatol. Int.* **18**, 5-10.

156. Zhu, M., Olee, T., Le, D.T., Roubey, R.A.S., Hahn, B.H., Woods, Jr., V.L. and Chen, P.P. (1999) Characterization of IgG monoclonal anti-cardiolipin/anti-β2-Glycoprotein I antibodies from two patients with antiphospholipid syndrome reveals three species of antibodies. *Br. J. Haematol.* **105**, 102-109.

157. Wagenknecht, D.R. and McIntyre, J.A. (1993) Changes in β2-Glycoprotein I antigenicity induced by phospholipid binding. *Thromb. Haemost.* **69**, 361-365.

158. Ichikawa, K., Khamashta, M.A., Koike, T., Matsuura, E. and Hughes, G.R.V. (1994) β2-Glycoprotein I reactivity of monoclonal anticardiolipin antibodies from patients with the antiphospholipid syndrome. *Arthritis Rheum.* **37**, 1453-1461.

159. Matsuura, E., Igarashi, Y., Yasuda, T., Triplett, D.A. and Koike, T. (1994) Anticardiolipin antibodies recognize β₂ glycoprotein I structure altered by interacting with an oxygen modified solid phase surface. *J. Exp. Med.* **179**, 457-462.

160. Pengo, V., Biasiolo, A. and Fior, M.G. (1995) Autoimmune antiphospholipid antibodies are directed against a cryptic epitope expressed when β₂ glycoprotein I is bound to a suitable surface. *Thromb. Haemost.* **73**, 29-34.

161. Chamley, L.W., Duncalf, A.M., Konarkowska, B., Mitchell, M.D. and Johnson, P.M. (1999) Conformationally altered β2 Glycoprotein I is the antigen for anti-cardiolipin autoantibodies. *Clin. Exp. Immunol.* **115**, 571-576.

162. Wang, S.X., Sun, Y.-T. and Sui, S.-F. (2000) Membrane-induced conformational change in human apolipoprotein H. *Biochem. J.* **348**, 103-106.
163. Willems, G.M., Janssen, M.P., Pelsers, M.M.A.L., Comfurius, P., Galli, M., Zwaal, R.F.A. and Bevers, E.M. (1996) Role of divalency in the high-affinity binding of anticardiolipin antibody β2-Glycoprotein I complexes to lipid membranes. *Biochemistry* **35**, 13833-13842.
164. Arnout, J., Wittevrongel, C., Vanrusselt, M., Hoylaerts, M. and Vermylen, J. (1998b) β2 glycoprotein I dependent Lupus Anticoagulants form stable bivalent antibody β-2-Glycoprotein I complexes on phospholipid surfaces. *Thromb. Haemost.* **79**, 79-86.
165. Blank, M., George, J., Barak, V., Tincani, A., Koike, T. and Shoenfeld, Y. (1998) Oral tolerance to low dose β2 Glycoprotein I: immunomodulation of experimental antiphospholipid syndrome. *J. Immunol.* **161**, 5303-5312.
166. Ruggeri, Z.M. and Ware, J. (1993) von Willebrand Factor. *FASEB J.* **7**, 308-316.
167. Sadler, J.E. (1998) Biochemistry and genetics of von Willebrand factor. *Annu. Rev. Biochem.* **67**, 395-424.
168. Ruggeri, Z.M. (1999) Structure and function of von Willebrand Factor. *Thromb. Haemost.* **82**, 576-584.
169. Shelton-Inloes, B.B., Titani, K. and Sadler, J.E. (1986) cDNA sequences for human von Willebrand factor reveal five types of repeated domains and five possible protein sequence polymorphisms. *Biochemistry* **25**, 3164-3171.
170. Titani, K., Kumar, S., Takio, K., Ericsson, L.H., Wade, R.D., Ashida, K., Walsh, K.A., Chopek, M.W., Sadler, J.E. and Fujikawa, K. (1986) Amino acid sequence of human von Willebrand factor. *Biochemistry* **25**, 3171-3184.
171. Marti, T., Roesselet, S., Titani, K. and Walsh, K.A. (1987) Identification of disulfide bridged substructures within human von Willebrand factor. *Biochemistry* **26**, 8099-8109.
172. Slayter, H., Loscalzo, J., Bockenstedt, P. and Handin, R.I. (1985) Native conformation of human von Willebrand protein. Analysis by electron microscopy and quasi-elastic light scattering. *J. Biol. Chem.* **260**, 8559-8563.
173. Heijnen, H.F.G., Koedam, J.A., Sandberg, H., Beeser-Visser, N.H., Slot, J.W. and Sixma, J.J. (1990) Characterization of human factor VIII and interaction with von Willebrand factor. An electron microscopic study. *Eur. J. Biochem.* **194**, 491-498.
174. Siedlecki, C.A., Lestini, B.J., Kottke-Marchant, K., Eppell, S.J., Wilson, D.L. and Marchant, R.E. (1996) Shear dependent changes in the three-dimensional structure of human von Willebrand factor. *Blood* **88**, 2939-2950.
175. Wagner, D.D. (1989) Storage and secretion of von Willebrand factor. In: Zimmermann, T.S. and Ruggeri, Z.M., eds. Coagulation and bleeding disorders. The role of factor VIII and von Willebrand factor. New York, M. Dekker, Inc., pp. 161-180.
176. Sixma, J.J., Schiphorst, M.E., Verweij, C.L. and Pannekoek, H. (1991) Effect of deletion of the A1 domain of von Willebrand factor on its binding to heparin, collagen and platelets in the presence of ristocetin. *Eur. J. Biochem.* **196**, 369-375.
177. Voorberg, J., Fontijn, R., Calafat, J., Janssen, H. van Mourik, J.A. and Pannekoek, H. (1991) Assembly and routing of von Willebrand factor variants: The requirements for disulfide-linked dimerization reside within the carboxy-terminal 151 amino acids. *J. Cell. Biol.* **113**, 195-205.
178. Lankhof, H., Damas, C., Schiphorst, M.E., IJsseldijk, M.J.W., Bracke, M., Furlan, M. Tsai, H.M., de Groot, P.G., Sixma, J.J. and Vink, T. (1997) von Willebrand factor without the A2 domain is resistant to proteolysis. *Thromb. Haemost.* **77**, 1008-1013.
179. Lankhof, H., Wu, Y.P., Vink, T., Schiphorst, M.E., Zerwes, H.-G., de Groot, P.G. and Sixma, J.J. (1997) Role of the glycoprotein Ib-binding A1 repeat and the RGD sequence in platelet adhesion to human recombinant von Willebrand factor. *Blood* **86**, 1035-1042.
180. Lankhof, H., van Hoeij, M., Schiphorst, M.E., Bracke, M., Wu, Y.-P., IJsseldijk, M.J.W., Vink, T., de Groot, Ph.G. and Sixma, J.J. (1996) A3 domain is essential for interaction of von Willebrand Factor with collagen type III. *Thromb. Haemost.* **75**, 950-958.
181. Foster, P.A., Fulcher, C.A., Marti, T., Titani, K. and Zimmermann, T.S. (1987) A major factor VIII binding domain resides within the amino-terminal 272 amino acid residues of von Willebrand factor. *J. Biol. Chem.* **262**, 8443-8446.
182. Ginsburg, D. (1999) Molecular genetics of von Willebrand disease. *Thromb. Haemost.* **82**, 585-591.
183. Vischer, U.M. and de Moerloose, Ph. (1999) von Willebrand factor: from cell biology to the clinical management of von Willebrand's disease. *Crit. Rev. Oncol. Hematol.* **30**, 93-109.
184. Mohlke, K.L., Nichols, W.C. and Ginsburg, D. (1999) The molecular basis of von Willebrand disease. *Int. J. Clin. Lab. Res.* **29**, 1-7.
185. Hoylaerts, M.F., Yamamoto, H., Nuyts, K., Vreys, I., Deckmyn, H. and Vermylen, J. (1997) von Willebrand factor binds to native collagen VI primarily via its A1 domain. *Biochem. J.* **324**, 185-191.
186. Mazzucato, M., Spessotto, P., Masotti, A., De Appollonia, L., Cozzi, M.R., Yoshioka, A., Perris, R., Colombatti, A. and De Marco, L. (1999) Identification of domains responsible for von Willebrand factor type VI collagen interaction mediating platelet adhesion under high flow. *J. Biol. Chem.* **274**, 3033-3041.
187. Andrews, R.K. and Berndt, M.C. (2000) Snake venom modulators of platelet adhesion receptors and their ligands. *Toxicon* **38**, 775-791.
188. Matsushita, T., Meyer, D. and Sadler, J.E. (2000) Localization of von Willebrand factor-binding sites for platelet glycoprotein Ib and botrocetin by charged-to-alanine scanning mutagenesis. *J. Biol. Chem.* **275**, 11044-11049.
189. Obert, B., Houllier, A., Meyer, D. and Girma, J.-P. (1999) Conformational changes in the A3 domain of von Willebrand factor modulate the interaction of the A1 domain with platelet glycoprotein Ib. *Blood* **93**, 1959-1968.
190. Sixma, J.J., Van Zanten, G.H., Huizinga, E.H., Van der Plas, R.M., Verkley, M., Wu, Y.P., Gros, P. and D Groot, P.G. (1997) Platelet adhesion to collagen: An update. *Thromb. Haemost.* **78**, 434-438.
191. Fujimoto, T., Ohara, S. and Hawiger, J. (1982) Thrombin-induced exposure and prostacyclin inhibition of the receptor for factor VIII/von Willebrand factor on human platelets. *J. Clin. Invest.* **69**, 1212-1222.
192. Ribes, J.A. and Francis, C.W. (1990) Multimer size dependence of von Willebrand factor binding to crosslinked or noncrosslinked fibrin. *Blood* **75**, 1460-1465.
193. Bienkowska, J., Cruz, M., Atiemo, A., Handin, R. and Liddington, R. (1997) The von Willebrand Factor A3 domain does not contain a metal ion-dependent adhesion site motif. *J. Biol. Chem.* **272**, 25162-25167.

92

194. Huizinga, E.G., van der Plas, R.M., Kroon, J., Sixma, J.J. and Gros, P. (1997) Crystal structure of the A3 domain of human von Willebrand factor: implications for collagen binding. *Structure* **5**, 1147-1156.

195. Celikel, R., Varughese, K.I., Madhusudan, Yoshioka, A., Ware, J. and Ruggeri, Z.M. (1998) Crystal structure of the von Willebrand factor A1 domain in complex with the function blocking NMC-4 Fab. *Nat. Struct. Biol.* **5**, 189-194.

196. Emsley, J. Cruz, M., Handin, R. and Liddington, R. (1998) Crystal structure of the von Willebrand Factor A1 domain and implications for the binding of platelet Glycoprotein Ib. *J. Biol. Chem.* 273, 10396-10401.

197. Qu, A. and Leahy, D.J. (1995) Crystal structure of the I-domain from the CD11a/CD18 (LFA-1, α$_L$β$_2$) integrin. *Proc. Natl. Acad. Sci. USA* **92**, 10277-10281.

198. Lee, J.O., Rieu, P., Arnaout, M.A. and Liddington, R. (1995a) Crystal structure of the A domain from the α subunit of integrin CR3 (CD11b/CD18). *Cell* **80**, 631-638.

199. Emsley, J., King, S.L., Bergelson, J.M. and Liddington, R.C. (1997) Crystal structure of the I domain from integrin α2β1. *J. Biol. Chem.* **272**, 28512-28517.

200. Emsley, J., Knight, C.G., Farndale, R.W., Barnes, M.J. and Liddington, R.C. (2000) Structural basis of collagen recognition by integrin α2β1. *Cell* **100**, 47-56.

201. Van der Plas, R.M., Gomes, L., Marquart, J.A., Vink, T., Meijers, J.C.M., de Groot, Ph.G., Sixma, J.J. and Huizinga, E.G. (2000) Binding of von Willebrand Factor to collagen type III: role of specific amino acids in the collagen binding domain of vWF, effects of neighboring domains. Accepted for publication by *Thromb. Haemost.*

202. Kraulis, P. (1991) Molscript: A program to produce both detailed and schematic plots of protein structures. *J. Appl. Crystallogr.* **24**, 946-950.

203. Merritt, E.A. and Bacon, D.J. (1997) Raster3D: photorealistic molecular graphics. *Meth. Enzymol.* **277**, 505-524.

204. Kessler, C.M., Floyd, C.M., Rick, M.E., Krizek, D.M., Lee, S.L. and Gralnick, H.R. (1984) Collagen-factor VIII/von Willebrand factor protein interaction. *Blood* **63**, 1291-1298.

205. Kaufman, R.J. and Pipe, S.W. (1999) Regulation of factor VIII expression and activity by von Willebrand factor. *Thromb. Haemost.* **82**, 201-208.

206. Lee, J.O., Bankston, L.A., Arnaout, M.A. and Liddington, R.C. (1995b) Two conformations of the integrin A domain (I domain): a pathway for activation? *Structure* **3**, 1333-1340.

207. Li, R., Rieu, P., Griffith, D.L., Scott, D. and Arnaout, M.A. (1998) Two functional states of the CD11b A domain: correlations with key features of two Mn^{2+}-complexed crystal structures. *J. Cell Biol.* **143**, 1523-1534.

208. Van Genderen, P.J.J., Vink, T., Michiels, J.J., van 't Veer, M.B., Sixma, J.J. and van Vliet, H.H.D.M. (1994) Acquired von Willebrand disease caused by an autoantibody selectively inhibiting the binding of von Willebrand factor to collagen. *Blood* **84**, 3378-3384.

209. Mohri, H., Hisanaga, S., Mishima, A., Fujimoto, S., Uezono, S. and Okubo, T. (1998) Autoantibody inhibits binding of von Willebrand factor to glycoprotein Ib and collagen in multiple myeloma: recognition sites present on the A1 loop and A3 domains of von Willebrand factor. *Blood Coag. Fibrinol.* **9**, 91-97.

210. Moake, J.L. and Chow, T.W. (1998) Increased von Willebrand factor (vWf) binding to platelets associated with impaired vWf breakdown in thrombotic thrombocytopenic purpura. *J. Clin. Apheresis.* **13**, 126-132.

211. Furlan, M. and Lämmle, B. (1999) Von Willebrand factor in thrombotic thrombocytopenic purpura. *Thromb. Haemost.* **82**, 592-600.

212. Baker, K.R. and Moake, J.L. (2000) Thrombotic thrombocytopenic purpura and the hemolytic-uremic syndrome. *Curr. Opin. Pediat.* **12**, 23-28.

213. Fessler, B.J. (1997) Thrombotic syndromes and autoimmune diseases. *Rheum. Dis. Clin. North Am.* **23**, 461-479.

214. Porta, C., Caporali, R. and Montecucco, C. (1999) Thrombotic thrombocytopenic purpura and autoimmunity: A tale of shadows and suspects. *Haematologica* **84**, 260-269.

215. Tefferi, A. and Nichols, W.L. (1997) Acquired von Willebrand disease: concise review of occurrence, diagnosis, pathogenesis, and treatment. *Am. J. Med.* **103**, 536-540.

216. Van Genderen, P.J.J. and Michiels, J.J. (1998) Acquired von Willebrand disease. *Baillieres Clin. Haematol.* **11**, 319-330.

217. Nitu-Whalley, I.C. and Lee, C.A. (1999) Acquired von Willebrand syndrome – report of 10 cases and review of the literature. *Haemophilia* **5**, 318-326.

218. Soff, G.A. and Green, D. (1993) Autoantibody to von Willebrand factor in systemic lupus erythematosus. *J. Lab. Clin. Med.* **121**, 424-430.

219. Macik, B.G. and Crow, P. (1999) Acquired autoantibodies to coagulation factors. *Curr. Opin. Hematol.* **6**, 323-328.

220. Mohri, H., Yamazaki, E., Suzuki, Z., Takano, T., Yokota, S. and Okubo, T. (1997) Autoantibody selectively inhibits binding of von Willebrand factor to glycoprotein Ib. Recognition site is located in the A1 loop of von Willebrand factor. *Thromb. Haemost.* **77**, 760-766.

221. Guariso, G., Ruffatti, A., Casonato, A., Drigo, P., Ghirardello, A. and Zancan, L. (1992) Antiphospholipid syndrome in a child with trisomy 21: the relationship between anticardiolipin G antibodies and the von Willebrand factor. *Clin. Exp. Rheumatol.* **10**, 613-616.

222. Lindsey, N.J., Dawson, R.A., Henderson, F.I., Greaves, M. and Hughes, P. (1993) Stimulation of von Willebrand factor antigen release by immunoglobulin from thrombosis prone patients with systemic lupus erythematosus and the anti-phospholipid syndrome. *Br. J. Rheumatol.* **32**, 123-126.

223. Schinco, P., Borchiellini, A., Tamponi, G., Montaruli, B., Garis, G., Bazzan, M., Pannocchia, A., Modena, V. and Pileri, A. (1997) Lupus anticoagulant and thrombosis: a role of von Willebrand factor multimeric forms. *Clin. Exp. Rheumatol.* **15**, 5-10.

224. Iwata, K., Seya, T., Yanagi, Y., Pesando, J.M., Johnson, P.M., Okabe, M., Ueda, S., Ariga, H. and Nagasawa, S. (1995) Diversity of sites for measles virus binding and for inactivation of complement C3b and C4b on membrane cofactor protein CD46. *J. Biol. Chem.* **270**, 15148-15152.

225. Sharma, A.K. and Pangburn, M.K. (1996) Identification of three physically and functionally distinct binding sites for C3b in human complement factor H by deletion mutagenesis. *Proc. Natl. Aacd. Sci. USA* **93**, 10996-11001.

226. Van der Poel, R.H.L., Meijers, J.C.M. and Bouma, B.N. (1999) Interaction between Protein S and Complement C4b binding Protein (C4BP). *J. Biol. Chem.* **274**, 15144-15150.
227. Blom, A.M., Webb, J., Villoutreix, B.O. and Dahlbäck (1999) A cluster of positively charged amino acids in the C4BP α-chain is crucial for C4b binding and Factor I cofactor function. *J. Biol. Chem.* **274**, 19237-19245.
228. Roubey, R.A.S. (1996) Immunology of the antiphospholipid antibody syndrome. *Arthritis Rheum.* **39**, 1444-1454.
229. Esmon, N.L., Smirnov, M.D. and Esmon C.T. (1997) Thrombogenic mechanisms of antiphospholipid antibodies. *Thromb. Haemost.* **78**, 79-82.
230. Koike, T., Ichikawa, K., Kasahara, H., Atsumi, T., Tsutsumi, A. and Matsuura, E. (1998) Epitopes on β2-GPI recognized by anticardiolipin antibodies. *Lupus* **7** (Suppl. 2), 14-17.
231. Corpet, F. (1988) Multiple sequence alignment with hierarchical clustering. *Nucl. Acids Res.* **16** (22), 10881-10890.239
232. Hansen, J.E., Lund, O., Engelbrecht, J., Bohr, H., Nielsen, J.O., Hansen, J.E.S. and Brunak, S. (1995) Prediction of O glycosylation of mammalian proteins: Specificity patterns of UDP-GalNAc:polypeptide *N*-acetylgalactosaminyltransferase. *Biochem. J.* **308**, 801 813.
233. Moore, M.D., DiScippio, R.G., Cooper, N.R. and Nemarrow, G.R. (1989) Hydrodynamic electron microscopic and ligand binding analysis of the Epstein-Barr virus/C3dg receptor (CR2). *J. Biol. Chem.* **264**, 20576-20582.
234. Di Scipio, R.G. (1992) Ultrastructures and interactions of complement factors H and I. *J. Immunol.* **149**, 2592-2599.
235. Stopar, D., Spruijt, R.B., Wolfs, C.J.A.M. and Hemminga, M.A. (1996) Local dynamics of the M13 Major Coat Protein in different membrane-mimicking systems. *Biochemistry* **35**, 15467-15473.
236. Mall, S., Sharma, R.P., East, J.M. and Lee, A.G. (1998) Lipid-protein interactions in the membrane: Studies with model peptides. *Faraday Discussions* **111**, 127-136.
237. Mangavel, C., Maget-Dana, R., Tauc, P., Brochon, J.C., Sy, D. and Reynaud, J.A. (1998) Structural investigations of basic amphipathic model peptides in the presence of lipid vesicles studied by circular dichroism, fluorescence, monolayer and modeling. *Biochim. Biophys. Acta* **1371**, 265-283.
238. de Planque, M.R.R., Kruijtzer, J.A.W., Liskamp, R.M.J., Marsh, D., Greathouse, D.V., Koeppe, R.E., de Kruijff, B. and Killian, J.A. (1999) Different membrane anchoring positions of tryptophan and lysine in synthetic transmembrane α-helical peptides. *J. Biol. Chem.* **274**, 20839-20847.
239. Brady, R.L., Dodson, E.J., Dodson, G.G., Lange, G., Davis, S.J., Williams, A.F. and Barclay, A.N. (1993) Crystal structure of domains 3 and 4 of rat CD4: relation to the NH$_2$-terminal domains. *Science* **260**, 979-983.
240. Bodian, D.L., Jones, E.Y., Harlos, K., Stuart, D.I. and Davis, S.J. (1994) Crystal structure of the extracellular region of the human cell adhesion molecule CD2 at 2.5 Å resolution. *Structure* **2**, 755-766.
241. Leahy, D.J., Aukhil, I. and Erickson, H.P. (1996) 2.0 Å crystal structure of a four-domain segment of human fibronectin encompassing the RGD loop and synergy region. *Cell* **84**, 155-164.
242. Horbach, D.A., van Oort, E., Donders, R.C.J.M., Derksen, R.H.W.M. and de Groot, P.G. (1996) Lupus anticoagulant is the strongest risk factor for both venous and arterial thrombosis in patients with systematic lupus erythematosus-Comparison between different assays for detection of antiphospholipid antibodies. *Thromb. Haemost.* **76**, 916-924.
243. Saxena, A., Gries, A., Schwarzenbacher, R., Kostner, G.M., Laggner, P. and Prassl, R. (1998) Crystallization and preliminary X-ray crystallographic studies on apolipoprotein H (β2 glycoprotein-I) from human plasma. *Acta Crystallog. D* **54**, 1450-1452.
244. Ravelli, R.B.G., Sweet, R.M., Skinner, J.M., Duisenberg, A.J.M. and Kroon, J. (1997) STRATEGY: a program to optimize the starting spindle angle and scan range for X-ray data collection. *J. Appl. Cryst.* **30**, 551-554.
245. Collaborative Computional Project No 4 (1994) The CCP4 suite: programs for protein crystallography. *Acta Crystallogr. D* **50**, 760-763.
246. Nicholls, A., Sharp, K.A. and Honig, B. (1993) GRASP: graphical representation and analysis of surface properties. *Biophys. J.* **64**, 166-170.
247. Wallace, A.C., Laskowski, R.A. and Thornton, J.H. (1995) LIGPLOT: A program to generate schematic diagrams of protein ligand interactions. *Prot. Eng.* **8**, 127-134.
248. Galli, M., Ruggeri, L. and Barbui, T. (1998) Differential effects of anti-β$_2$-Glycoprotein I and antiprothrombin antibodies on the anticoagulant activity of activated protein C. *Blood* **91**, 1999-2004.
249. Ieko, M., Ichikawa, K., Triplett, D.A., Matsuura, E., Atsumi, T., Sawada, K.I. and Koike, T. (1999) β$_2$ Glycoprotein I is necessary to inhibit protein C activity by monoclonal anticardiolipin antibodies. *Arthritis Rheum.* **42**, 167-174.
250. Bouma, B., de Groot, Ph.G., van den Elsen, J.M.H., Ravelli, R.B.G., Schouten, A., Simmelink, M.J.A., Derksen, R.H.W.M., Kroon, J. and Gros, P. (1999) Adhesion mechanism of human β2-Glycoprotein I to phospholipids based on its crystal structure. *EMBO J.* **18**, 5166-5174.
251. Schwarzenbacher, R., Zeth, K., Diederichs, K., Gries, A., Kostner, G.M., Laggner, P. and Prassl, R. (1999 Crystal structure of human beta2-glycoprotein-I: implications for phospholipid binding and the antiphospholipid syndrome. *EMBO J.* **18**, 6228-6239.
252. Brandt, J.T. (1993) Antibodies to β2-glycoprotein I inhibit phospholipid dependent coagulation reactions. *Thromb. Haemost.* **70**, 598-602.
253. Arnout, J., Vanrusselt, M., Wittevrongel, C. and Vermylen, J (1998). Monoclonal antibodies against β-2 Glycoprotein I: Use as reference material for Lupus Anticoagulant tests. *Thromb Haemost* **79**, 955-958.
254. Atsumi, T., Khamashta, M.A., Amengual, O., Donohoe, S., Mackie, I., Ichikawa, K., Koike, T. and Hughes, G.R.V. (1998) Binding of anticardiolipin antibodies to protein C via β$_2$-glycoprotein I (β$_2$-GPI): a possible mechanism in the inhibitory effect of antiphospholipid antibodies on the protein C system. *Clin. Exp. Immunol.* **112**, 325-333.
255. Niemeier, A., Willnow, T., Dieplinger, H., Jacobsen, C., Meyer, N., Hilpert, J. and Beisiegel, U. (1999) Identification of megalin/gp330 as a receptor for lipoprotein(a) in vitro. *Arterioscler. Thromb. Vasc. Biol.* **19**, 552-561.
256. Kanalas, J.J. (1992) Analysis of plasmin binding and urokinase activation of plasminogen bound to the Heymann nephritis autoantigen, gp330. *Arch. Biochem. Biophys.* **299**, 255-260.
257. Kanalas, J.J. (1993) Effect of the nephritogenic autoantibody of Heymann's nephritis on plasminogen-binding to gp330 and activation by urokinase. *Biochim. Biophys. Acta* **1225**, 101-106.

258. Gliemann, J. (1998) Receptors of the low density lipoprotein (LDL) receptor family in man. Multiple functions of the large family members via interaction with complex ligands. *Biol. Chem.* **379**, 951-964.
259. Chattopadhyaya, R., Meador, W.E., Means, A.R. and Quiocho, F.A. (1992) Calmodulin structure refined at 1.7 Å resolution. *J. Mol. Biol.* **228**, 1177-1192.
260. Butler, J.E., Ni, L., Brown, W.R., Joshi, K.S., Chang, J., Rosenberg, B. and Voss, E.W., Jr. (1993) The immunochemistry of sandwich ELISAs—VI. Greater than 90% of monoclonal and 75% of polyclonal anti-fluorescyl capture antibodies (Cabs) are denatured by passive adsorption. *Mol. Immunol.* **30**, 1165-1175.
261. Butler, J.E., Navarro, P. and Sun, J. (1997) Adsorption-induced antigenic changes and their significance in ELISA and immunological disorders. *Immunol. Invest.* **26**, 39-54.
262. Brighton, T.A., Dai, Y.-P., Hogg, P.J. and Chesterman, C.N. (1999) Microheterogeneity of β-2 glycoprotein I: implications for binding to anionic phospholipids. *Biochem. J.* **340**, 59-67.
263. Chattopadhyaya, R., Meador, W.E., Means, A.R. and Quiocho, F.A. (1992) Calmodulin structure refined at 1.7 Å resolution. *J. Mol. Biol.* **228**, 1177-1192.
264. Halkier, T. and Magnusson, S. (1988) Contact activation of blood coagulation is inhibited by plasma factor XIII b-chain. *Thromb. Res.* **51**, 313-324.
265. Pittoni, V., Ravirajan, C.T., Donohoe, S., Machin, S.J., Lydyard, P.M. and Isenberg, D.A. (2000) Human monoclonal anti phospholipid antibodies selectively bind to membrane phospholipid and β_2-glycoprotein I (β_2-GPI) on apoptotic cells. *Clin. Exp. Immunol.* **119**, 533-543.
266. Hörkkö, S., Miller, E., Dudl, E., Reaven, P., Curtiss, L.K., Zvaifler, N.J., Terkeltaub, R., Pierangeli, S.S., Branch, D.W., Palinski, W. and Witztum, J.L. (1996) Antiphospholipid antibodies are directed against epitopes of oxidized phospholipids. *J. Clin. Invest.* **98**, 815-825.
267. Hörkkö, S., Miller, E., Branch, D.W., Palinski, W. and Witztum, J.L. (1997) The epitopes for some antiphospholipid antibodies are adducts of oxidized phospholipid and β_2 glycoprotein 1 (and other proteins). *Proc. Natl. Acad. Sci. USA* **94**, 10356-10361.
268. Hasunuma, Y., Matsuura, E., Makita, Z., Katahira, T., Nishi, S. and Koike, T. (1997) Involvement of β_2 glycoprotein I and anticardiolipin antibodies in oxidatively modified low-density lipoprotein uptake by macrophages. *Clin. Exp. Immunol.* **107**, 569-573.
269. Kalafatis, M., Jenny, R.J. and Mann, K.G. (1990) Identification and characterization of a phospholipid-binding site of bovine factor Va. *J. Biol. Chem.* **265**, 21580-21589.
270. Lecompte, M.-F., Bouix, G. and Mann, K.G. (1994) Electrostatic and hydrophobic interactions are involved in factor Va binding to membranes containing acidic phospholipids. *J. Biol. Chem.* **269**, 1905-1910.
271. Gilbert, G.E. and Baleja, J.D. (1995) Membrane-binding peptide from the C2 domain of factor VIII forms an amphipathic structure as determined by NMR spectroscopy. *Biochemistry* **34**, 3022-3031.
272. Kamerling, J.P. and Vliegenthart, J.F.G. (1989) Mass spectrometry. In: Lawson, A.M. (ed.): Clinical biochemistry: principles, methods, applications, Vol. 1, Walter de Gruyter, Berlin, 176-263.
273. Gerwig, G.J. and Vliegenthart, J.F.G. (2000) Analysis of glycoprotein-derived glycopeptides. In: Jollès, P. and Jörnvall, H. (eds.): Proteomics in functional genomics. Birkhäuser Verlag, Basel, 159-186.
274. Kaufmann, R. (1995) Matrix-assisted laser desorption ionization (MALDI) mass spectrometry: a novel analytical tool in molecular biology and biotechnology. *J. Biotechnology* **41**, 155-175.
275. Harvey, D.J. (1996) Matrix-assisted laser desorption/ionisation mass spectrometry of oligosaccharides and glycoconjugates. *J. Chromatogr. A* **720**, 429-446.
276. Bligh, E.G. and Dyer, W.J.A. (1959) Rapid method for total lipid extraction and purification. *Can. J. Biochem. Physiol.* **37**, 911-917.
277. Esnouf, R.M. (1997) An extensively modified version of MolScript that includes greatly enhanced colouring capabilities. *J. Mol. Graph. Model.* **15**, 132-134, 112-113.
278. Gerwig, G.J. and Damm, J.B.L. (1998) General strategies for the characterization of carbohydrates from recombinant glycoprotein therapeutics. In: Subramanian, G. (ed.): Bioseparation and bioprocessing, Vol. II, Ch. 12, Wley-VCH, Weinheim, 325-375.
279. Lee, T. (1998) Biosynthesis and possible biological functions of plasmalogens. *Biochim. Biophys. Acta* **1394**, 129-145.
280. Horrocks, L.A. (1968) The alk-1-enylgroup content of mammalian myelin phosphoglycerides by quantitative two dimensional thin-layer chromatography. *J. Lipid Res.* **9**, 469-472.
281. Rouser, G., Fleischer, S. and Jamamoto, A. (1970) Two dimensional thin-layer chromatography separation of polar lipids and determination of phospholipids by phosphorus analysis of spots. *Lipids* **5**, 494-496.
282. Dougherty, D.A. and Stauffer, D.A. (1990) Acetylcholine binding by a synthetic receptor: implications for biological recognition. *Science* **250**, 1558-1566.
283. Verdonk, M.L., Boks, G.J., Kooijman, H., Kanters, J.A. and Kroon, J. (1993) Stereochemistry of charged nitrogen aromatic interactions and its involvement in ligand-receptor binding. *J. Comput. Aided Mol. Des.* **7**, 173-182.
284. Padlan, E.A., Cohen, G.H. and Davies, D.R. (1985) On the specificity of antibody/antigen interaction: phosphocholine binding to McPC603 and the correlation of three-dimensional structure and sequence data. *Ann. Inst. Pasteur Immunol.* **136C**, 271-276.
285. Olson, R., Nariya, H., Yokota, K., Kamio, Y. and Gouaux, E. (1999) Crystal structure of Staphylococcal LukF delineates conformational changes accompanying formation of a transmembrane channel. *Nat. Struct. Biol.* **6**, 134-140.
286. Thompson, D., Pepys, M.B. and Wood, S.P. (1999) The physiological structure of human C-reactive protein and its complex with phosphocholine. *Structure* **7**, 169-177.
287. Wu, R., Svenungsson, E., Gunnarsson, I., Andersson, B., Lundberg, I., Schäfer Elinder, L. and Frostegård, J. (1999) Antibodies against lysophosphatidylcholine and oxidized LDL in patients with SLE. *Lupus* **8**, 142-150.
288. Romero, F.I., Atsumi, T., Tinahones, F.J., Gómez-Zumaquero, J.M., Amengual, O., Khamashta, M.A. and Hughes, G.R.V. (1999) Autoantibodies against malondialdehyde-modified lipoprotein(a) in antiphospholipid syndrome. *Arthritis Rheum.* **42**, 2606-2611.

289. Brosche, T. and Platt, D. (1998) The biological significance of plasmalogens in defense against oxidative damage. *Exp. Gerontol.* **33**, 363-369.
290. Hörkkö, S., Bird, D.A., Miller, E., Itabe, H., Leitinger, N., Subbanagounder, G., Berliner, J.A., Friedman, P., Dennis, E.A.,Curtiss, L.K., Palinski, W. and Witztum., J.L. (1999) Monoclonal autoantibodies specific for oxidized phospholipid-protein adducts inhibit macrophage uptake of oxidized low-density lipoproteins. *J. Clin. Invest.* **103**, 117-128.
291. Mohri, H., Yoshioka, A., Zimmerman, T.S. and Ruggeri, Z.M. (1989) Isolation of the von Willebrand factor domain interacting with platelet glycoprotein Ib, heparin, and collagen and characterization of its three distinct functional sites. *J. Biol. Chem.* **264**, 17361-17367.
292. Cruz, M.A., Yuan, H., Lee, J.R., Wise, R.J. and Handin, R.I. (1995) Interaction of the von Willebrand Factor (vWF) with collagen. *J. Biol. Chem.* **270**, 10822-10827.
293. Colombatti, A. and Bonaldo, P. (1991) The superfamily of proteins with von Willebrand factor-type A-like domains: One theme common to components of extracellular matrix, hemostasis, cellular adhesion and defense mechanisms. *Blood* **77**, 2305-2315.
294. Perkins, S.J., Smith, K.F., Williams, S.C., Haris, P.I., Chapman, D. and Sim, R.B. (1994) The secondar structure of the von Willebrand factor type A domain in factor B of human complement by Fourier-transform infrared spectroscopy. Its occurrence in collagen type-VI, type-VII, type-XII and type-XIV, the integrins and other proteins by averaged structure predictions. *J. Mol. Biol.* **238**, 104-119.
295. Michishita, M., Videm, V., Arnaout, M.A. (1993) A novel divalent cation-binding site in the A domain of the β_2 integrin CR3 (CD11b/CD18) is essential for ligand binding. *Cell* **72**, 857-867.
296. Bockenstedt, P., McDonagh, J. and Handlin, R.I. (1986) Binding and covalent cross linking of purifie vonWillebrand factor to native monomeric collagen. *J. Clin. Invest.* **78**, 551-556.
297. Cruz, M.A., Bienkowska, J., Liddington, R. and Handin, R.I. (1997) Identification of the collagen binding site in the vWF-A3 domain by molecular structure and site-specific mutagenesis. Blood 90, 23A (abstract).
298. Hale, J.E. (1995) Irreversible, oriented immobilization of antibodies to Cobalt iminodiacetate resin for use as immunoaffinity media. Anal. Biochem. **231**, 46-49.
299. Dübel, S., Breitling, F., Fuchs, P., Zewe, M., Gotter, S., Welschof, M., Moldenhauer, G. and Little, M. (1994) Isolation of IgG antibody Fv-DNA from various mouse and rat hybridoma cell lines using the polymerase chain reaction with a simple set of primers. *J. Immunol. Methods* **175**, 89-95.
300. Carrol, W.L., Mendel, E. and Levy, S. (1988) Hybridoma fusion cell lines contain an aberrant kappa transcript. *Mol. Immunol.* **25**, 991-995.
301. Kabat, E.A., Wu, T.T., Perry, H.M., Gottesman, K.S. and Foeller, C. (1991) "Sequences of proteins of immunological interest", 5th ed. Bethesda MD: US National Institutes of Health. Vol 1.
302. Navazza, J. (1994) AMoRe: an automated package for molecular replacement. *Acta Crystallogr. A* **50**, 157-163.
303. Blundell, T.L. and Johnson, L.N. (1976) Protein Crystallography. Academic Press, New York.
304. Van den Elsen, J.M., Herron, J.N., Hoogerhout, P., Poolman, J.T., Boel, E., Logtenberg, T., Wilting, J., Crommelin, D.J., Kroon, J. and Gros, P. (1997) Bactericidal antibody recognition of a PorA epitope of Neisseria meningitidis: crystal structure of a Fab fragment in complex with a fluorescein-conjugated peptide. *Proteins* **29**, 113-125.
305. Brünger, A.T. (1990) Extension of molecular replacement: A new search strategy based on Patterson correlation refinement. *Acta Crystallogr. A* **46**, 46-57.
306. Bedzyk, W.D., Johnson, L.S., Riordan, G.S., and Voss Jr., E.W. (1989) Comparison of variable region primary structures within an anti-fluorescein idiotype family. J. Biol. Chem. 265, 18615-18620.
307. Herron, J.N., He, X.-M., Mason, M.L., Voss Jr., E.W. and Edmundson, A.B. (1989) Three-dimensional structure of a fluorescein-Fab complex crystallized in 2-methyl-2, 4-pentanediol. *Proteins* **5**, 271-280.
308. Banfield, M.J., Barker, J.J., Perry, A. and Brady, R.L. (1998) Function from structure? The crystal structure of human phosphatidylethanolamine-binding protein suggests a role in membrane signal transduction. *Structure* **6**, 1245-1254.
309. Stanfield, R.I., Fieser, T.M., Lerner, R.A. and Wilson, I.A. (1990) Crystal structure of an antibody to a peptide and its complex with peptide antigen at 2.8 Angstroms. *Science* **248**, 712-719.
310. Oxvig, C., Lu, C. and Springer, T.A. (1999) Conformational changes in tertiary structure near the ligand binding site of an integrin I domain. *Proc. Natl. Acad. Sci. USA* **96**, 2215-2220.
311. Kamata, T., Puzon, W. and Takada, Y. (1994) Identification of putative ligand binding sites within I domain of integrin α2β1 (VLA-2, CD49b/CD29). *J. Biol. Chem.* **269**, 9659-9663.
312. Kamata, T. and Takada, Y. (1994) Direct binding of collagen to the I-domain of integrin α2β1 (VLA-2, CD49b/CD29) in a divalent cation-independent manner. *J. Biol. Chem.* **269**, 26006-26010.
313. Smith, C., Estavillo, D., Emsley, J., Bankston, L.A., Liddington, R.C. and Cruz, M.A. (2000) Mapping the collagen binding site in the I domain of the glycoprotein Ia/IIa (integrin $\alpha_2\beta_1$). *J. Biol. Chem.* **275**, 4205-4209.
314. Roth, G.J., Titani, K., Hoyer, L.W. and Hickey, M.J. (1986) Localization of binding sites within human von Willebrand factor for monomeric type III collagen. *Biochemistry* **25**, 8357-8361.

--- Summary ---

The integrity of blood circulation is a prerequisite for life; its malfunctioning is a leading cause of morbidity and mortality in developed countries. For that reason the haemostatic system is a critical component of homeostasis. In *Chapter I* an overview is given of the biophysical and biochemical characterization of two human plasma proteins that serve important functions in haemostasis: β_2-glycoprotein I (β2gpI) and von Willebrand factor (vWf). β2gpI has a proposed role in clearance of thrombogenic apoptotic cells and in coagulation. Moreover, β2gpI is the key target of auto-antibodies in the auto-immune disease anti-phospholipid syndrome (APS), resulting in thrombotic complications. β2gpI binds with its fifth C-terminal short concensus repeat (SCR) domain to anionic lipids. This affinity is increased by complexation of β2gpI in divalent β2gpI-antibody complexes, which results in shielding of anionic surfaces that are necessary in coagulation. Binding to anionic lipids is possibly the primary involvement of β2gpI in coagulation. Multimeric vWf has a key function in the haemostatic system when an arterial vessel wall is damaged. Multi-domain vWf contains the binding site for collagen located in its A3 domain. When an arterial vessel wall is ruptured, binding of the A3 domain to exposed collagen is a first step in haemostasis, that facilitates recruitment of platelets for formation of a blood clot. The function of vWf can be disturbed by quantitative and qualitative alterations of the protein and by non-self compounds that induce spontaneous platelet aggregation. Disturbed vWF function results in bleeding tendencies or thrombotic complications. Structural insights into adhesion of β2gpI to lipids and of vWf-A3 to collagen are of valuable help in understanding their role in homeostasis and in yielding insight into the molecular origin of, for example, coagulation disorders.

β_2-Glycoprotein I

In *Chapter II* we describe the crystal-structure elucidation of β2gpI from human plasma. The structure is solved at 2.7 Å resolution with the multiple isomorphous replacement method and reveals that β2gpI has an elongated fish-hook like arrangement of its five globular SCR domains. Half of the fifth domain has a unique face created by a six-residue insertion and a 19-residue C-terminal extension, together with some rearrangement of parts of the SCR-like core. Based on this structure and on biochemical data we propose a model for adhesion to anionic lipids. A large patch of 14 cationic residues provides favorable electrostatic interactions with anionic surfaces, and an exposed membrane-insertion loop containing a typical Trp-Lys sequence yields specificity for lipids. The lipid-adhesion site is located at the tip and outer curve of the β2gpI fish-hook. From the crystal structure we infer that in the lipid-bound state, domains one to four point away from the lipid layer. Domains three and four are partly shielded for protein-protein interactions by the four N-glycans attached to these domains. Domains one and two are fully exposed and may provide binding sites in apoptosis, APS and coagulation. In *Chapter III* we address β2gpI-protein complex formation in solution using gel-filtration chromatography. β2gpI forms a stable complex with IgG 22F6

which has properties common to auto-antibodies that are active in APS. This indicates that lipid adhesion is not always a prerequisite for formation of active β2gpI-antibody complexes. β2gpI does not form complexes in solution with protein C and protein S which are anticoagulants. Complex formation between protein S and its inhibitor C4B binding protein lowers the concentration of free protein S, which results in inhibition of the anticoagulant function of protein S. The complex of protein S and C4B binding protein remains stable, even in the presence of β2gpI. Therefore, our experiments do not reveal further evidence that supports an anticoagulant function of β2gpI by maintaining the level of free protein S. With our binding experiments we cannot establish previously reported high-affinity complexation between β2gpI and calmodulin. Stable complexes putatively only form *in vivo* when β2gpI is bound to lipids. In *Chapter IV* we describe structural differences between intact β2gpI and an isoform of β2gpI (denoted β2gpI *1) that has lost its ability to adhere to anionic lipids and that is present in plasma during oxidative stress. With gas chromatography-mass spectrometry and thin-layer chromatography we show that β2gpI *1 has bound phosphatidyl-choline (PC) or choline plasmalogen, and, to a lesser extent, sphingomyelin. The crystal structure at 3.0 Å resolution of β2gpI *1 indicates a binding pocket for a glycerophosphorylcholine moiety located within the adhesion site for anionic lipids. The choline moiety is buried deeply inside the pocket and is surrounded by an anionic residue and two aromatic residues; these are aspects common to several PC-binding proteins. With C-terminal sequencing, carbohydrate analysis and mass spectrometry we show that, neither enzymatic cleavage at Ala314-Phe315, nor mutation Trp316Ser, cleavage of sialic acid residues, or differences in N-glycan content, account for the observed difference in lipid-adhesive properties of β2gpI *1. Therefore, specific binding of a neutral lipid seems to be fully responsible for blocking adhesion to anionic membranes. Based on these findings we discuss a possible role for β2gpI *1 in defense mechanisms during oxidative stress. The crystal structure of β2gpI *1, together with the structures of β2gpI, which was partially cleaved at Lys317-Thr318 (Ref. 250), and of intact β2gpI[251], also provides new insights that contribute to a more detailed anionic lipid-adhesion model. In the *Appendix* to *Chapter IV* we address recently discerned specific structural radiation damage of proteins upon exposure of crystals to very intense X-ray beams of a third-generation synchrotron. We describe a new method for refinement of partially broken disulfide bonds which appear to be present in β2gpI *1. Effects of specific structural radiation damage include complete cleavage of the carboxyl group of one Glu residue and partial cleavage of all eleven disulfide bonds, observed in the most severely affected crystal of β2gpI *1. After refinement differences among disulfide bonds in position of the S_γ-atom and in electron density accounting for the partially broken bonds suggest that solvent-exposed bonds are more susceptible to radiation than buried bonds. Comparison of the severely affected structure of β2gpI *1 with that of virtually not damaged β2gpI *1 (*Chapter IV*) shows that specific structural radiation damage is localized to acidic residues and cystines. No changes in the global conformation of β2gpI *1 are observed. This implies that the structural implications presented in *Chapter IV* are not compromised by radiation damage.

Von Willebrand factor A3-domain

In *Chapter V* we describe the crystal-structure determination of the vWf (Se-Met) A3-domain, in its complex with a Fab fragment of antibody RU5, which inhibits binding of vWf to collagen. With this structure we aimed at locating the collagen-binding site in the A3 domain of vWf. The structure is solved at 2.0 Å resolution by molecular replacement using the anomalous signal of the seleno methionines. The epitope of RU5 involves residues that are part of an α-helix and three solvent-exposed loops, located at the 'bottom' side of A3. Comparison with other structures of A3 shows that RU5 binding does not induce long-range conformational changes. Instead, RU5 most likely blocks collagen binding by steric hindrance, which implies that the collagen-binding site is located at or close to the epitope of RU5 near the bottom side of A3. Surprisingly, the collagen-binding site of vWf-A3 is located distant from the top face of the domain where collagen-binding sites are found in homologous integrin I-domains. Apparently, vWf-A3 and integrin I-domains bind collagen in fundamentally different ways. The structure of A3-RU5 provides an excellent starting point for further exploration of the collagen-binding site by means of site-directed mutagenesis.

--- Samenvatting ---

Het goed functioneren van onze bloedsomloop is een essentiële voorwaarde voor een gezond bestaan. Dit wordt geïllustreerd door het feit dat hart- en vaatziekten de meeste ziekte- en sterftegevallen veroorzaken in de ontwikkelde landen. Het haemostase systeem maakt dan ook een belangrijk onderdeel uit van de homeostase. In *Hoofdstuk I* wordt een overzicht gegeven van de biofysische en biochemische karakterisering van twee humane plasma-eiwitten die een belangrijke functie vervullen in haemostase: β_2-glycoproteïne I (β2gpI) en von Willebrand factor (vWf). Aan β2gpI wordt een functie toegeschreven gerelateerd aan het verwijderen van trombogene apoptotische cellen uit de bloedbaan en in de proteïne C-afhankelijke anti-stollingscascade. Daarnaast is β2gpI het belangrijke antigeen voor auto-antilichamen die aanwezig zijn in personen die lijden aan de auto-immuunziekte 'anti-fosfolipiden syndroom' (APS), een ziekte die onder andere wordt gekenmerkt door een sterk verhoogd risico voor trombose. Het vijfde C-terminale 'short concensus repeat' (SCR) domein van β2gpI bindt aan anionische lipiden. Deze affiniteit wordt sterk verhoogd onder invloed van complexvorming van β2gpI in divalente β2gpI-antilichaamcomplexen, wat leidt tot het afschermen van anionische oppervlakken die belangrijk zijn in anti-stollingsprocessen. Deze afscherming wijst op de mogelijk belangrijke factor van β2gpI in de bloedstolling. Multimeer vWf speelt een sleutelrol in het haemostase systeem als een slagaderlijke vaatwand beschadigd raakt. Multi-domein vWf heeft een bindingsplaats voor collageen, welke gelokaliseerd is in het A3 domein. Wanneer een bloedvat beschadigd is, is binding van het A3 domein aan blootgesteld collageen één van de eerste stappen in haemostase. Deze binding is essentieel voor het rekruteren van bloedplaatjes ten behoeve van het vormen van een bloedstolsel. Het functioneren van vWf kan verstoord raken door kwantitatieve en kwalitatieve veranderingen van het eiwit en door bepaalde lichaamsvreemde stoffen die spontane klontering van bloedplaatjes veroorzaken. Verstoring van de functie van vWf leidt tot interne bloedingen of tot trombose. Structuurinformatie over de binding van β2gpI aan lipiden en over binding van vWf-A3 aan collageen is van groot belang om de rol van deze eiwitten in de homeostase te begrijpen en om inzicht te verkrijgen in de moleculaire grondslag van, bijvoorbeeld, verstoorde bloedstolling.

β_2-Glycoproteïne I

In *Hoofdstuk II* wordt de opheldering beschreven van de kristalstructuur van β2gpI dat uit humaan bloedplasma is gezuiverd. De structuur is bepaald tot een resolutie van 2.7 Å met behulp van de meervoudige isomorfe vervangingsmethode en laat zien dat de vijf globulaire SCR domeinen van β2gpI een zeer uitgerekte vishaak-achtige rangschikking hebben. De ene helft van het vijfde domein vormt een unieke zijde die gevormd wordt door een insertie van zes aminozuren en een verlenging bestaande uit negentien aminozuren; dit gaat samen met enige herrangschikking van delen van de SCR basisstructuur. Gebaseerd op deze structuur en op beschikbare biochemische gegevens stellen wij een model op die de binding van β2gpI aan anionische lipiden beschrijft. Een groot oppervlak bestaande uit veertien kationische aminozuren verschaft gunstige elektrostatische interacties met anionische componenten; een

vrijelijk beschikbaar membraan anker, bestaande uit onder andere een typische tryptofaan-lysine sequentie, zorgt voor specificiteit van β2gpI voor anionische lipiden. De bindingsplaats voor membranen bevindt zich aan de punt en tevens aan de buitenzijde van de kromming van het vishaakje dat β2gpI vormt. Uit de kristalstructuur leiden we af dat wanneer β2gpI gebonden is aan lipiden, domeinen één tot en met vier ver weg van het membraanoppervlak en in de oplossing steken. Domeinen drie en vier zijn door hun N-gebonden suikers gedeeltelijk afgeschermd voor eiwit-eiwit interacties. Domeinen één en twee zijn volledig beschikbaar voor eiwit-eiwit interacties en bevatten mogelijk bindingsplaatsen die een rol spelen in apoptose, APS en bloedstolling. In *Hoofdstuk III* richten we ons met behulp van gelfiltratie chromatografie op het bestuderen van de vorming van β2gpI-eiwit complexen in oplossing. β2gpI vormt een stabiel complex met het antilichaam '22F6' dat eigenschappen gemeen heeft met die welke waargenomen worden voor auto-antilichamen die actief zijn in APS. Deze waarneming duidt erop dat de binding aan membranen niet altijd een vereiste is voor het vormen van actieve complexen tussen β2gpI en auto-antilichamen. β2gpI vormt in oplossing geen complex met proteïne C of met proteïne S, die betrokken zijn in anti-stollingsprocessen. Complexvorming tussen proteïne S en C4B binding protein resulteert in een verlaagde proteïne S concentratie, waardoor de remmende werking van proteïne S op bloedstolling vermindert. Het complex tussen proteïne S en C4B bindend eiwit blijft zelfs zeer stabiel in aanwezigheid van β2gpI. Dientengevolge leveren onze experimenten geen aanvullend bewijs dat een functie voor β2gpI als anti-stollingsfactor ondersteunt: β2gpI zou de concentratie aan vrij proteïne S reguleren. Met onze bindingsexperimenten kunnen we niet de eerder gepubliceerde hoge affiniteit van β2gpI voor calmoduline aantonen. Het is mogelijk dat stabiele complexen alleen *in vivo* gevormd worden, als β2gpI gebonden is aan lipiden. In *Hoofdstuk IV* beschrijven we de waargenomen verschillen tussen de structuur van intact β2gpI en van een gelijkende vorm van β2gpI (aangeduid met β2gpI *1) die echter niet meer aan anionische lipiden kan binden en die gedurende oxidatieve stress aanwezig is in het bloed. Met behulp van gaschromatografie gecombineerd met massaspectrometrie en met dunne-laag chromatografie laten we zien dat β2gpI *1 een fosfatidylcholine (PC) of een choline plasmalogeen molecuul gebonden heeft en in mindere mate een sfingomyeline molecuul. De kristalstructuur van het β2gpI-lipide complex, die bepaald is tot een resolutie van 3.0 Å, suggereert dat zich een bindingsplaats voor een glycerofosfaatcholine eenheid bevindt in het midden van de bindingsplaats voor anionische membranen. De choline eenheid bevindt zich op de bodem van de bindingsplaats en wordt omringd door een anionisch aminozuur en twee aromatische aminozuren; deze aspecten worden algemeen waargenomen voor meerdere PC-bindende eiwitten. Door middel van C-terminale aminozuurbepaling, suikeranalyse en massaspectrometrie tonen we aan dat noch een enzymatische knip tussen Ala314 en Phe315, noch de mutatie Trp316Ser, noch het wegknippen van siaalzuur, noch mogelijke verschillen in het gehalte aan N-gebonden suikers, een rol spelen in de waargenomen verminderde affiniteit van β2gpI *1 voor anionische lipiden. Daarom lijkt de specifieke binding van een neutraal lipide volledig verantwoordelijk te zijn voor het blokkeren van de mogelijkheid om aan anionische membranen te binden. Gebaseerd op deze bevindingen halen we in de discussie een mogelijke rol aan voor het β2gpI-lipide complex in het verdedigingssysteem gedurende oxidatieve stress. Naast de gedetailleerde structuurinformatie die we verkregen hebben over de aspecten die van invloed zijn op de binding aan anionische lipiden, verschaft de kristalstructuur van β2gpI *1, te zamen met de structuren van β2gpI, dat gedeeltelijk geknipt was tussen Lys317 en Thr318 (Ref. 250) en intact β2gpI[251], nieuwe inzichten die bijdragen aan een meer gedetailleerd model voor de adhesie van β2gpI aan anionische lipiden. In de *Appendix* bij *Hoofdstuk IV* richten we ons op recent onderkende specifieke stralingsschade aan de structuur van eiwitten, die veroorzaakt wordt door het bestralen van kristallen met

zeer intense röntgenbundels van een derde-generatie synchrotronbron. We beschrijven een methode voor de verfijning van zwavelbruggen die gedeeltelijk verbroken zijn; deze zijn namelijk aanwezig in β2gpI *1. De effecten van specifieke stralingsschade op de structuur zijn onder andere het volledig afsplitsen van een carboxyl groep van één Glu residu en het gedeeltelijke verbreken van alle elf zwavelbruggen, zoals is waargenomen voor het zwaarst aangetaste kristal van β2gpI *1. De na de verfijning waargenomen verschillen tussen zwavelbruggen voor wat betreft de positie van de S_γ-atomen en de electronendichtheid ter plekke van de gedeeltelijk verbroken zwavelbruggen, suggereren dat zwavelbruggen die in de periferie van de eiwitstructuur liggen meer vatbaar zijn voor stralingsschade dan zwavelbruggen die zich binnenin de eiwitstructuur bevinden. Wanneer de zwaar aangetaste structuur van β2gpI *1 vergeleken wordt met die van β2gpI *1, die niet noemenswaardig is aangetast (*Hoofdstuk IV*), blijkt dat de specifieke stralingsschade beperkt blijft tot anionische aminozuren en cystines. We nemen geen veranderingen waar van de globale conformatie van β2gpI *1. Dit houdt in dat de gevolgtrekkingen op basis van de structuur van β2gpI *1, zoals beschreven in *Hoofdstuk IV*, niet gecompromitteerd zijn door niet-verdisconteerde effecten van stralingsschade.

Von Willebrand factor A3-domein

In *Hoofdstuk V* beschrijven we de bepaling van de kristalstructuur van het vWf (seleno-methionine) A3-domein in complex met een Fab fragment van het antilichaam 'RU5' dat de binding van vWf aan collageen remt. Met behulp van deze structuur proberen we de bindingsplaats voor collageen in het A3 domein te lokaliseren. De structuur is bepaald op een resolutie van 2.0 Å met behulp van de moleculaire vervangingsmethode, die ondersteund werd door het gebruik van het anomaal signaal van seleno-methionine residuen in A3. Het epitoop van RU5 omvat residuen die deel uitmaken van een α-helix en van drie lussen die aan het oppervlak van het A3 molecuul liggen. Al deze residuen liggen in de onderzijde van A3. Na vergelijking met andere A3 structuren blijkt dat binding van RU5 geen conformatie-veranderingen over lange afstand bewerkstelligt. In plaats daarvan lijkt RU5 collageen binding te voorkomen door middel van sterische hindering. Dit impliceert dat de bindingsplaats voor collageen zich binnen of dichtbij het epitoop van RU5 bevindt en dus in de buurt van de onderzijde van A3. Het is opmerkelijk dat de bindingsplaats van vWf-A3 voor collageen zich ver van de bovenzijde van het A3 domein bevindt omdat hier de bindingsplaatsen voor collageen aangetoond zijn in homologe I domeinen van integrines. Het is dus aannemelijk dat vWf-A3 en de I domeinen van integrines collageen op fundamenteel uiteenlopende wijzen binden. De structuur van A3-RU5 verschaft een uitstekend startpunt voor een verder onderzoek naar de bindingsplaats voor collageen, door middel van plaats-specifieke mutagenese.

--- Curriculum Vitae ---

Barend Bouma werd geboren op 21 november 1972, te Deventer. De middelbare school werd in 1991 afgerond met het behalen van het Voorbereidend Wetenschappelijk Onderwijs diploma aan de Gemeentelijke Scholengemeenschap Doetinchem. In datzelfde jaar werd begonnen met de voltijdsstudie Scheikunde aan de Universiteit Utrecht. In augustus 1992 werd het propaedeuse-diploma gehaald. Gedurende de doctoraalfase werd een bijvak van zes maanden gevolgd bij de vakgroep Vaste Stof Chemie (Prof. Dr G. Blasse). In augustus 1995 werd het doctoraalprogramma van Scheikunde afgerond met als hoofdvak Kristal- & Structuurchemie onder begeleiding van Dr. L.M.J. Kroon-Batenburg en Prof. Dr J. Kroon. De onderzoeksspecialisatie omvatte tevens een stage periode van drie maanden bij Akzo-Nobel, te Velp (Dr. E.A. Klop). Alvorens het doctoraaldiploma in november 1995 in ontvangst te nemen (met genoegen), werd ter voorbereiding op een aansluitend promotie-onderzoek drie maanden onderzoek verricht binnen de faculteit Biologie, bij de vakgroep Biomoleculaire Celbiologie (Prof. Dr W.P.M. Hoekstra en Drs. C. Jansen). Tijdens de studie werd in 1994 deelgenomen aan het vierde symposium van de KNCV Sectie Scheikunde-onderwijs (Amsterdam) en aan de A.I.O.-school "Kristal- en Structuuronderzoek" en in 1995 aan het zestiende Europees Kristallografisch Congres (Lund, Zweden). Op het KNCV symposium en op het Europees congres werd onderzoek gepresenteerd dat tijdens het groot bijvak en het hoofdvak verricht werd.

Van december 1995 tot januari 2000 werd onderzoek verricht als Assistent in Opleiding bij de Sectie Kristal- & Structuurchemie, die onderdeel is van het Bijvoet Centrum voor Biomoleculair Onderzoek van de Universiteit Utrecht. Het in dit proefschrift beschreven onderzoek werd verricht onder leiding van Prof. Dr J. Kroon, Dr. P. Gros en Dr. Ph.G. de Groot (Universitair Medisch Centrum, Divisie Haematologie, Universiteit Utrecht). Tevens werd onderzoek verricht onder leiding van Prof. Dr K.W.A. Wirtz (Sectie Biochemie van Lipiden, Centrum voor Biomembranen en Lipiden Enzymologie, Universiteit Utrecht). Resultaten van het in dit proefschrift beschreven onderzoek werden onder andere gepresenteerd op bijeenkomsten van de Studiegroep Eiwitonderzoek (Lunteren, 1999) en de Studiegroep Kristal- en Structuuronderzoek (Lunteren, 1999) van de Stichting Chemische Wetenschappen Nederland, op de bijeenkomst van de Nederlandse Vereniging voor Trombose en Haemostase (Amsterdam, 1999) en tijdens het International Union of Crystallography XVIII Congres (Glasgow, Schotland, 1999). In 1996 werd deelgenomen aan een NATO/FEBS zomerschool over "Cell signalling and targetting" (Spetsai, Griekenland) en aan de EMBO cursus "Data collection" (Cambridge, Engeland).

--- Publications ---

1. Komatsu, H., **Bouma, B.**, Gros, P., Wirtz, K.W.A., Taraschi. T.F. and Janes, N. (2000) Activity of phosphatidylinositol transfer protein is sensitive to ethanol and membrane curvature, Biochem. J. 348, 667-673.
2. **Bouma, B.**, de Groot, Ph.G., van den Elsen, J.M.H., Ravelli, R.B.G., Schouten, A., Simmelink, M.J.A., Derksen, R.H.W.M., Kroon, J. and Gros, P. (1999) Adhesion mechanism of human β_2-glycoprotein I to phospholipids based on its crystal structure. EMBO J. 18, 5166-5174.
3. **Bouma, B.**, Kooijman, H., Kroon, J., Grech, E. and Brezinski, B. (1999) 1,8-Bis-(dimethylaminomethyl)naphthalene squaric acid (2/1) complex dihydrate. Acta Cryst. C 55, 1824-1826.
4. Tuscher, O., Lorra, C., **Bouma, B.**, Wirtz, K.W.A. and Huttner, W.B. (1997) Cooperativity of phosphatidylinositol transfer protein and phospholipase D in secretory vesicle formation from the TGN. Phosphoinositides as a common denominator? FEBS Lett. 419, 271-275.
5. Kroon-Batenburg, L.M.J., **Bouma, B.** and Kroon, J. (1996) Stability of cellulose structures studied by MD simulations. Could mercerized cellulose II be parallel? Macromolecules 29, 5695-5699.
6. **Bouma, B.** and Klop, E.A. (1995) Refinement of the POK-α fibre crystal structure by two different least-squares procedures. (Internal company publication of Akzo-Nobel, Velp, The Netherlands)
7. **Bouma, B.** and Blasse, G. (1995) Dependence of luminescence of titanates on their crystal structure. J. Phys. Chem. Solids 56, 261-265.
8. **Bouma, B.**, Westerman, J., Dekker, N., Gros, P. and Wirtz, K.W.A. Activation of phosphatidylinositol transfer protein α and β isoforms from inclusion bodies requires phosphatidylcholine with different acyl-chain length. (submitted).
9. **Bouma, B.**, Huizinga, E.G., Schiphorst, M.E., Sixma, J.J., Kroon, J. and Gros, P. Structure of a von Willebrand Factor A3-domain Fab complex points to a location for the collagen-binding site. (submitted).
10. **Bouma, B.**, Gros, P., Kroon, J. and de Groot, Ph.G. Structural and functional aspects of β_2-glycoprotein I. (*Review*, in preparation).
11. **Bouma, B.**, Simmelink, M.J.A., Westerman, J., de Groot, Ph.G., Gerwig, G.J., Kroon, J. and Gros., P. Inactive β_2-glycoprotein I carries a neutral phospholipid molecule. (in preparation).